UNIVERSITY MICROFILMS, ANN ARBOR, MICH.

L. C. Card no. Mic 58-3647

CLINE, James Edward. BETA AND GAMMA DECAYS FROM SOME ODD-ODD, SELF-CONJUGATE NUCLEI AND THEIR ISOBARIC NEIGHBORS.

University of Michigan, Ph. D., 1958
Physics, nuclear

Negative Microfilm Received from University

# BETA AND GAMMA DECAYS FROM SOME ODD-ODD, SELF-CONJUGATE NUCLEI AND THEIR ISOBARIC NEIGHBORS

by

James E. Cline

A dissertation submitted in partial fulfillment
of the requirements for the degree of
Doctor of Philosophy in the
University of Michigan
1957

Doctoral Committee:

Assistant Professor Paul R. Chagnon, Co-chairman
Associate Professor Robert W. Pidd, Co-chairman
Associate Professor Paul V. C. Hough
Professor Kenneth M. Case
Professor Wilfred Kaplan

# BETA AND GAMMA DECAYS FROM SOME ODD-ODD, SELF-CONJUGATE NUCLEI AND THEIR ISOBARIC NEIGHBORS

James E. Cline

The present experiment was undertaken to study the properties of the N = Z, A = 4n + 2 (n = integer) nuclei and their adjacent isobaric neighbors by time and energy analyses of the positrons and gamma-rays emitted from the unstable nuclei in these groups. The specific groups studied were those with A = 38, A = 30 and A = 26. The objectives of this research were: (1) To obtain information about the level schemes and spacings of the N = Z nuclei, especially with regard to the relative spacings of the two lowest-lying levels in these nuclei; (2) to obtain more accurate ft values than presently exist for the positron decays from the (N = Z) nuclei; and (3) to obtain the lifetime of the heretofore-never-observed (N = Z - 2) member of these triads.

The studied nuclei were produced by $(\gamma,n)$ and $(\gamma,n^dp)$ photonuclear reactions using the 20 cps, pulsed, 85 mev bremsstrahlung beam of the University of Michigan electron synchrotron. Development of adequate shielding allowed the technique of scanning the targets (by scintillation detectors) in the position in which they were activated by the x-ray beam. A system was developed which would control the bombardment time and the time between bombardment periods, allowing the compilation of decay curves which extended for several half-lives of the decay. Positron decay half-lives were measured by a coincidence technique which involved counting the annihilation radiation by two counters placed on opposite sides of a thick target.

$Log_{10}ft$ values for the positron decays of $K^{38m}$, $K^{38}$, $P^{30}$ and $Al^{26}$ were obtained; the values were $(3.48 \pm 0.06)$, $(4.89 \pm 0.07)$, $(4.81 \pm 0.07)$ and $(3.38 \pm 0.07)$ respectively. A series of three energy determinations, consisting of energy measurements of the positron and gamma transitions in the decays of $K^{38}$ and $K^{38m}$, yielded the result that the $(T = 0, J = 3^+)$ is the ground state of $K^{38}$ and that the $(T = 1, J = 0^+)$ level lies $(210 \pm 190)$ kev above.

Branching in the positron decay of $Ca^{38}$ to a level at $(3.5 \pm 0.14)$ mev in $K^{38}$ has led to a half-live determination for the decay of $Ca^{38}$ of $(0.66 \pm 0.05)$ seconds, and a tentative identification of the level in $K^{38}$ as a $(T = 0, J = 1^+)$ level. A search for a similar branching of the $S^{30}$ decay, specifically to a 690 kev level in $P^{30}$ (previously identified in two separate experiments as having $J = 0$ (implying $T = 1$) and $T = 0$ (implying $J = 1^+$) ), with a negative result has led to the belief that the state has both $T = 0$ and $J = 0$ (in violation of the usual coupling rules in the $N = Z, A = 4n + 2$ nuclei); branching would not be expected to occur in any appreciable amount to such a level.

The positron decays from the mirror nuclei $Ca^{39}$, $S^{31}$ and $Si^{27}$ were also studied and these decays yielded $log_{10}ft$ values of $(3.65 \pm 0.06)$ $(3.79 \pm 0.07)$ $(3.41 \pm 0.07)$ respectively. Such values are consistent with the fact that the decays should be superallowed transitions.

Of interest also were the relative yields from the $(\gamma, n^d p)$ and $(\gamma, n)$ reactions. These were measured to be $0.40 \pm 0.05$, $0.43 \pm 0.05$ and $0.16 \pm 0.04$ for the bombardment of $Ca^{40}$, $S^{32}$ and $Si^{28}$ respectively by 85 mev bremsstrahlung. The ratio was $0.13 \pm 0.03$ and $0.11 \pm 0.03$ for bombardment of $Si^{28}$ by 60 mev and 40 mev bremsstrahlung respectively.

Interpretations are made of these ratios with respect to themselves and to data of other investigators.

## ACKNOWLEDGMENTS

The author wishes to express his sincere appreciation to the members of his committee for their guidance and interest in this work. The author is particularly indebted to Dr. Paul R. Chagnon and Dr. Robert W. Pidd for their many ideas and suggestions and for their continued encouragement throughout the work, to Messrs. H. A. Westrick, O. Haas, G. Edict and J. Hobart for their cooperation and skill in the construction of the apparatus, to Mr. A. B. Miller for his assistance in running the synchrotron and in recording the data, and to his wife, Molly, without whose cooperation this work would have been impossible.

The author also wishes to express his appreciation to the United States Atomic Energy Commission for support of this work under Contract AT(11-1)-150.

TABLE OF CONTENTS


| | | Page |
|---|---|---|
| ACKNOWLEDGMENTS | | ii |
| LIST OF TABLES | | v |
| LIST OF FIGURES | | vi |
| I. | INTRODUCTION | 1 |
| | A. Historical Background | 1 |
| | B. The Experiment | 4 |
| | C. Results | 7 |
| II. | INTRODUCTION OF THEORETICAL BACKGROUND | 11 |
| | A. Fermi Theory of Beta-Decay | 11 |
| | B. Theory of Isobaric Spin | 14 |
| | C. The Shell Model of the Nucleus | 16 |
| III. | GENERAL DESCRIPTION OF THE N = Z, A = 4N + 2 NUCLEI AND THEIR ISOBARIC NEIGHBORS | 19 |
| | A. Application of Beta-Decay Theory to (A = 4n + 2) Nuclei | 19 |
| | B. Energy Level Schemes for the (A = 4n + 2) Nuclei | 24 |
| | C. Energy Level Schemes for the Mirror Nuclei | 30 |
| IV. | EXPERIMENTAL EQUIPMENT AND TECHNIQUES | 32 |
| | A. Synchrotron | 33 |
| | B. The X-Ray Beam | 33 |
| | C. Shielding | 36 |
| | D. Apparatus and Techniques for Measuring Half-Lives | 39 |
| | 1. Coincidence Technique | 39 |
| | 2. Beam "Knock-Out" System | 46 |
| | 3. Detection Equipment | 55 |
| | 4. Time Analyzer | 60 |
| | 5. Data Analysis and Errors | 64 |
| | E. Apparatus and Techniques for Making Energy Measurements | 66 |

TABLE OF CONTENTS (CONT'D)


| | Page |
|---|---|
| 1. Positron Endpoint Determination Equipment and Techniques Targets | 66 |
| 2. Gamma-Ray Energy Measurements | 75 |
| V. DESCRIPTION OF ENERGY LEVEL AND DECAY SCHEMES IN SPECIFIC NUCLEI: RESULTS OF THE MEASUREMENTS | 78 |
| A. $Ca^{38}$, $K^{38}$, $A^{38}$ | 78 |
| 1. Energy Level and Decay Schemes | 78 |
| 2. Experimental Results and Analysis | 83 |
| 3. Summary and Conclusions | 96 |
| B. $S^{30}$, $P^{30}$, $Si^{30}$ | 99 |
| 1. Energy Level and Decay Schemes | 99 |
| 2. Experimental Results and Analysis | 102 |
| 3. Summary and Conclusions | 106 |
| C. $Si^{26}$, $Al^{26}$, $Mg^{26}$ | 108 |
| 1. Energy Level and Decay Schemes | 108 |
| 2. Experimental Results and Analysis | 112 |
| 3. Summary and Conclusions | 116 |
| D. Decay From the Mirror Nuclei, $Ca^{39}$, $S^{31}$, $Si^{27}$ | 117 |
| 1. Energy Level and Decay Schematics | 117 |
| 2. Experimental Results and Analysis | 119 |
| 3. Summary and Conclusions | 126 |
| VI. RELATIVE YIELDS FROM THE $(\gamma,n)$ AND THE $(\gamma,n^dp)$ REACTIONS ON $Ca^{40}$, $S^{32}$ and $Si^{28}$ | 127 |
| A. Deuteron Emission Photonuclear Reactions | 128 |
| B. Results and Analysis | 129 |
| C. Summary and Conclusions | 132 |
| VII. SUMMARY AND CONCLUSIONS | 134 |
| BIBLIOGRAPHY | 136 |

## LIST OF TABLES


| Table | | Page |
|---|---|---|
| I | Results of the Measurements of the Decays From the Nuclei in the Nuclear Triad with (A = 38)..... | 84 |
| II | Results of the Measurements of the Decays From the Nuclei in the Nuclear Triad with (A = 30)..... | 104 |
| III | Results of the Measurements of the Decays From the Nuclei in the Nuclear Triad with (A = 26)..... | 114 |
| IV | Theoretical Values of the Nuclear Matrix Elements for the Positron Decay of the Mirror Nuclei, $Ca^{39}$, $S^{31}$, and $Si^{27}$..... | 119 |
| V | Results of the Measurements of the Decays From the Mirror Nuclei..... | 120 |
| VI | List of Ratios of Relative Yields From $(\gamma,n)$ and $(\gamma,n^dp)$ Reactions in $Ca^{40}$, $S^{32}$, and $Si^{28}$..... | 130 |

LIST OF FIGURES


| Figure | | Page |
|---|---|---|
| 1 | Segrè Chart of Nuclei in Region 1a < Z < 2a, Showing (A = a + b) Nuclei and Mirror Nuclei and Their Decay Modes | 3 |
| 2 | Energies (in MeV) of Lowest T = 0 and T = 1 States in Odd-Odd, N = Z Nuclei, Relative to Ground State of Neighboring Even-Even N = Z + 2 Isotope | 26 |
| 3 | Typical Energy Level Diagram for (A = 4N + 2) Nuclear Chain | 29 |
| 4 | Thin Target Photon Spectrum (Lead) | 35 |
| 5 | Photograph of X-Ray Beam Taken at Entrance Port to Experimental Area | 37 |
| 6 | Photograph of X-Ray Beam Taken at Exit Port From Experimental Area | 37 |
| 7 | Cross-Section of Synchrotron Area, Showing Synchrotron, Concrete Shielding and Beam-Trapping Arrangement | 40 |
| 8 | Plot of Gamma-Ray Absorption Coefficients Vs. Target Thickness, for Maximum 180° Coincidence Counting Rate From Thick Targets | 45 |
| 9 | Diagram of Target-Counter Arrangement Used in Coincidence Detection of the Annihilation Radiation | 47 |
| 10 | Master Timer Control Circuit | 51 |
| 11 | Plot of Optimal Bombarding Times for Given Observation Times in Units of Half-Lives of the Nuclear Decay Being Observed | 54 |
| 12 | Circuit Diagram for Photocathode Pulser | 57 |
| 13 | Detection System Block Diagram | 59 |
| 14 | Diagram of Time Analyzer | 61 |
| 15 | Diagram of Target-Counter Arrangement Used in the Detection of Positrons From an Activated Target | 68 |

LIST OF FIGURES (CONT'D)


| Figure | | Page |
|---|---|---|
| 16 | Energy Level Diagram for the Nuclei, $A^{38}$, $K^{38}$, $Ca^{38}$ | 80 |
| 17 | Fractional Intensity x of $(0^+ \rightarrow 1^+)$ Transition in $\beta^+$ Decay of the Z = N + 2, A = 4n + 2 Nuclei, $\Delta$ Equals Height of $8^+$ State Above $1^+$ State in N = Z Nuclei | 82 |
| 18 | Decay Curve for $K^{38}$ | 85 |
| 19 | Decay Curve for $K^{38m}$ | 86 |
| 20 | Kurie Plot of Positron Spectrum From $K^{38}$ and $K^{38m}$ | 88 |
| 21 | Gamma-Ray Spectrum From the Decay of $K^{38}$ and $K^{38m}$ Showing Calibration Spectrum from $Na^{24}$ | 90 |
| 22 | Decay Curve for Argon Gamma-Ray | 92 |
| 23 | Gamma-Ray Spectrum from Calcium Targets Showing 2.2 mev Gamma-Ray from Argon and 3.5 mev Gamma-Ray, Specifically Obtained Only from a Calcium Target | 93 |
| 24 | Decay Curve of Gamma-Ray Found from the Bombardment of a Calcium Target | 94 |
| 25 | Energy Level Diagram for Nuclei $S^{30}$, $P^{30}$, $Si^{30}$ | 101 |
| 26 | Decay of $P^{30}$ | 103 |
| 27 | Kurie Plot of Positron Spectrum from the Decay of $P^{30}$ | 105 |
| 28 | Gamma-Ray Spectrum from Sulfur Target, Energy Region 0 → 1.0 mev | 107 |
| 29 | Energy Level Diagram for Nuclei: $Mg^{26}$, $Al^{26}$, $Si^{26}$ | 110 |
| 30 | Decay Curve for $Si^{27}$ and $Al^{26}$ for 85 mev Bombarding Energy | 113 |
| 31 | Kurie Plot of Positron Spectrum from $Al^{26}$ | 115 |
| 32 | Decay Curve for $Ca^{39}$ | 121 |
| 33 | Decay of $S^{31}$ | 123 |
| 34 | Kurie Plots of the Positron Spectra from the Mirror Nuclei | 125 |

# CHAPTER I

# INTRODUCTION

## A. Historical Background.

Although a great quantity of information has been compiled concerning the properties of many nuclei, there remain a vast number of nuclei about which relatively little is known. A few of these nuclei fall into a group called the odd - odd, self - conjugate nuclei, implying that they contain an even number of nucleons, an odd number of both neutrons and protons and that the numbers of neutrons and of protons are equal. These nuclei are often called the odd - odd, $(A = 4n + 2)$ nuclei, n being an integer. The members of this group are for the most part beta unstable, decaying with rather short half-lives to even-even isobars (even numbers of neutrons and protons). Due primarily to the fact that the decay half-lives are so short, direct information about spin, magnetic moments, quadrupole moments, etc. is relatively rare for these nuclei. Some of the desired information, however, may be obtained from the study of beta and gamma decays in the $(4n + 2)$ nuclei, if techniques are developed which enable one to study the short-lived decays. The majority of the information that has been obtained concerning beta decay was compiled with the use of long-lived sources. These sources either contained long-lived beta emitters, or contained nuclei in long-lived isomeric states, the decay from which precipitated a short-lived beta-decay. In the analysis of such decays, it was possible to remove the sources from the activating area and analyze them in a background-free station. If beta transitions with short half-lives, which do not follow such isomeric transitions, are to be

studied, the experimental techniques must be such as to create and analyze the nuclei in essentially the same position, with any background radition shielded out.

Investigations which are described in this thesis were directed with the sole purpose of obtaining more information about the $(A = 4n + 2)$, $N = Z$ nuclei. However, not only the self-conjugate nuclei were studied. Due primarily to the interest in the $(N = Z)$ nuclei, much has been predicted from a theoretical standpoint concerning the properties of their $(N = Z - 2)$ and $(N = Z + 2)$ isobaric neighbors. The odd-odd nucleus and its adjacent isobars form an isobaric triad. The $(N = Z + 2)$ member of the group is generally stable (i.e. for $Z > 7$), while the other two members of the group are positron unstable. In some cases, the proton-rich member of the different groups (i.e. the isobar with $N = Z - 2$) has never been observed, although the half-live and endpoint energy of the positron decay from these nuclei have been predicted. Consequently any observation of the decays from the $(N = Z - 2, A = 4n + 2)$ nuclei would constitute the discovery of a new nuclide. A Segre chart, showing the nuclei of interest, is presented in figure 1.

Energy endpoint measurements of the positron transitions among the members of a $(4n + 2)$ triad can yield valuable information concerning the position of some of the states (with respect to one another). This was particularly true in the nucleus $K^{38}$, where the relative position of the two lowest states has long been in doubt.

A half-life measurement, in conjunction with a positron energy endpoint determination, can yield an ft value for a given beta-decay

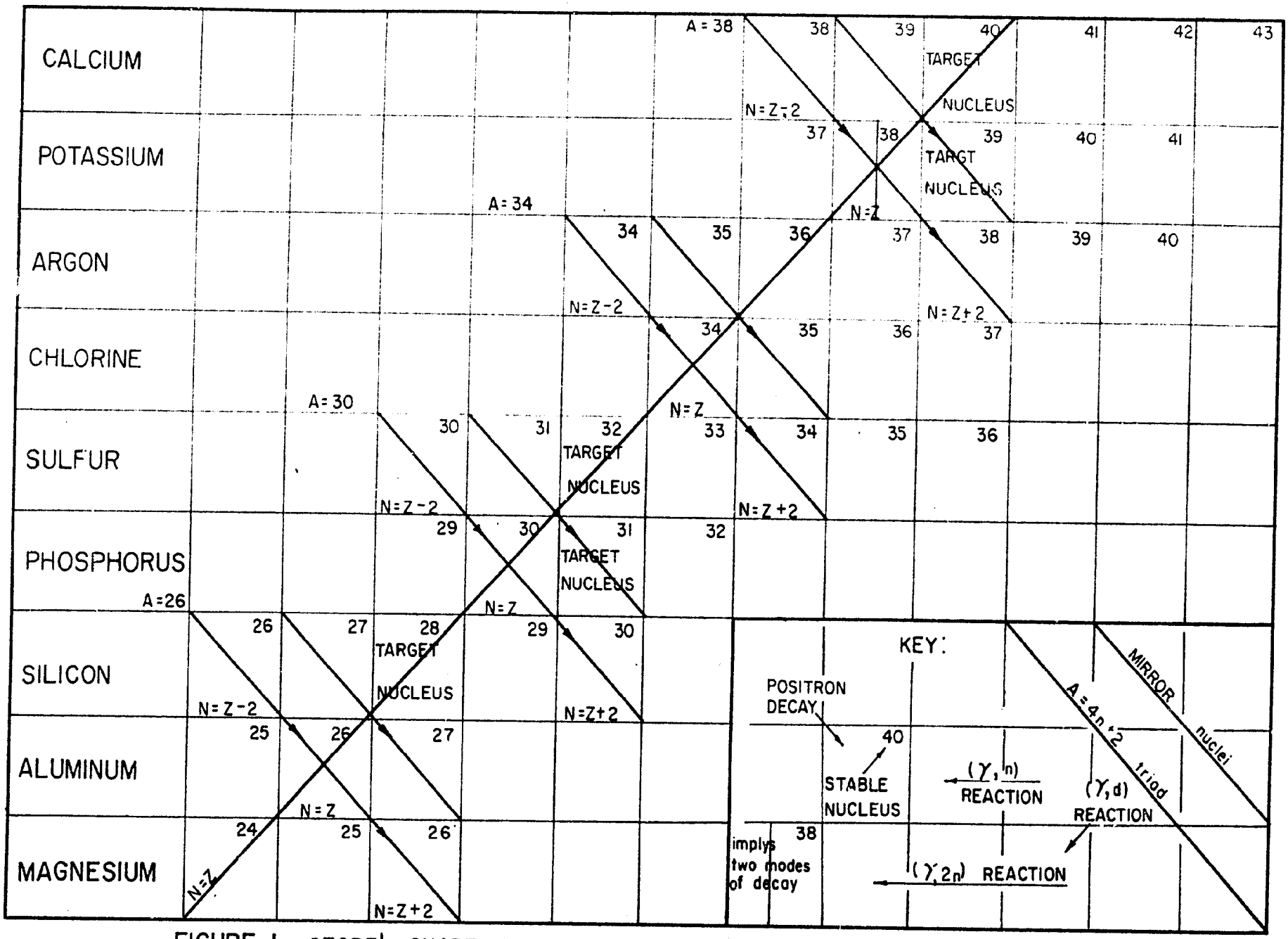


FIGURE I. SEGRE' CHART OF NUCLEI IN REGION $12 \leq Z \leq 20$, showing (A = 4n + 2) NUCLEI AND MIRROR NUCLEI AND THEIR DECAY MODES

which establishes the degree of allowedness for that transition. Once the allowedness is established, if the T and J values of one of the two states involved in the transition are also known, T and J values may usually be uniquely assigned to the other state as well. In addition, if in a given beta-decay a branching occurs to an excited level of the daughter nucleus, an observation and energy measurement of the resulting gamma transition from the excited level may lead to a positive assignment of energy and total angular momentum and isobaric-spin quantum numbers for the excited level. A half-life measurement of this gamma-ray should yield the half-life of the positron decay proceeding the gamma-ray.

Thus it is seen that a great deal of information may be obtained from a detailed study of the beta and gamma transitions among the nuclei in the $(4n + 2)$ isobaric triads.

B. The Experiment.

The nuclei studied in this experiment have short half-lives and were produced artificially by photonuclear reactions, using the bremsstrahlung beam of the University of Michigan electron synchrotron. The photonuclear reactions used to produce the nuclei were the $(\gamma,n)$, $(\gamma,2n)$ and $(\gamma,n^dp)$ reactions which require an initial photon energy of about 25 mev. The x-ray beam consists of bursts of photons, each burst being about 30 microseconds duration and the time between bursts being 50 milliseconds. It was therefore possible to bombard and observe in continuous operation, leaving the targets and the counters in a fixed position, and gating the counting system on during the period between beam bursts. For the compilation of decay curves (from which half-life determinations

were made), it became necessary to extend this time between photon bursts. A system was therefore developed which controlled the injection of the electrons into the synchrotron, thus controlling both the bombarding time and the time between bombardment periods. The ratio of these two times could be set to any prescribed value, and the total duration of the control period was 50 seconds. This time could be extended to 5000 seconds by the use of an auxiliary instrument but in so doing, the extension would increase proportionately the duration of the controlling steps.

A principal difficulty involved in the use of such a technique is that of a high background flux, tending to mask out the actual signal from the target. The major contributor to the background counting rate were neutrons, electro-and photoproduced both internal and external to the synchrotron proper, although scattered bremsstrahlung also presented significant effects. To reduce the unwanted background the experimental area was enclosed by concrete shielding walls one meter thick. Collimation of the x-ray beam before it was directed into the room through a port in the forward wall, also served toward the end of reducing the background. Targets were then placed in the beam just inside the entrance port.

The irradiated target was a thick sample in which the positrons would stop and annihilate. Two scintillation detectors, placed on opposite sides of the target and discriminated so as to allow only the 511 kev two-quantum annihilation gamma-rays to be accepted by the detection system, were operated in coincidence. The method had two distinct advantages over the standard methods used in beta spectroscopy. The first

of these was that it allowed the use of thick targets (~10 gms/cm$^2$) with the attendant relatively high counting rates. This allowed the compilation of decay-curves composed of sufficient counts to allow half-life determinations with standard deviations of about 2%. The second advantage lay in the fact that it reduced the background counting rate relative to the signal counting rate. Any particles other than positrons annihilating in the target would be rejected by the counting system and the only background would be that of accidental coincidences and that of cosmic-rays which created pairs, the positron annihilating in either one of the crystals or in the target. The number of accidental coincidences could be calculated from a knowledge of the resolving time of the coincidence system.

Other measurements made in this experiment consisted of positron endpoint energy determinations and gamma-ray energy determinations. These measurements involved the use of single scintillation detectors, and hence, no coincidence technique could be used to reduce the background. However, it was still possible, at least in the gamma-ray energy determinations to employ thick targets, similar to those used in obtaining the decay-curves. For the positron endpoint determinations, the signal to background ratio was quite bad due to the low counting rates connected with the use of the necessarily thin targets. The proportionately large background, although measured and subtracted from the data, introduced errors into the results which are difficult to estimate. Nevertheless, it is felt that most of the energy determinations were accurate to about 5%.

Using the described techniques, the following (A=4n+2) nuclei were studied: $Ca^{38}$, $K^{38}$, $A^{38}$, $S^{30}$, $P^{30}$, $Si^{30}$, $Si^{36}$, $Al^{26}$ and $Mg^{26}$. Since the synchrotron had to be run at 85 mev, for intensity reasons, many additional nuclei were produced by photonuclear reactions on the target isotopes, other than those which produced the nuclei of primary interest. Some of the more abundant byproduct nuclei were the mirror nuclei $Ca^{39}$, $S^{31}$ and $Si^{27}$. Since these nuclei are positron emitters, were produced in relatively high abundance and are of some theoretical interest, they were studied as well.

Furthermore, the data allowed an estimate of the relative yields for some of the photonuclear reactions used in this experiment. In particular, the ratio of the yields from the $(\gamma,n^{d}p)$ reaction and the $(\gamma,n)$ reaction has been measured (for a peak bombarding energy of 85 mev) on the following nuclides: $Ca^{40}$, $S^{32}$ and $Si^{28}$. The ratio was also measured in $Si^{28}$ for peak x-ray energies of 60 mev and 40 mev.

C. Results.

The results of this research fall into several catagories since many types of measurements were made. Half-life measurements of the positron decay from the unstable odd-odd, self-conjugate nuclei, coupled with endpoint measurements have yielded ft values for the decays which are consistent with the type of transitions which should occur. In particular, the values of $\log_{10}$ ft for the positron-decay from $K^{38}$, $K^{38m}$, $P^{30}$ and $Al^{26}$ were measured respectively to be 4.89, 3.48, 4.81 and 3.38. The reported values have errors of about 2%. The $\log_{10}$ ft values for the positron-decay from the mirror nuclei $Ca^{39}$, $S^{31}$ and $Si^{27}$ were found to be 3.65, 3.79 and 3.41 respectively. These values also have standard deviations of about .2%,

and are consistent with the assumption that the positron-decays are superallowed transitions.

The two lowest states in $K^{38}$, namely the (T = 1,J = 0 +) and the (T = 0,J = 3 +) states were measured to have an energy separation of about 200 kev (with an error of about 8%), with the (T = 0,J = 3 +) state being the lower state. This separation was determined from measurements of the endpoint energy of the positron-decays from the two levels, and from an energy measurement of the gamma transition from the first excited level in $A^{38}$ to which the (T = 0,J = 3 +) state in $K^{38}$ decays.

A search for gamma transitions which follow a branching in the positron-decay from the (Z = N + 2) nuclei led to two results. The first of these was the identification of a 3.5 mev gamma-ray, observed only with the bombardment (by the x-ray beam) of a calcium target, as being from the decay of an excited level in $K^{38}$ following a branching in the positron-decay of $Ca^{38}$ to that level. A half-life measurement was made of this gamma-ray and the resulting value is 0.66 seconds, which is in accordance with the predicted value of the half-life of $Ca^{38}$. The 3.5 mev excited state in $K^{38}$ was identified from experimental and theoretical arguments as being either a (T = 1,J = 0 +) or a (T = 0,J = 1 +) level, with the latter assignment being the preferred assignment. Since $Ca^{38}$ had heretofore never been observed, this result is also construed as the identification of the new isotope with a half-life of 0.66 seconds.

A similar searching for a gamma transition following a branching in the decay of $S^{30}$ to an excited level in $P^{30}$, with a negative result, yielded the second result. A level in $P^{30}$ had been found by several investigators and had been seemingly conflicting identified as having (J = 0),

implying (T = 1), and independently, as having (T = 0), implying (J = 1). Either of these assignments would have led to a state to which a branching in the decay of $S^{30}$ would occur. The fact that a gamma transition from the state was not observed in this experiment indicates that both previous identifications were correct, and that the state has (T = 0,J = 0) which is in violation of the semi-emperical rules governing the creation of low-lying states in odd-odd, (N = Z) nuclei. Such a state could arise from a mixed nucleon configuration in $P^{30}$ and branching in the positron-decay from the (T = 1, 0 +) ground state of $S^{30}$ would be forbidden.

The ratios for the relative production of nuclei by the $(\gamma,n^dp)$ and $(\gamma,n)$ photonuclear reactions on the target nuclei $Ca^{40}$, $S^{32}$ and $Si^{28}$ were measured to be 0.40, 0.43 and 0.16 respectively for a peak bombarding energy of 85 mev. This ratio was also measured for $Si^{28}$ at bombarding energies of 60 mev and 40 mev with results 0.13 and 0.11 respectively. These results carry errors of about 15% and confirm the results of other investigators who found that the yield from the $(\gamma,n^dp)$ process is too high to be consistent with the Weisskopf-Ewing theory of the compound nucleus. The fact that the ratio for the bombardment of $Si^{28}$ is so much lower than the corresponding ratio in the other isotopes indicates that another state is created in $Al^{26}$ by the $(\gamma,n^dp)$ process which has a very long half-life and would not have been observed in these measurements.

The following report, which describes the theory behind these measurements and the experimental details themselves as well as the results, is broken up in the following manner. Chapter II introduces briefly the theories of beta-decay, isobaric spin and the nuclear shell

model. These are presented for the sake of reference and include those points which are pertinent to the (A = 4n + 2) and mirror nuclei. The next chapter applies these theories in more detail to specific nuclei and their associated decay schemes. The remaining chapters describe the experimental approach, the results and the analysis of these results.

## CHAPTER II

## INTRODUCTION OF THEORETICAL BACKGROUND

### A. Fermi Theory of Beta - Decay.

The first theory of beta decay which successfully accounted for the continuous beta spectrum and for the shape of the spectrum was offered by Fermi[1] in 1934. It is based on the hypothesis that a neutrino is emitted from the nucleus along with the electron. This neutrino may be emitted with any energy up to the maximum energy involved in the decay of the nucleus. The total energy is then shared by the neutrino, the beta particle, and the product nucleus, and the division of energy is a function of the angles between the three particles. In this paper were introduced the Fermi selection rules for beta decay. The theory was soon extended to take into consideration the remaining types of interactions between heavy and light particles[2].

In the formulation of the general theory of beta decay, Fermi expressed the probability per unit time for a beta transition by the equation of time dependent perturbation theory

$$P = \frac{2\pi}{\hbar} \left| \mathcal{H}'_{if} \right|^2 \delta(E). \qquad \text{II-1}$$

$\mathcal{H}'_{if}$ is the interaction matrix element and $\rho(E)$ is the energy density of final states.

Since the emitted particles have half-integer spin and move with velocities equal to (neutrino) or approaching (beta particles) the velocity of light, they must be described by Dirac's relativistic wave equation. A

restriction that the interaction Hamiltonian must be relativistically invariant allows only five forms for the matrix element. An example of one of these forms is the vector interaction matrix element which can be expressed as[3]

$$\left( |\mathcal{H}'_{if}| \right)_v = G_v p_v (u_e^*, u_\nu^*) |\int 1|^2 \qquad \text{II-2}$$

1 represents the unit operator and the notation $|\int 1|$ is defined by $|\int O| = \sum_{n=1}^{A} \int \varphi_f^* O \tau_n + \varphi_i d\tau$ where O represents some operator, $\varphi_f$ and $\varphi_i$ represent the nuclear wavefunctions for the final and initial nucleus respectively, and $\tau_n +$ represents an operator which, when operating on any proton wave function, converts it into a neutron wave function. $G_v$ is the coupling constant for the vector interaction. $p_v(u_e^*, u_\nu^*)$ is a function of $u_e^*$ and $u_\nu^*$ (the complex conjugates of the electron and neutrino wave functions respectively) and, in the case of the vector interaction, the unit operator.

In the limit of non-relativistic nucleons in the nucleus, the scalar nuclear matrix element reduces to the expression which represents the vector matrix element. Similarly, the pseudo-vector interaction nuclear matrix element reduces to the expression for the tensor matrix element. The pseudo-scalar interaction, in this limit, vanishes. Any beta decay may then be described by a linear combination of the two remaining forms of the nuclear matrix element.

In order to evaluate the function $p(u_e^*, u_\nu^*)$ in equation II-2, an expansion of the electron and neutrino wave functions is made in terms of spherical harmonics. The major contribution comes from the first non-vanishing term in the expansion. If the first term in the

expansion does not vanish, then the decay is termed an allowed decay. If the second term is the first non-vanishing term, then the decay is said to be first - forbidden. Each degree of forbiddenness implies a smaller transition probability and hence a longer half-life for the decay.

There are two classes of allowed transitions, namely allowed and favored (generally called superallowed), and allowed but unfavored (generally called allowed). The distinction between the two has to do with the overlap of the nuclear wave functions. For superallowed transitions the overlap is complete (i.e. the nuclear wave functions are identical in the parent and daughter nuclei), while in allowed transitions, the overlap is not perfect.

The shape of the continuous allowed beta spectrum may be expressed as the probability per unit time that the beta-particle is observed with total energy between E and E + dE by

$$p(E)dE = K_2 F(E,Z)g(E, E_o) \left[ G_F^2 \left| \int 1 \right|^2 + G_{G.T.} \left| \int \sigma \right|^2 \right] \qquad \text{II-3}$$

where $K_2$ is a known constant, g a known function of E, the energy of the emitted beta particle, and $E_o$ is the maximum beta energy. F(E,Z) is a known function of E and Z, the charge of the daughter nucleus. $|\int \sigma|$ symbolizes the nuclear matrix element for the tensor and pseudo-scalar interaction where $\vec{\sigma}$ represents the Pauli spin matrices. $G_F$ and $G_{G-T}$ are the Fermi and Gamow - Teller interaction coupling constants respectively where $G_F = (G_S + G_V)$ and $G_{G.T.} = (G_A + G_T)$

Equation II-3 has been integrated to yield

$$B = ft\left[ G_F^2 \left| \int 1 \right|^2 + G_{G.T.} \left| \int \sigma \right|^2 \right] \qquad \text{II-4}$$

t is the half-life of the decay, f an integral which corrects the half-life

for the effects of the nuclear Coulomb field and for the energy distribution of the beta particles and B is a universal constant for allowed beta decays.

The ft value for a given beta-decay is proportional to the inverse square of the total nuclear matrix element. The constant of proportionability, B, may be calculated. Empirically, the ft values of various beta-transitions have been grouped into different classes, each class corresponding to a different degree of allowedness. If the nuclear matrix elements can be evaluated, the theoretical value of ft may be compared to the measured experimental value and conclusions may be drawn concerning the changes in spin, parity, and orbital angular momentum associated with the transitions.

B. Isobaric Spin.

The evaluation of the nuclear matrix elements $|\int 1|^2$ and $|\int \sigma|^2$ is greatly facilitated by the use of the concept of isobaric spin. Isobaric spin was first introduced under the name of isotopic spin by Cassen and Condon[4] in 1936, and by Wigner[5] in 1937. The name isobaric spin, which seems to be more appropriate, is becoming in recent years the more common name.

In the concept of isobaric spin, the nucleon is treated as a single entity having two charge states, the neutron and the proton. A single wave function is then formed for the nucleus which contains both the proton wave functions and the neutron wave functions. The basic requirement for such a description is that nuclear forces are charge independent. The formalism may be written in such a form that the functions

which describe the nucleons as being either protons or neutrons take the exact form of the Pauli spin functions of atomic spectroscopy. The name is then derived from the fact that the isobaric-spin plays essentially the same role as the electron spin does in Russel-Saunders (spin-orbit) coupling. In neither case do the spins enter directly into the Hamiltonian, but enter, rather, through the Pauli exclusion principle. They both govern the symmetry of the spatial wave functions which, in turn, determine the energy of a given configuration level.

The generalized Pauli principle then states that the total nuclear wave function must be anti-symmetric with respect to the exchange of any two nucleons. The quantum number, T, introduced by the symmetry properties involving isobari spin functions is called the isobaric spin quantum number. It is a "good" quantum number so long as the assumption of charge independence of nuclear forces is valid. The isobaric-spin vector $\vec{T}$ of a nuclear system is defined by $\vec{T} = \frac{1}{2} \sum_j \vec{t}_j$ where $\vec{t}_j = \left[ t_1(j), t_2(j), t_3(j) \right]$ is the isobaric-spin operator of the $j^{th}$ nucleon. In the stationary state of a nucleus the third component of the vector $\vec{T}$ has as its characteristic value $T_3 = \frac{(Z-N)}{2}$ .

Two of the isobaric-spin operators were used by Fermi in his original theory of beta decay even before the introduction of the concept of isobaric spin by Cassen and Condon. Since its introduction, isobaric-spin has become increasingly more important in nuclear physics. The concept has been applied to the theories of beta decay, multipole radiation [6,7,8] and nuclear reactions [8,9,10]. Such applications have, in general, been successful in predicting different degrees of forbiddenness for some

transitions than would be predicted by the selection rules involving angular momentum and parity alone.

C. The Shell Model of the Nucleus.

Some of the nuclear matrix elements involved in the theory of beta decay may be evaluated only on the basis of some definite model of nuclear structure. Throughout the relatively short history of nuclear physics there have been many such models proposed. The model which has been the most successful in explaining some of the aspects of nuclear spectroscopy is based on the independent particle model, developed primarily to explain the existence of certain "basic" numbers connected with nuclear structure.

The existence of such numbers was first noted in 1917 when Harkins[11] pointed out that nuclei with even numbers of protons or neutrons are more stable than those with odd numbers. Elasser[12,13] found that special numbers of protons or neutrons form particularly stable configurations. This was the first note of the "magic numbers" associated with nuclear structure. The existence of such numbers was further substantiated by the high abundance of natural isotopes with 2,8,14,20,28,50,82,126 neutrons or protons in the nucleus. High abundance of a nuclear species usually goes with high binding energies. Overwhelming evidence for the existence of these "magic numbers" now exists in several forms. It exists in the fact that beta-ray emission energies are abnormally high whenever the neutron or proton number of the daughter nucleus assumes a "magic" value. Further evidence for their existence is found in the fact that the radiative-capture cross-sections for nuclie with N=50,82,126 are much lower than those of their neighbors. The existence of such numbers has been interpreted

as indicating that neutrons and protons within the nucleus are arranged into shells, like electrons in atoms.

To describe such a shell-like structure, the independent particle model of the nucleus assumes that the nucleons in the nucleus move under the influence of a common potential V(r) and that the interaction between the nucleons may be treated as a small perturbation. The most successful theory, based on such a description, has been that offered independently by Haxel, Suess, and Jensen[14], and by Mayer[15] in 1949. In this theory, the common potential is assumed to be an oscillator potential for radii less than the nuclear radius, and zero for radii greater than the nuclear radius. A further assumption is that there exists a spin-orbit coupling which splits the terms where $j = \ell + 1/2$ and $j = \ell - 1/2$ by reducing the energy of those terms ($j = \ell + 1/2$) in which the intrinsic spin is parallel to the orbital angular momentum and conversely. This effect is assumed to increase with increasing values of $\ell$. The parameters are then adjusted to give rise to closed nucleon levels occuring at the experimentally observed "magic numbers".

The internal motion of the nucleus can be described by the superposition of all semi-independent motions of the individual nucleons. Each nucleon in an orbit can be characterized by individual quantum numbers, which determine an individual nucleon energy level. According to Pauli's exclusion principle, these levels are filled successively with neutrons and protons independently. Whenever two successive levels are widely separated, the complete filling of the lower one, either with protons or with neutrons, corresponds to a shell closure, just as in the case of the electronic shells of the rare gas elements.

A number of semi-empirical rules have evolved from the use of such a nuclear shell model which explain qualitatively and, in many cases, quantitatively, numerous properties of nuclei. One of these rules states that an even number of nucleons of the same type in a state of a given j will nearly always arrange themselves to give a total angular momentum 0 in the ground state. Hence the angular momentum of any shell with an even population is zero, and the ground state angular momentum of any shell with odd population must equal the angular momentum of the odd (unpaired) particle. This particular rule allows unique predictions of the nuclear spins of the ground states for a great number of the nuclei (e,g, all even - even nuclei must have ground state spin zero). The shell - model is particularly useful in evaluating beta decay nuclear matrix elements since the model may be used to estimate nuclear wave functions.

## CHAPTER III

## GENERAL DESCRIPTION OF THE N = Z, A = 4N + 2 NUCLEI AND THEIR ISOBARIC NEIGHBORS

There are, at present, fifteen known members of the odd-odd, self-conjugate group of nuclei, starting with the deuteron and ending with $Cu^{58}$. Of this group, only $H^2$, $Li^6$, $B^{10}$, and $N^{14}$ are stable; their properties have been thoroughly investigated[16]. The other nuclei of this group decay by positron emission, going to their even-even isobars with (N = Z + 2). In turn, the self-conjugate nucleus is formed from the decay of its isobar with (Z = N + 2). Isobaric-spin triplet nuclear wave functions are common to each of the three nuclei in these triads. Eigenstates corresponding to these wave functions are thus found in each of the nuclei and are (T = 1) states. Corresponding eigenstates among the three nuclei are displaced from one another by the Coulomb energy and by the neutron-proton mass difference. The center nuclei in these triads, the self-conjugate nuclei, also have isobaric-spin singlet states which correspond to the isobaric singlet eigenfunctions of the nuclear Hamiltonian. Since the (N = Z) nuclei have odd numbers of nucleons of both types, the J value for the lowest isobaric singlet state in each of these nuclei may be predicted fairly unambiguously with the aid of Nordheim's coupling rules[17].

### A. Application of Beta-Decay Theory to (A = 4n + 2) Nuclei.

In each of the (A = 4n + 2) triads, there is only one stable nucleus. The triplet groups with $A \leq 14$ have as the stable member the self conjugate nucleus, while the N = Z + 2 nucleus is a negatron emitter. In the triads with $A > 14$, the N = Z + 2 nucleus is the stable member, the other two nuclei being positron unstable. The following discussion will

primarily concern the nuclei with ($A = 4n + 2$) and with $A \geq 14$.

The positron decays between the lowest-lying isobaric-spin triplet levels in these nuclei are all superallowed transitions (with $|\Delta J| = 0$, $J = 0^+$), while the decays to or from the singlet levels are generally allowed transitions ($|\Delta J| = 1$). In some cases, in particular $Al^{26}$, the lowest singlet state has a high J value and decays by a higher order transition. The selection rules for the superallowed and the allowed transitions may be summarized by

$$\pi_i = \pi_f, \begin{cases} |\Delta J| = |\Delta T| = 0 & \text{superallowed.} \\ |\Delta J| = |\Delta T| = 1 & \text{allowed.} \end{cases} \qquad \text{III-1}$$

In actuality, there exist two distinct classes of superallowed transitions; those that occur between the ($T = 1$, $J = 0^+$) states of the ($A = 4N + 2$) nuclei, and those that occur between the ground ($T = 1/2$) states of mirror nuclei (i.e. a pair of isobars in which one nucleus has one more proton than neutron and the other nucleus has one less proton than neutron).

The nuclear matrix elements for the Fermi interactions and for the Gamow-Teller interactions are given respectively by[18]

$$|\int 1|^2 = \sum_{M_f} \left| \int \psi_f^* \sum_i t_+^i \psi_i \, d\tau \right|^2 = \sum_{M_f} \left| \int \psi_f^* T_+ \psi_i \, d\tau \right|^2, \qquad \text{III-2}$$

and

$$|\int \sigma|^2 = \sum_{M_f} \sum_x \left| \int \psi_f^* \sum_i t_+^i \sigma_x^i \psi_i \, d\tau \right|^2. \qquad \text{III-3}$$

$\psi_i$ and $\psi_f$ are the total nuclear eigenfunctions which depend upon all the nucleons. $t_+$ is the isobaric-spin operator which transforms a proton wave function into a neutron wave function and its properties are defined in complete analogy to those of the Pauli spin operator $\sigma_+$ by

$$t_+\pi = (t_x + i\ t_y)\pi, \qquad \text{III-4}$$

where $\pi$ is the function upon which it operates. $t_x$ and $t_y$ are the x and y components of single nucleon isobaric spin. The third component $t_z$ represents the charge of a nucleon, being 1/2 for protons and -1/2 for neutrons, $T_+ = \sum_i t_+^i$. The sums are to be taken over all components of the Pauli spin operator $\vec{\sigma}$, and over all M values of the final level.

The Fermi interaction matrix element is seen from equation III-2 to be zero unless the levels of the parent and daughter nucleus belong to the same isobaric spin multiplet and have the same isobaric-spin quantum number T. In this case, if the nuclear eigenfunctions are pure functions (i.e. arise from a single shell model nucleon configuration), $\psi_i$ and $\psi_f$ are identical except for Coulomb terms, and equation III-2 may be solved exactly[19], yielding

$$|\int 1|^2 = T(T+1) - T_{Z_1} T_{Z_2}. \qquad \text{III-5}$$

This evaluation depends in no way upon any nuclear model but only upon assumption of charge independence of nuclear forces.

The matrix elements for the Gamow-Teller interactions are not so easily evaluated. If a single nucleon is involved, transitions are allowed only between states of the same $\ell$, since the operator $\sigma$ can at most flip the spin. The matrix elements can then be calculated with the aid of any independent particule model of nuclear structure. Mayer and Jensen[18]

evaluate the matrix elements for such a case and the results are listed as follows:

$$\text{a)} \quad |\int\sigma|^2 = \frac{j+1}{j} \quad ; \quad j_i = j_f = \ell + 1/2$$

$$\text{b)} \quad |\int\sigma|^2 = \frac{j}{j+1} \quad ; \quad j_i = j_f = \ell - 1/2 \qquad \text{III-6}$$

$$\text{c)} \quad |\int\sigma|^2 = \frac{2j_f+1}{\ell+1/2} \quad ; \quad j_i = \ell + 1/2,\ j_f = \ell - 1/2$$
$$j_i = \ell - 1/2,\ j_f = \ell + 1/2 \ .$$

For the superallowed transitions in which ($|\Delta J| = |\Delta T| = 0$, $J = 0^+$), the Fermi interaction provided the only contribution to the total nuclear matrix element, since the Gamow-Teller selection rules distinctly forbid $J = 0^+ \rightarrow 0^+$ transitions. The states involved in these transitions are members of an isobaric triplet with ($T = 1$) and with one of the nuclei having ($T_Z = 0$), by equation III-5, $|\int 1|^2 = 2$ for these transitions.

Nuclear matrix elements may be calculated as well for the other class of superallowed transitions, the positron decay of mirror nuclei. In this case $T = 1/2$, and $T_Z = \pm 1/2$ for the parent and daughter nucleus respectively. The Fermi interaction matrix element does not vanish for the mirror transitions since the nuclear ground states of the two nuclei involved form an isobaric spin doublet. $|\int 1|^2$ assumes the value one for these transitions. Since these decays are not expressly classed as forbidden by the Gamow-Teller selection rules, the total nuclear matrix element also has a non-vanishing contribution from the Gamow-Teller matrix element $|\int\sigma|^2$.

In a typical mirror transition, $Ca^{39}(\beta^+)\ K^{39}$, the ground states of both $Ca^{39}$ and $K^{39}$ have ($J = 3/2^+$, $T = 1/2$). These values arise from a

single (1d 3/2) hole in the proton level in $K^{39}$. The Gamow-Teller nuclear matrix element may be calculated from equation III-6-b, the result being $|\int\sigma|^2 = 0.6$.

For positron transitions between nuclei of the isobaric triad for which ($|\Delta J| = |\Delta T| = 1$)(i.e. transitions from isobaric triplet levels to isobaric singlet levels, or conversely) the Gamow-Teller interaction nuclear matrix element is the only non-zero component of the total nuclear matrix elements. The states with ($T = 0$) in the ($A = 4n + 2$) nuclei arise from two-particle configurations, and the matrix elements may not be calculated from equations III-6. The matrix elements for some of these allowed transitions have been calculated assuming L-S coupling[20,21]. Mayer and Jensen[18] list the results for these calculations and also for their calculations which assume j-j coupling. The agreement between the calculations for the two coupling schemes is very poor, and both disagree with the experimental values.

Equation II-4 may be written in the form

$$C = ft\left((1-x)|\int 1|^2 + x|\int\sigma|^2\right) , \qquad \text{III-7}$$

where

$$x = \frac{G^2_{G.-T.}}{(G^2_{G.T.} + G_F^2)} \quad , \text{ and } C = \text{const.}$$

If the nuclear matrix elements can be calculated, and the ft value measured experimentally, each beta-decay should yield a plot of C vs. x which is a straight line. Since the matrix elements are easily evaluated for the beta decay of mirror nuclei, such a plot may be made for each mirror transition

for which the ft value has been measured. A common intersection for all such plots should yield the values of C and x, universal constants for all allowed and superallowed beta transitions. Winther[22] has made such an analysis and the results, determined by a least squares fit of the intersections of these plots, when inserted into equation III-7 yield the expression

$$\log_{10} ft = 3.7 - \log_{10}|M|^2 \quad ,$$

where

$$|M|^2 = |\int 1|^2 + |\int \sigma|^2 \quad ,$$

and is the total nuclear matrix element.

B. Energy Level Schemes for the (A = 4n + 2) Nuclei.

The (4n + 2), self-conjugate nuclei are the only nuclei with more than one value of isobaric-spin among their low-lying states. In many such nuclei, the lowest (T = 1) level is actually the ground state, which is contrary to the usual rule that the ground state has the minimum possible value of T(i.e. $T = |T_Z| = |\frac{Z-N}{2}|$). In particular, the ground state of $Cl^{34}$ has been identified as having (T = 1), and $(J = 0^+)$ [23]. The $(T = 0, J = 3^+)$ level in $Cl^{34}$ lies about 100 kev above the ground state. More recently, the ground state assignment in $Sc^{42}$ has been given to a $(T = 1, J = 0^+)$ level[24]. This was the only assignment which was consistent with the measured half-life of 0.62 seconds and with j-j coupling, which is the more probable coupling scheme in this heavy an element.

Moszkowski and Peaslee[25] point out that it is an interesting question to investigate the relation between the lowest lying (T = 1) and (T = 0) levels and to search for some systematic behavior. In the elements with low Z, the

(T = 0) state is certainly the ground state. As progression is made toward higher Z elements, the lowest (T = 0) state becomes energetically higher with respect to the lowest (T = 1) state. The lowest (T = 1) state in the self-conjugate nucleus should be energetically higher than its corresponding level in the (N = Z + 2) isobar, the ground state, by the Coulomb energy and the neutron-proton mass difference. If this separation in energy between the corresponding (T = 1) states is calculated, using the equation for neutral atoms,

$$E_{(T=1)} = 0.60(A-2)A^{-1/3} - 0.78 \quad , \qquad \text{III-9}$$

remarkable agreement is made with the experimentally measured energy differences. A comparison is made between the theoretical and the experimental energy separations in figure 2. The solid line represents the energies which were calculated from equation III-9. In making the calculations, the nucleus was assumed to be a uniformly charged sphere at radius $R = 1.4 \times 10^{-13} A^{1/3}$ cms. It is noticed from figure 1 that the experimental curve seems to increase with A faster than equation III-9 would indicate. This has been attributed to the neglect of the Coulomb exchange term[26,27,28] in the calculation. The exchange term is significant for small values of Z and has been used to resolve the discrepancy between nuclear radii computed from electron scattering measurements and from measurements of the energies involved in the decay of mirror nuclei. Also shown in figure 2 is the dashed line which shows the experimental values of the energy difference between the lowest (T = 0) state in the self-conjugate nuclei and the ground (T = 1) state of the N = Z + 2 isobar. It is noticed that the two experimental curves cross in the neighborhood of $Cl^{34}$ and $K^{38}$, indicating a shift

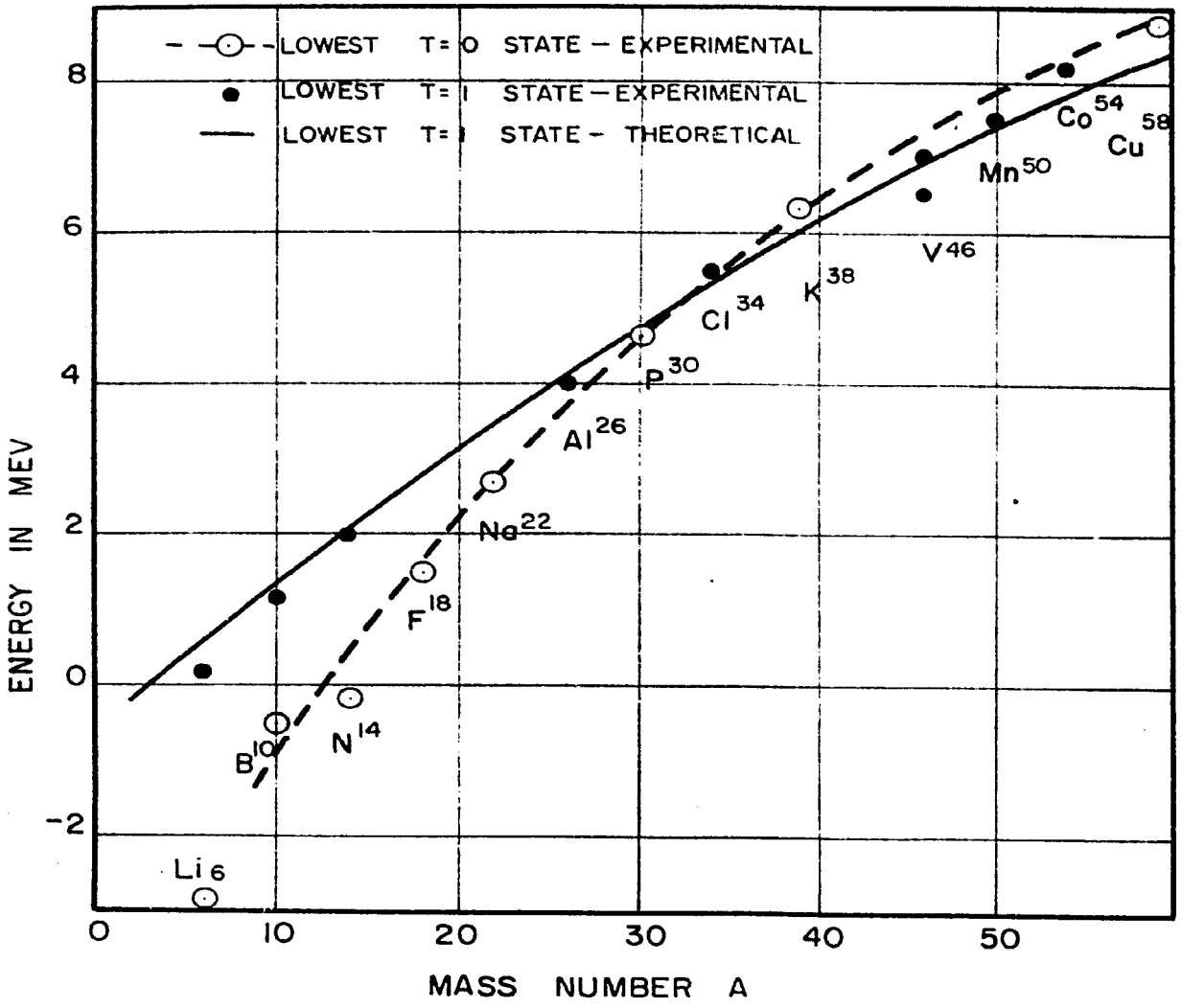


FIGURE 2. ENERGIES (neutral atom) OF LOWEST T=0 AND T=1 STATES IN ODD-ODD, N=Z NUCLEI, RELATIVE TO GROUND STATE OF NEIGHBORING EVEN-EVEN N=Z+2 ISOBAR

in the ground state of the (N = Z) nucleus from a (T = 0) state to a (T = 1) state.

The even-even nuclei of the isobaric triads necessarily have only (T = 1) levels as their low-lying states. These nuclei have an even number of nucleons of each type outside of the shell-model core of closed orbits. Since the outer nucleons are all in the same levels, the states arising from such a configuration must have even parity. The nuclear wave functions, being isobaric triplet functions, must be antisymmetric in their spin and space functions with respect to the interchange of any two nucleons. Thus, under rotations of 180°, the wave functions must be invariant, restricting the resulting J values to the even values. The low-lying states of the even-even nuclei, with (A = 4n + 2) have even parity, even values of J, and (T = 1). The ground state should be a ($T = 1, J = 0^+$) state.

To these (T = 1) states correspond states in the (N = Z) nuclei. However, in addition to the (T = 1) states, the odd-odd nuclei also have states which arise from nuclear eigenfunctions which are antisymmetric in the isobaric spin function. The lowest (T =0) states also have even parity since they are formed from a configuration of two nucleons, a proton and a neutron, in the same level. One of Nordeim's rules[17] states that for those nuclei in which the odd neutron and the odd proton have parallel intrinsic spins and orbital momenta, or have anti-parallel spins and angular momenta, the angular momenta tend to add, although not necessarily to the highest possible value. This rule may be used to predict the J values of the lowest (T = 0) states since all self-conjugate, odd-odd nuclei fall into this group. The low-lying levels arising from these configurations

must have wave functions which are symmetric in the spin and space functions. The nuclear wave functions satisfying such a symmetry property are those associated with odd values of J.

A rule may then be formulated concerning the assignment of unique T and J values to the low-lying states of the odd-odd nuclei[25]. This rule states that for odd-odd, N = Z nuclei with neutrons and protons in equivalent orbits the low-lying (T = 0) levels have odd J, while the low-lying (T = 1) levels have even values of J. As has been demonstrated, this rule strictly holds for states arising from j-j coupling. The rule has been found to hold quite well even for L - S coupling. If the states evolve from a mixture of configurations, this rule could, of course, be violated. An example of such a violation appears to occur in a low-lying excited state of $S^{30}$. This will be discussed in the section devoted to sulfur in chapter V.

A typical energy level diagram for the (A = 4n + 2) triads is shown in figure 3. The energy separation between the ($T = 1, 0^+$) state of the (Z = N + 2) nucleus and the corresponding state in the (N = Z) nucleus may be estimated by the use of equation III-9. The ground state of the (Z = N + 2) nucleus is connected through positron decay to the similar state in the self-conjugate nucleus. If ($T = 0, J = 1^+$) state also exists energetically lower than the ground state of the (Z = N + 2) nucleus, a branching in the positron decay will occur to this state. The nucleus will then decay by M1 radiation from the ($T = 0, 1^+$) level to the ($T = 1, 0^+$) level and/or by E2 radiation to the ($T = 0, 3^+$) state if this is the lowest (T = 0) level. The odd-odd, N = Z nuclei with A > 14 are also positron unstable. If the lowest isobaric-spin singlet state in the odd-odd nucleus has (J = 1), regardless of its position with respect to

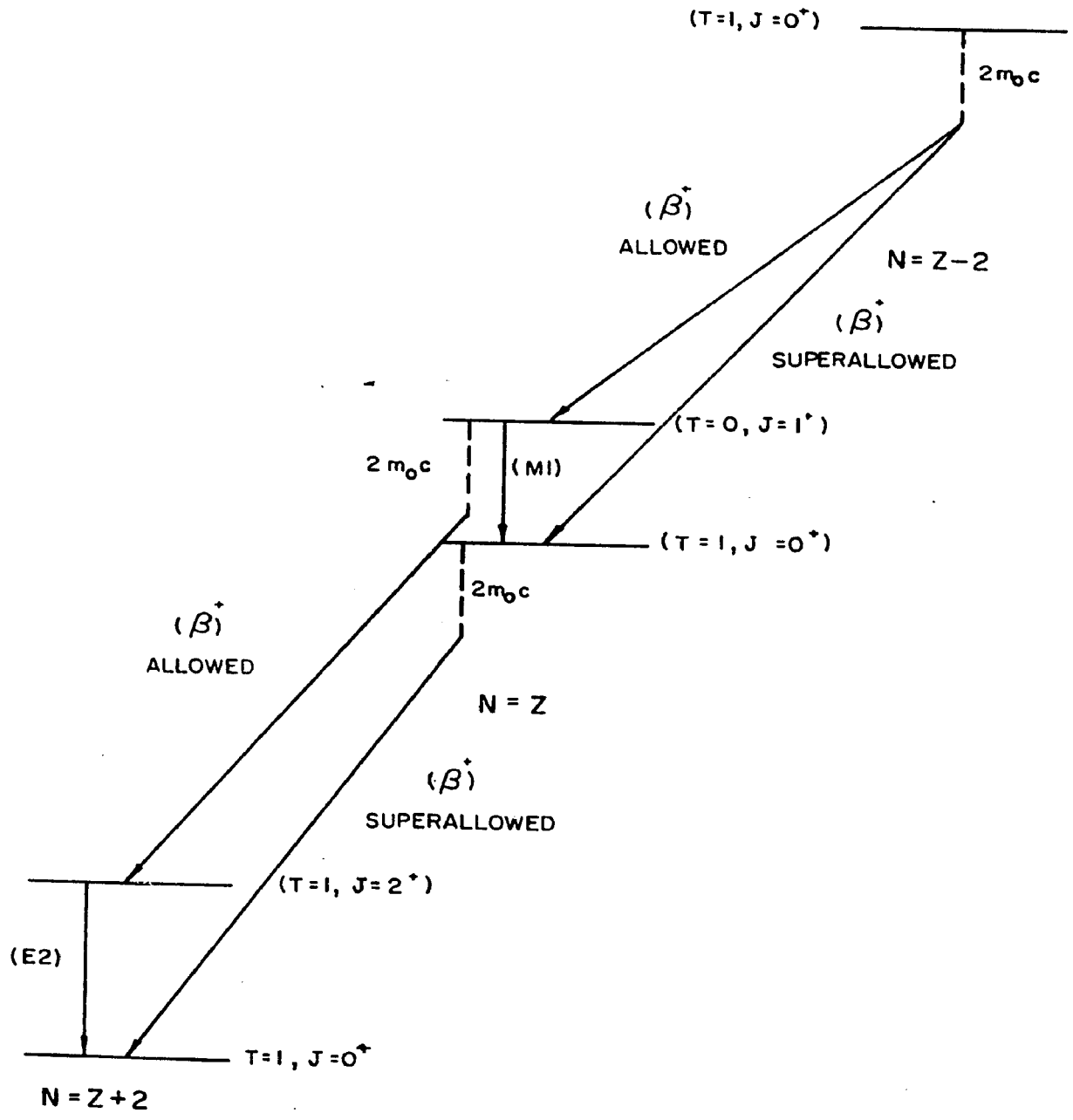


FIGURE 3. TYPICAL ENERGY LEVEL DIAGRAM FOR (A = 4N + 2) NUCLEAR CHAINS

the ($T = 1,0^+$) level, positron decay will occur from the state to the ($J = 2^+$) excited level in the stable ($N = Z + 2$) nucleus. The ($J = 2^+$) level is then connected by E2 radiation to the ($T = 1,0^+$) ground state. Independent positron decay will also occur in this case from the ($T = 1,0^+$) level in the ($N = Z$) nucleus to the ($T = 1,0^+$) ground state of the ($N = Z + 2$) isobars. If, however, the lowest ($T = 0$) level in the self-conjugate nucleus has ($J = 1^+$), then either this state or the ($T = 1,0^+$) state, depending upon which of the two is the ground state, will be connected by a single positron decay to the ground state of the ($N = Z + 2$) nucleus. The two states in the ($N = Z$) nucleus will be connected by M1 radiation with a half-life much shorter than the half-life of any positron decay from the energetically higher state, even though such positron decay might be superallowed. If the singlet level is the lower, then the decay will be an allowed decay; if the triplet level is the ground state, then the decay will be superallowed. The ft value for the transition would indicate which of the two levels is the lower.

C. Energy Level Schemes for the Mirror Nuclei.

The energy level picture for the mirror nuclei is much simpler than that for the ($4n + 2$) triads. The ground states of the two nuclei form the states of an isobaric doublet with ($T = 1/2$). For the nuclei studied in this research, $J = 1/2^+$, $3/2^+$, or $5/2^+$. The ground state of the nucleus with ($Z = N + 1$) decays to the ground state of the ($N = Z + 1$) nucleus by a superallowed positron transition. There should be no branching to an excited state in the daughter nucleus. Such a branching would involve a forbidden transition since the low-lying excited states in such

nuclei would either have $T = 1/2$ and presumably not $J = 1/2^+$, or would have $(T = 3/2, J = 1/2^+)$.

## CHAPTER IV

## EXPERIMENTAL EQUIPMENT AND TECHNIQUES

The experimental apparatus that is required to produce artificial isotopes by photonuclear processes, and to analyze the decay from these isotopes, consists of a source of high energy gamma-radiation, a target, and a detection system. The University of Michigan electron synchroton provides such a source of high energy photons if a target is put into the path of the electron beam.

The experimental measurements involved in this research were of three basic types. The first of these was that of accurately measuring half-lives which were of the order of seconds, and of extending the techniques to measure those longer half-lives which were also of interest in the experiment. This meant that the half-life measurements had to be carried out for several half-lives of the decays. The other two types were both energy measurements; that of measuring the energy end-points of the positron decay spectra from the activated target samples, and that of detecting and performing energy analysis of the gamma transitions following the positron decays.

The dominant experimental problems which were common to all three groups of measurements were those of high background flux and of low signal intensity. The solution of these problems involved the use of extensive shielding to reduce the background to tolerable limits. It was also deemed necessary to develop multichannel data recording equipment in order to obtain the number of counts necessary for reliable counting statistics in a period of time short enough that any systematic errors would not seriously

affect the data. These systematic errors could be caused by drifts in the electronic equipment and also in the synchrotron beam itself.

A. Synchrotron.

The electron orbit in the synchrotron consists of four quadrants of radius 40 inches and four straight sections of length 30 inches. A straight section lies between adjacent quadrant sections. The electrons are injected into one of the straight sections at an energy of about 500,000 electron volts and are accelerated during the initial portion of the 20 cycle per second magnetic cycle by a frequency modulated oscillator. When the electrons approach the velocity of light, the frequency modulated accelerator is turned off, and a constant frequency oscillator is turned on to accelerate the electrons for the remainder of the acceleration period. The maximum electron energy that can be obtained with the present magnet excitation system is 85 mev. To force the electron beam to hit a prescribed target, it is necessary to turn off the fixed frequency oscillator before the peak magnetic field is reached. As the magnetic field continues to increase, the orbit of the electron beam shrinks until the beam hits the the target which is located in the straight section diametrically opposite the injection straight section.

B. The X-Ray Beam.

When a relativistic electron passes through a target, most of the energy lost is radiated in the form of a continuous energy distribution of photons. Since the initial electrons are essentially uni-directional, the photons emitted are contained in a cone containing all energies less than or equal to the final energy of the electron beam. The solid angle of this cone may be approximately expressed by $\Omega = \frac{m_o c^2}{E_o}$, where $\Omega$ is the solid

angle subtended by the cone and $E_o$ is the energy of the incident electron.

The x-ray energy spectrum[29] created by an electron passing through an infinitely thin lead target is shown in figure 4 for several electron energies. Actually, the electron target was a sheet of tungsten 6 mils thick. The curves for a lead target may be used because the spectrum shape is insensitive to small changes in the atomic number of the target. The finite thickness of the target also has a negligible effect on the spectrum shape, but does affect the solid angle of the bremsstrahlung cone, since the electrons undergo multiple scattering as they pass through the target.

The x-ray beam comes off tangent to the electron orbit at the target position, and passes through an opening in the synchrotron guide magnet provided by the extended return legs of two magnet sections. Since the beam has passed out of the synchrotron race track, it is diffused slightly in passing through approximately 3/4 inch of porcelain in the "donut" section. This diffusion, in conjunction with the effect of the finite thickness of the electron target, necessitates further defining of the bremsstrahlung beam in order to have a "clean", well localized beam in which to place experimental targets.

For the purpose of defining the beam, two lead collimators were incorporated. That closest to the machine was a block of lead 5 inches by 5 inches in cross-section and 12 inches in length. Through this block there was a hole 1/2 inch in diameter on the side toward the machine, tapering out to 5/8 inch diameter at the opposite end. This collimator was located as close to the bremsstrahlung source as was physically possible, about 4 feet away. The second collimator was a block of lead 8 inches

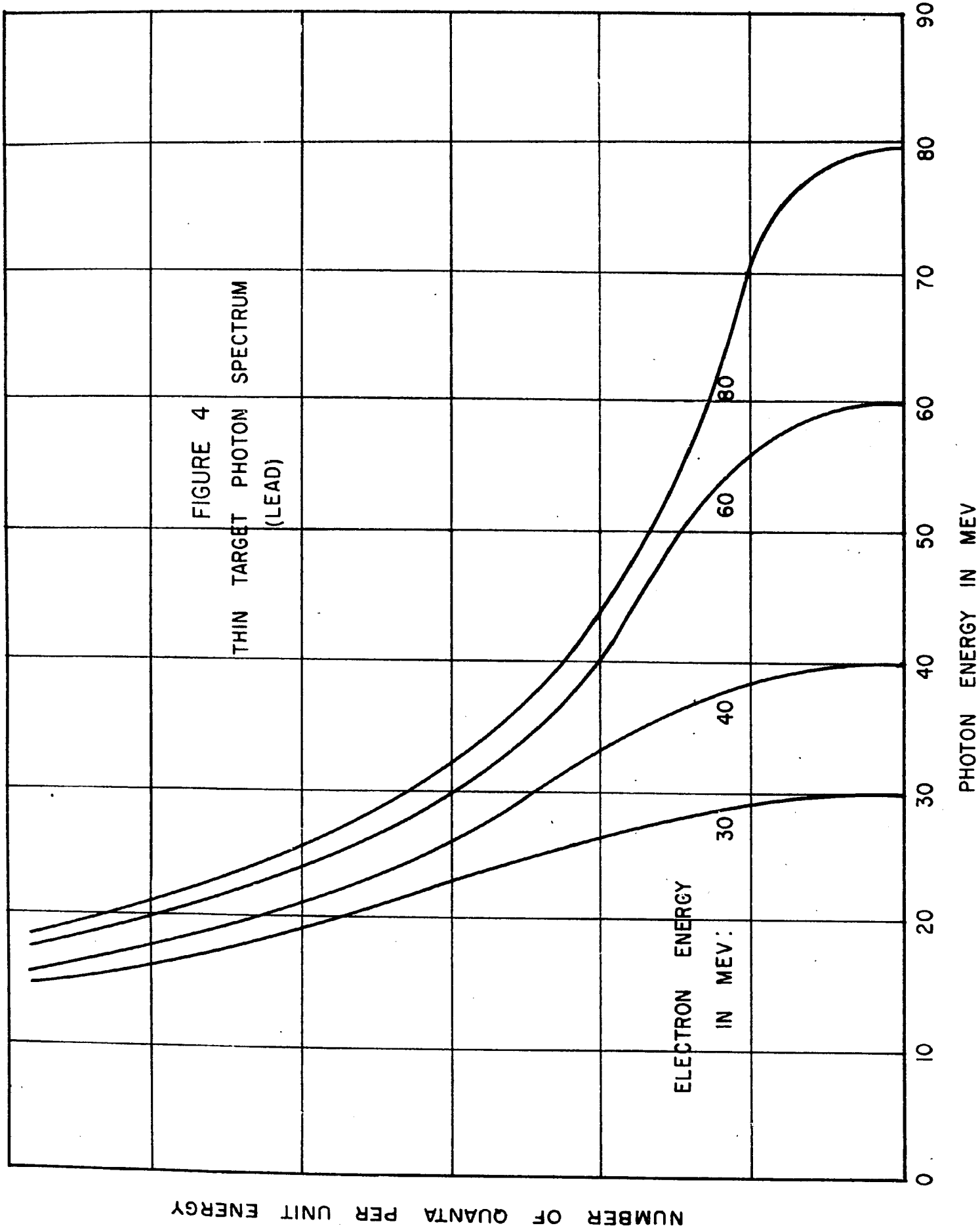
FIGURE 4
THIN TARGET PHOTON SPECTRUM
(LEAD)
ELECTRON ENERGY IN MEV:
80
60
40
30
NUMBER OF QUANTA PER UNIT ENERGY
PHOTON ENERGY IN MEV
0
10
20
30
40
50
60
70
80
90

thick through which there was a 1 inch hole. Between the two collimators was placed an ionization chamber which was used to monitor the beam and to normalize the experimental runs to one another. Three feet beyond the second collimator lay the experimental area, which was 11 feet in length. The alignment of these collimators was accomplished with photographic techniques, using a 5 inch by 7 inch film holder loaded with standard no-screen x-ray film behind a 1/8 inch lead sheet. In the lead sheet was cut a one inch hole; lead cross-hairs were placed intersecting at right angles in the center of the hole. In this manner, the beam could be located within 1/32 of an inch.

As a result of the alignment and collimation of the beam, there was a well defined bremsstrahlung beam. At the entrance to the experimental area the beam was 1 1/2 inches in diameter. This dimension had increased to 4 inches at the point where the beam left the experimental area. Figures 5 and 6 are photographs of the beam taken at the entrance and exit points of the experimental area.

C. Shielding.

When this experiment was first initiated, the photomultiplier and the crystal were located in the same room as the accelerator. The background was so intense as to overshadow completely decay radiation from any activated target. Various shielding techniques were employed, none of which proved successful in that even with large amounts of both neutron shielding (i.e. paraffin and borax) and lead, no distinction could be found between the data taken with a target in place, and that taken with no target.

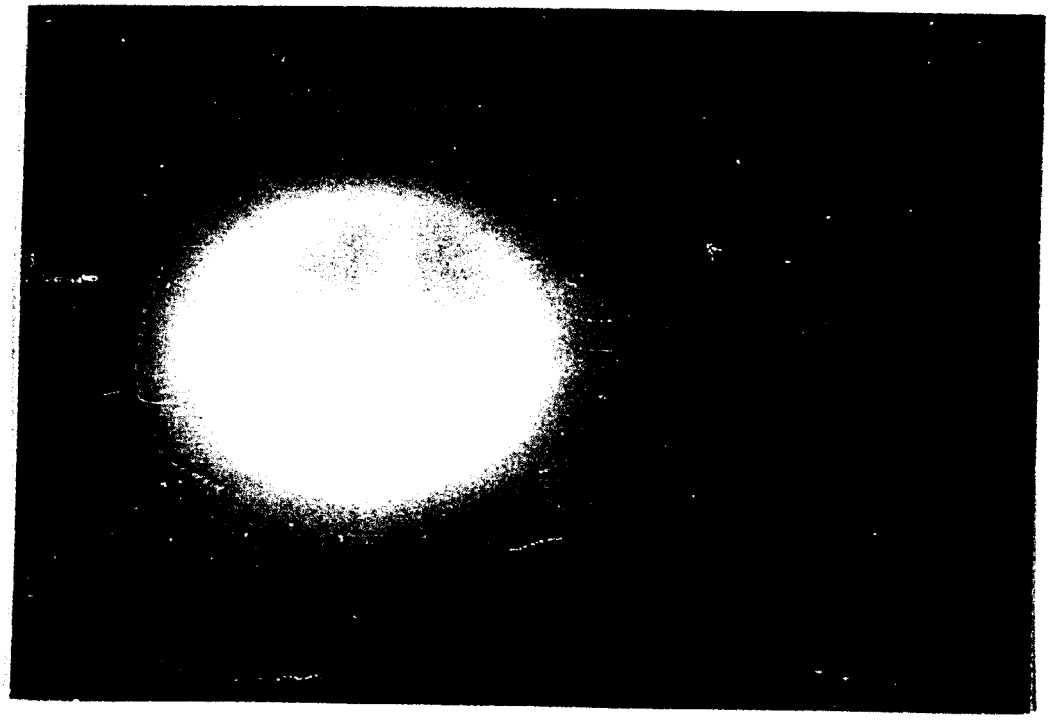

Figure 5. Photograph of X-Ray Beam Taken at Entrance Port to Experimental Area.

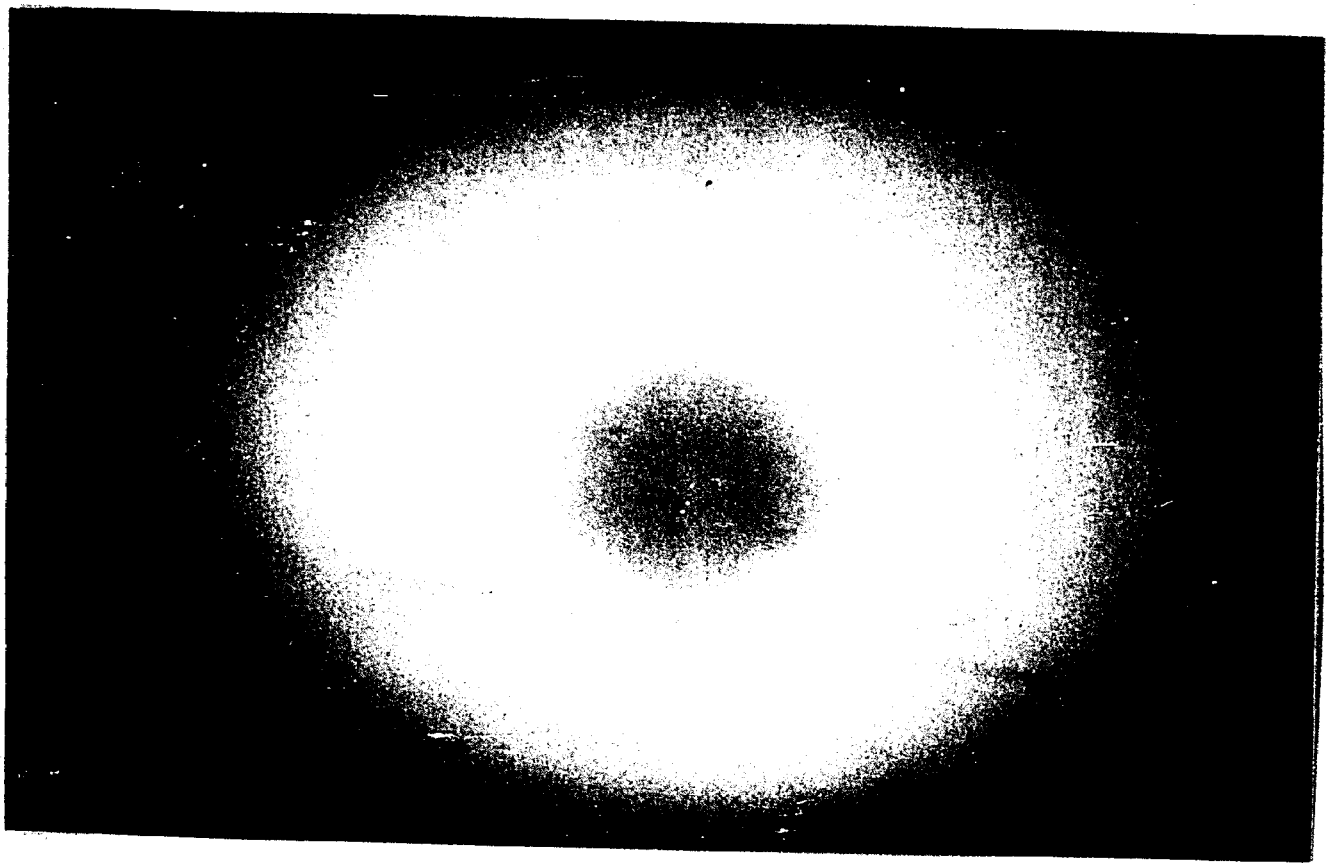

Figure 6. Photograph of X-Ray Beam Taken at Exit Port From Experimental Area.

The results of these attempts at shielding did indicate, however, the nature of the background radiation. Two equally annoying components were to be found in this background; scattered bremsstrahlung and neutrons electroproduced and photo-produced in the internal target, the walls of the vacuum chamber, and so on. Moreover, the background flux was determined to be nearly independent of the position of the scintillation detector in the synchrotron room itself, so long as the counter was in the plane of the electron orbit.

It was decided to construct an experimental room which would serve the dual purpose of reducing the background to a reasonable level, and of allowing personnel to enter the room without completely turning off the machine. The most efficient (i.e. cheap and effective) material from which to construct a wall for such a purpose is concrete. The mean free path of fast neutrons in most common materials is of the order of 25 cms. In addition, a flux of 85 mev gamma-rays is reduced to 1/e of its initial value in 18 cms of concrete. Taking both of these values into account, the walls were made of concrete one meter thick.

The room was constructed of concrete blocks, each block weighing about 3,000 lbs. Each wall consists of two rows of these blocks, staggered so as to allow no straight path into the room. The ceiling, also one meter thick, was constructed of two overlapping layers of blocks. The room's internal dimensions are 11 ft. long by 8 ft. wide by 7 ft. tall. The portion of the wall immediately adjacent to the synchrotron was made of a heavy concrete. This concrete has a density of 250 lbs./ft.$^3$ instead of the normal 130 lbs./ft.$^3$, the increase in density being obtained by the use of barium sulfate as an aggregate. This type of concrete was

used in the construction of the Ford nuclear reactor located on the north campus of the University of Michigan.

After passing through the second collimator, the bremsstrahlung beam enters the experimental room through a 7 inch diamter hole in the concrete wall. The beam, after passing through the experimental area, is stopped in a concrete cave before it should pass into the synchrotron control room. To attenuate any back scattering of radiation into the experimental room, the beam stopping wall of this cave was constructed of a water tank 28 inches thick backed by one foot of lead and one foot of concrete located in the control room. In front of this water tank was placed an ionization chamber which was used as a monitor by the synchrotron operator. The effectiveness of such an arrangement is shown in the fact that the countable background in the experimental room between beam pulses has been reduced to the order of the expected cosmic ray intensity. In addition, there is no health problem due to excessive radiation from the bremsstrahlung beam in the synchrotron control room. A diagram showing the synchrotron, collimators, and shielding is given in figure 7.

D. Apparatus and Techniques for Measuring Half-Lives.

1. Coincidence Technique

In making the measurements of the half-lives of the beta decays from ($A = 4n + 2$) and mirror nuclei, advantage was taken of the fact that the emitted particles were positrons. If the positrons were stopped in the target material, annihilation of the positrons occurred with the subsequent release, in the main, of two quanta with energy $m_o c^2$. These quanta were emitted 180° apart and it was possible to

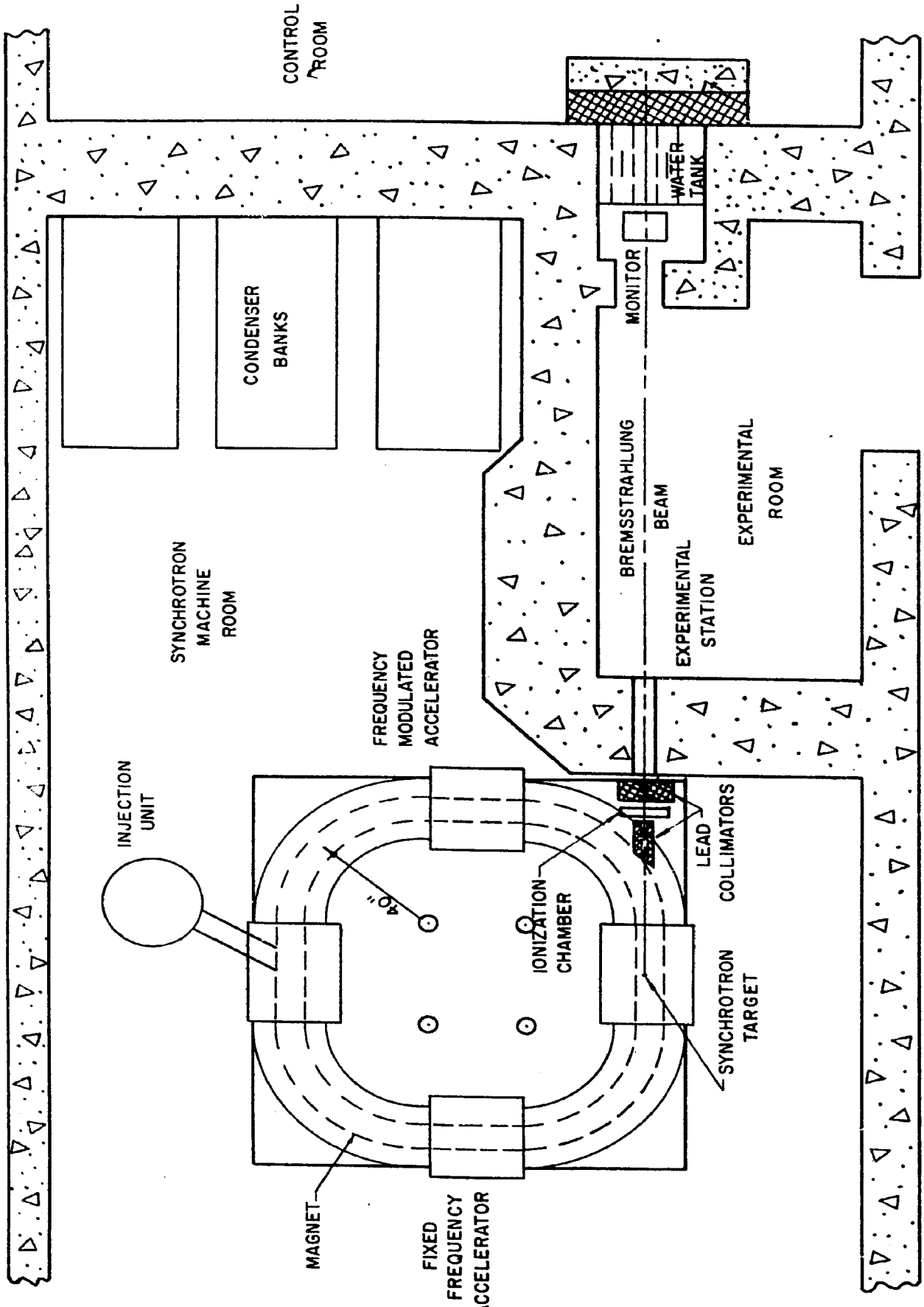


FIGURE 7. CROSS-SECTION OF SYNCHROTRON AREA, SHOWING SYNCHROTRON, CONCRETE SHIELDING AND BEAM-TRAPPING ARRANGEMENT

operate two scintillation counters, placed on opposite sides of the target, in coincidence to detect these photons. Only pulses in the 511 kev annihilation peak were accepted from either counter. The counting of the annihilation radiation permitted the use of much thicker targets than are normally used in beta spectroscopy. The use of both energy discrimination and coincidence analysis reduced the background to the order of cosmic ray intensity.

The observed counting rate was corrected for the accidental coincidences by the equation

$$N_{acc} = 2N_1N_2\tau \quad , \qquad \text{IV-1}$$

where $N_{acc}$ is the accidental counting rate, $N_1$ and $N_2$ are the counting rates in each counter respectively, and $\tau$ is the resolving time of the coincidence circuit. $\tau$ was experimentally determined by placing a source of $Cs^{137}$, of a strength comparable to the strengths of the radiation from the targets bombarded by the bremsstrahlung beam, in the target position between the two counters and observing the coincidence counting rate. $Cs^{137}$ should be expected to give rise to no coincidences in counters placed 180° apart and any observed coincidences could be attributed to accidental coincidences. The value of $\tau$ obtained from such measurements was 6 microseconds. This value was corroborated by similar measurements using source of $Zn^{65}$.

Using a relation for the range of positrons in materials given by [30]

$$R_p = 0.526 \frac{E}{MEV} - 0.094 \quad 5ms/cm^2 \quad , \qquad \text{IV-2}$$

a calculation may be performed which maximizes the observed counting rate (a function of target thickness, positron energy, and gamma-ray absorption coefficient of the target material) with respect to target thickness. In the calculation, only those positrons which annihilate in the target are treated as being available to produce coincidences. Furthermore, the target is assumed to be placed in an x-ray beam of constant intensity over the entirety of the target.

Consider a target of thickness t and an element of this target dx, at a distance x from the left.

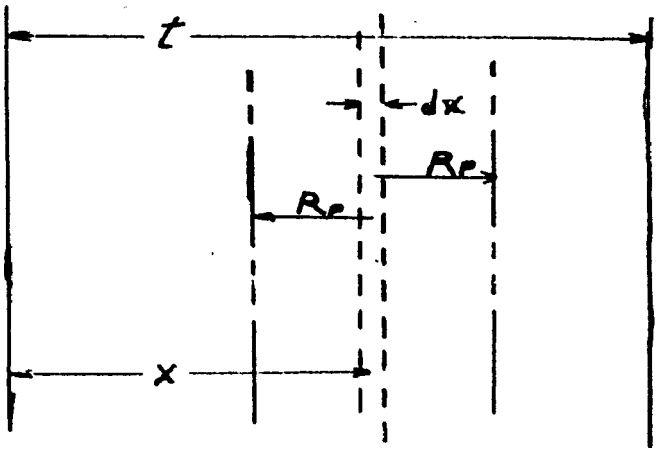


The positrons emitted in this region travel a distance $R_p$, given by equation IV-2, before annihilating. The total number of positrons emitted to the left with an energy E, which annihilate in the target, is given by

$$N^1(E) = \int_{R_p}^{t} n(E)dx = n(E)(t-R_p) \qquad \text{IV-3}$$

where n(E) is the energy distribution of the emitted particles. Clearly, this situation is symmetric with respect to particles

emitted to the right and left, so the total number of positrons which annihilate in the target is $2N'(E)$. In order to obtain the number of annihilations from positrons of all energies, equation IV-3 must be integrated over all energies. Approximating $n(E)$ by $CE^2(E_o-E)^2$, where C contains all factors which do not contain the energy, such an integration yields as the total number of annihilations in the target,

$$N = 2C \int_o^{E_o} E^2(E_o-E)^2 \,(t-aE+b)dE$$
$$= 2C\left[(t+0.094)\left(\frac{E_o^5}{30}\right) - 0.526\left(\frac{E_o^6}{60}\right)\right]. \qquad \text{IV-4}$$

Some of the annihilation radiation is absorbed in traversing the target. The sum of the paths that the two quanta must follow in leaving the target is equal to the thickness of the target itself. Hence the final expression for the number of pairs of quanta emitted from the target may be written as

$$N = 2C\left[(t + 0.094)\left(\frac{E_o^5}{30}\right) - 0.526\left(\frac{E_o^6}{60}\right)\right] e^{-\mu t}, \qquad \text{IV-5}$$

where $\mu$ is the absorption coefficient for 0.511 mev gamma-radiation in the target material. Maximizing this expression with respect to t, the target thickness, yields the final equation which expresses the optimum target thickness as a function of the gamma-ray absorption coefficient and the positron endpoint energy,

$$t = \frac{1}{\mu} - 0.094 + 0.263\, E_o \quad . \qquad \text{IV-6}$$

$E_o$ is the positron endpoint in mev. $\mu$ is the absorption coefficient

in $cm^2/gm$ for 0.511 mev gamma-rays for the material of which the target is composed, and t is the target thickness in $gm/cm^2$. A graph of this function is shown in figure 8.

The results of such a calculation indicate that the maximum counting rate, for the target materials of interest in this experiment, (i.e. calcium, potassium, sulfur, phosphorus, and silicon), occurs for targets nearly two inches thick. Since the bremsstrahlung beam at the experimental station was essentially a cylinder 1 1/2 inches in diameter, targets could be used which filled up the entire cross-section of the beam cylinder. The targets themselves were composed of the powdered sample of the element, with the exceptions of calcium, where $CaH_2$ was used, and potassium, where a solid piece of potassium was used.

The target holder consisted of a cylindrical iron can 1 1/2 inches in diameter, supported by an aluminum rod screwed into a fitting soldered to one side of the can. The arrangement was such that no part of the aluminum supporting rod was exposed to the photon beam. The target cans were made air tight so that they could be used to contain such reactive substances as $CaH_2$ and K metal. Iron was chosen as the material of the target chambers due to its structural strength, and also due to the fact that natural iron is composed primarily of $Fe^{56}$ (91.6%) which should contribute little or no background radiation when bombarded by the x-ray beam. This was confirmed by bombarding a target of iron filings and observing the activity produced in such a target by photonuclear reactions. A drawing showing the target and detectors in relation to the

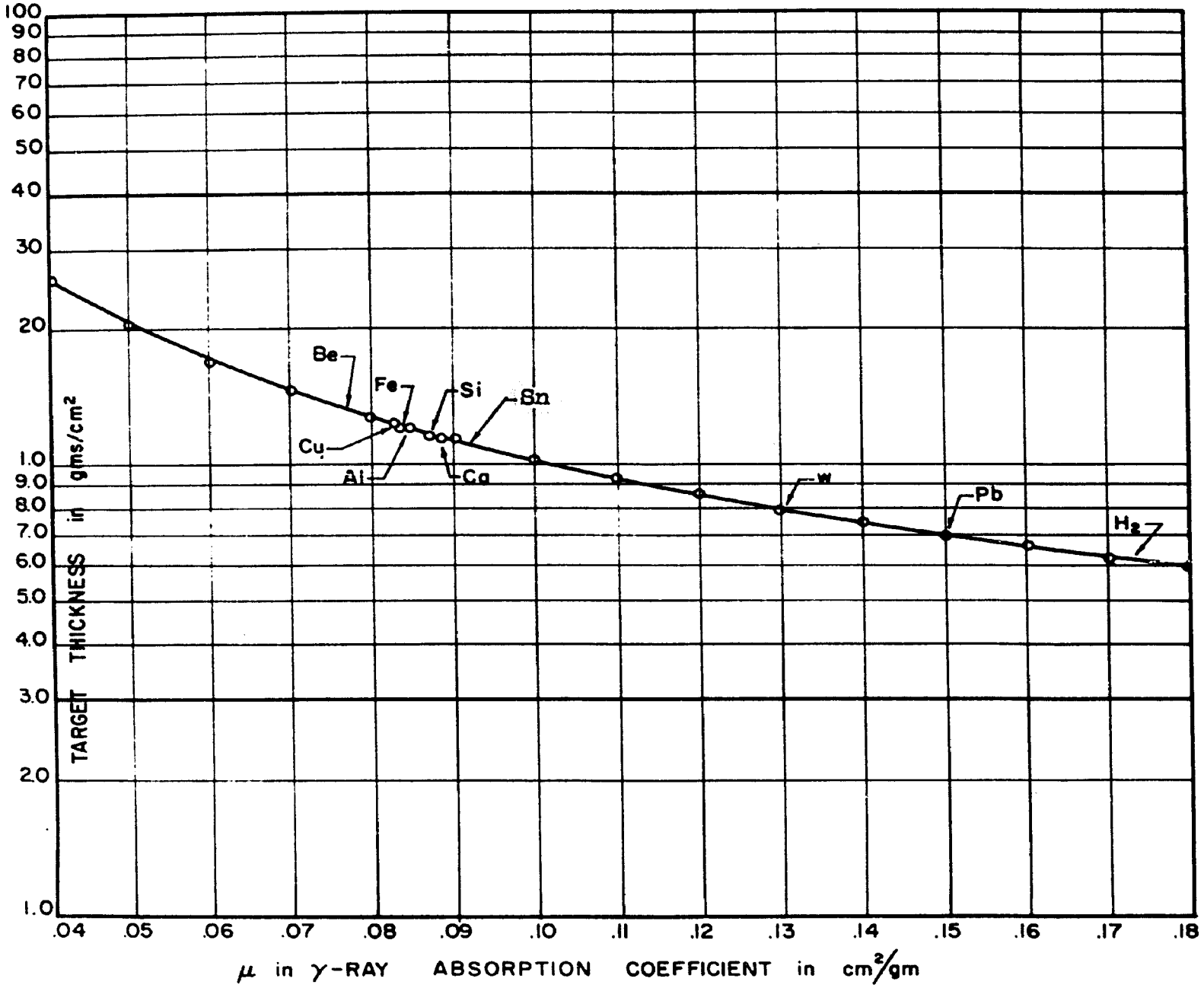


FIGURE 8. PLOT OF $\gamma$ ABSORPTION COEFFICIENTS
vs.
TARGET THICKNESS FOR MAX. 180 COINCIDENCE
COUNTING

bremsstrahlung beam is shown in figure 9.

2. Beam "Knock-Out" System

The values of the half-lives measured in this experiment fell into two distinct groups. those that were between 0.5 seconds and 7 seconds fell into the first group, and those longer than 1 minute fell into the second group. Measurements of half-lives longer than 1 minute involved, for the most part, simply turning the synchrotron off after a suitable bombardment time, and measuring the amount of decay radiation, as a function of time, in 50 second intervals. To measure shorter half-lives, however, required much different techniques.

Since the background in the room had been so effectively reduced, it was possible to scan the targets in the position in which they had been bombarded by the bremsstrahlung beam. Under normal synchrotron operation (i.e. 20 beam pulses/sec), the x-ray beam pulse is 30 microseconds in length, and there is a dead time between the pulses of nearly 50 milliseconds. This dead time was not of sufficient duration to permit accurate measurements of decay half-lives which were the order of seconds in length.

A system was therefore developed which allowed blocking out of the synchrotron beam for longer periods of time. The system consisted mainly of one control circuit which was named the master timer control. The master timer cyclically performed three functions: "knocking out" beam, providing a gating signal for the counting portion of the operation cycle, and reseting itself to start the cycle over again.

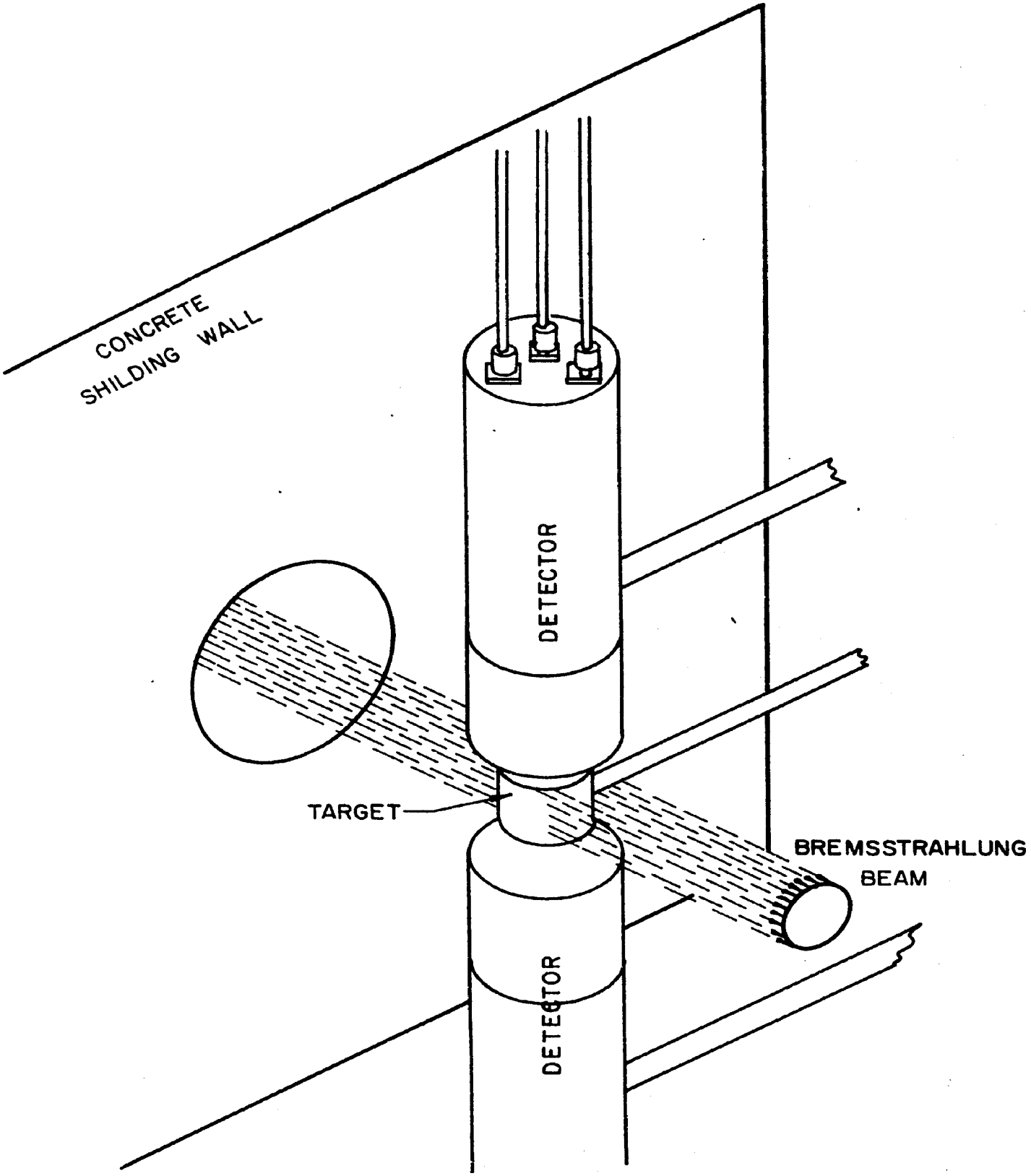


FIGURE 9. DIAGRAM OF TARGET – COUNTER ARRANGEMENT USED IN COINCIDENCE DETECTION OF THE ANNIHILATION RADIATION.

Injection of the electrons into the synchrotron is timed by the use of a peaking strip which is attached across one leg of the synchrotron guide field magnet. This peaking strip is a strip of high mu material (e.g. mu metal) which is placed shunting one of the magnet legs and has two coils of wire wrapped around it. One of the coils carries a biasing current which magnetically saturates the mu metal strip in a direction opposing the usable portion of the sinusoidal magnetic guide field. When the magnetic guide field reaches a value such as to unsaturate the strip, a change of flux through the mu metal occurs which produces an emf pulse in the second coil. This pulse is shaped and used to trigger electron injection into the synchrotron. If the biasing current were sharply reduced, the electrons would be injected into the synchrotron before the magnetic guide field was of sufficient value to guide them in the donut orbit of one meter radius. Consequently, the injected electrons would not be accelerated.

This is the method which was used to "knock out" the beam. A vacuum tube was installed in parallel with the output of the regulated power supply which supplies the biasing current to the peaking strip. Normally this tube was biased off so that it provided an infinite resistance shunt across the output. When the beam was to be "knocked out", the master timer put out a signal which was used to bias this shunting tube on. This, in turn, shunted some of the output current through the vacuum tube, reducing the current through the peaking strip winding. In this manner injection occurred 10 to 20 microseconds early, and the beam was so effectively "knocked out" that there was no measurable background from the synchrotron at

any time during the "knock out" period.

The master timer control was able to perform the two functions of "knocking out" the beam and of providing a variable length gate signal for the counting period, at any time, in 50 millisecond steps, up to the time of reset. The reset time could be set to any time, also in 50 millisecond steps, up to a maximum of 50 seconds. An auxiliary circuit which consisted of a scale of 1,000 could be used to extend this time up to nearly 14 hours, but would, of course, proportionally increase the duration of the controlling steps. The reset pulse was used to reset the timing system and to bias off the shunting tube, allowing electron injection to occur again at the proper time. The master timer consisted of a scale of 1,000, using three GS10C dekatron tubes in a decade arrangement. The cathodes of each tube were connected to the terminals of four ten-position rotary switches connected in parallel. Twelve rotary switches were arranged in four parallel groups of three switches. The three output terminals of each group were connected through a coincidence circuit to the triggering grid of a 2021 thyratron tube, each of the four groups having its separate coincidence and thyratron circuit. One of the thyratrons was connected so as to remain fired when triggered. The plate signal on this tube, after undergoing phase inversion, was used to provide the bias for the tube shunting the peaking strip current supply. All remaining thyratrons were connected so as to self-extinguishing. Two of them were used to provide the "on" and "off" triggers for the flip-flop circuit, used to generate the counting period gate. The third was used to provide a trigger for the reset

system which would extinguish the first thyratron and reset the dekatron tubes to the zero cathodes. Those pulses scaled off by this timer control circuit were the same peaking strip pulses used to trigger electron injection into the synchrotron. A circuit diagram for the master timer control is shown in figure 10.

The use of this control system permitted an accurate time analysis of nuclear decays. The operation cycle consisted of bombarding the target material with the bremsstrahlung beam for a given number of peaking strip pulses, and "knocking out" the beam for a number of pulses, during which time a time analysis of the decay radiation was made. At the end of this counting period, the timer was reset and the cycle was started over. This operation cycle was repeated many times in order to obtain good statistics in the number of counts observed in the time channels.

To make these runs in a minimum length of time, the problem arose as to what to make the value of k (the length of the bombardment time) for a given length of observation time, p. After one burst of beam there are n' active nuclei in the target. There is then a dead time of $t_o$ seconds before the next pulse of beam. During this time, some of the n' nuclei have decayed so that there are only

$$n_1 = n^1 e^{-\lambda t_o} \qquad \text{IV-7}$$

active nuclei in the target. $\lambda$ is the decay constant for the radioactive nuclei of interest. If this process is repeated k times, the number of artificially created nuclei in the target before the $(k + 1)^{st}$

# MASTER TIMER CONTROL CIRCUIT

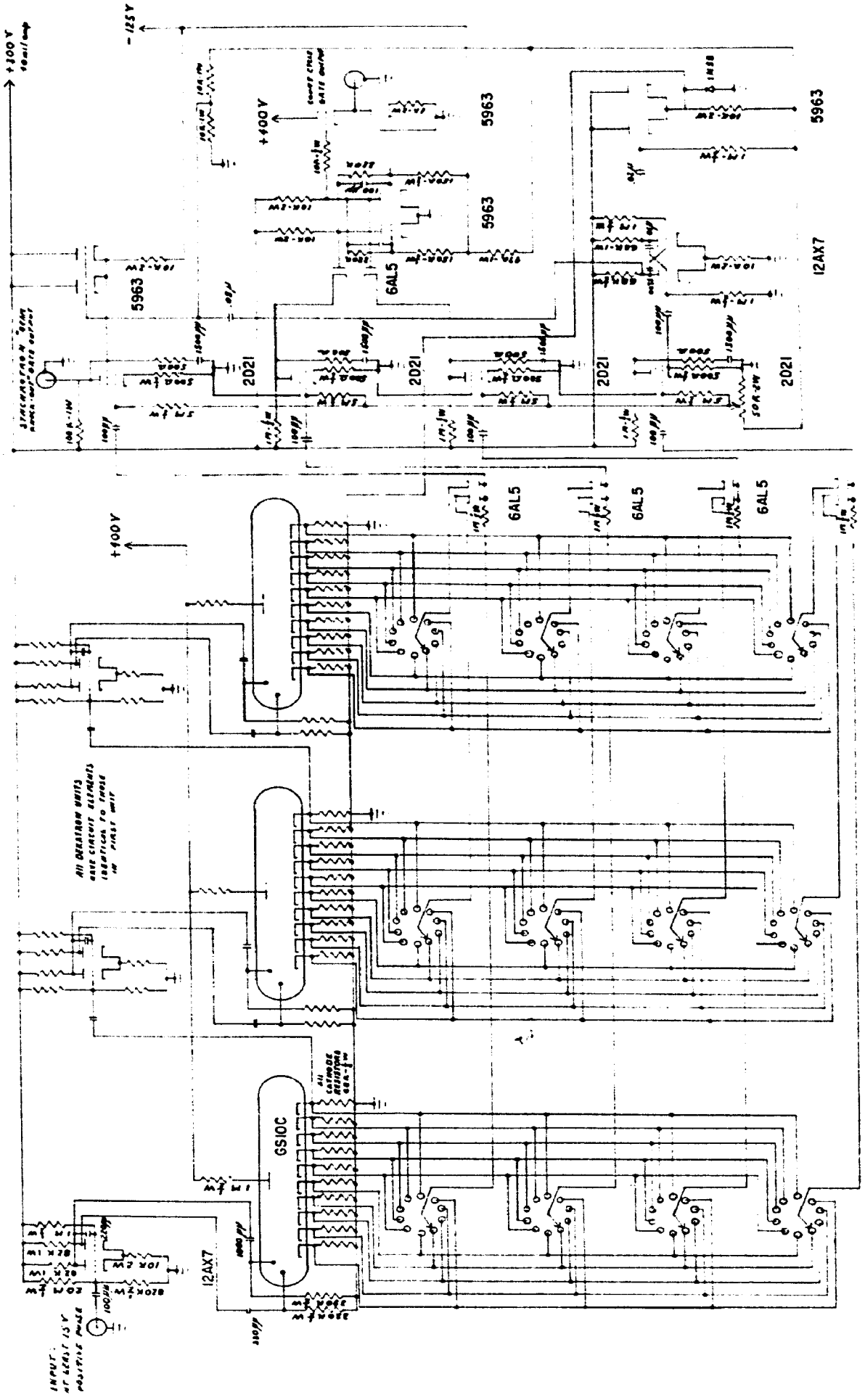


FIGURE 10

pulse is

$$n_k = n^1 \sum_{n=1}^{k} e^{-n\lambda t_o} = n^1 \left( \frac{e^{-\lambda t_o} - e^{-k\lambda t_o}}{1 - e^{-\lambda t_o}} \right) . \qquad \text{IV-8}$$

There are then p pulses of "silence" during which the target nuclei decay and the target is scanned by the counters. After this time there are

$$n_{k_p} = n_k e^{-p\lambda t_o} \qquad \text{IV-9}$$

radioactive nuclei remaining in the target. This process builds up as the synchrotron goes through more cycles of operation. After m cycles of such operation, there are left in the target

$$n_{kpm} = n_{kp} \left( \sum_{\alpha=0}^{m-1} e^{-\alpha\lambda(p+k)t_o} \right) \qquad \text{IV-10}$$

active nuclei. This process rapidly reaches an equilibrium for short-lived decays. Assuming such an equilibrium state, there are, in the target sample,

$$n_{kp\infty} = n_{kp} \left( \frac{1}{1-e^{-\lambda(k+p)t_o}} \right) \qquad \text{IV-11}$$

nuclei of interest.

Before an observation of the decay radiation from the target is made, there is a bombardment period of k pulses duration. There are finally

$$N = n_{kp\infty} e^{-k\lambda t_o} + nk \qquad \text{IV-12}$$

radioactive nuclei in the target at the beginning of an observation period. The total number of decays during this period is then expressed by

$$N = \int_{o}^{pt_o} \lambda N e^{-\lambda t} dt = N\left(1 - e^{-p\lambda t_o}\right) \quad . \qquad \text{IV-13}$$

The average number of counts per second is expressed by

$$N/sec = \frac{\epsilon N}{(k+p)t_o} \quad , \qquad \text{IV-14}$$

where $\epsilon$ converts total number of decays into the number of counts seen by a counter of finite size. If an experimental run is characterized by a total number of counts $N_t$, the time to complete such run is given by

$$T = \frac{N_t}{N/sec}$$

$$= \frac{N_t t_o(1-e^{-\lambda t_o})}{n^1\epsilon(1-e^{-p\lambda t_o})} \left[ \frac{(k+p)(1-e^{-(k+p)\lambda t_o})}{e^{-\lambda t_o} - e^{-k\lambda t_o}} \right] \qquad \text{IV-15}$$

This function is then minimized with respect to k .

$$\frac{dT}{dk} = 0 = \left( \frac{N_t t_o(1-e^{-\lambda t_o})}{n^1\epsilon(1-e^{-p\lambda t_o})} \right) \left[ \frac{(1-e^{-(k+p)\lambda t_o}) + (k+p)(\lambda t_o e^{-(k+p)\lambda t_o})}{(e^{-\lambda t_o} - e^{-k\lambda t_o})} \right.$$

$$\left. - \frac{(k+p)(1-e^{-(k+p)\lambda t_o})(\lambda t_o e^{-k\lambda t_o})}{(e^{-\lambda t_o} - e^{-k\lambda t_o})^2} \right] \quad , \qquad \text{IV-16}$$

or

$$\lambda t_o(k+p) = \frac{(1-e^{-(k+p)\lambda t_o})(e^{-\lambda t_o} - e^{-k\lambda t_o})}{e^{-k\lambda t_o}(1-e^{-(p+1)\lambda t_o})} \qquad \text{IV-17}$$

By assuming a value of $\lambda t_o$ consistent with the half-lives studied, a graphical solution of equation IV-17 may be made. The optimum values of $\lambda k t_o$ for given values of $\lambda p t_o$ are shown in figure 11 in units of the

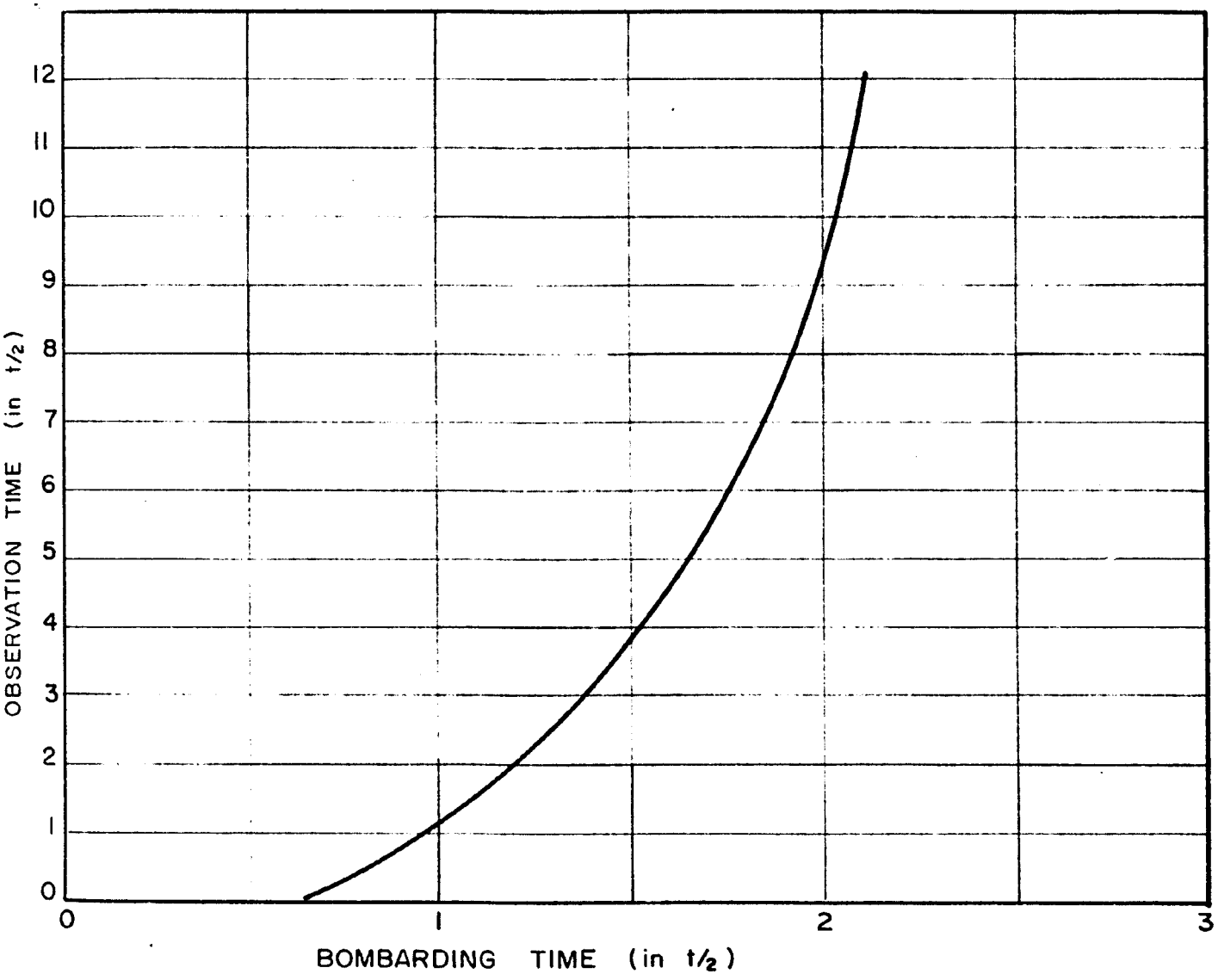


FIGURE II. PLOT OF OPTIMAL BOMBARDING TIMES FOR GIVEN OBSERVATION TIMES IN UNITS OF HALF-LIVES OF THE NUCLEAR DECAY BEING OBSERVED

half-life of the decay studied.

3. Detection Equipment.

The basic unit of the detection system used in this portion of the experiment consisted of two scintillation counters. Each counter was composed of a 1 1/2 inch by 1 1/2 inch NaI(Tl) scintillation crystal mounted, in one counter, on a Dumont 6292 photomultiplier tube, and in the other counter, on an R.C.A. 6342 photomultiplier tube. A magnetic shield, consisting of alternate cylindrical layers of 10 mil hypersil foil and 5 mil aluminum foil, 9 layers in all, was placed around the photomultiplier tube, separated from the glass envelope by 1/4 inch.

The crystal, photomultiplier, magnetic shielding, socket, and internal wiring were then enclosed in a three inch diameter light - tight brass pipe. The crystal end of each counter was covered with a piece of 20 mil copper foil, soldered to the brass casing. The photomultipliers were operated with a positive high voltage so that, in operation, the photocathodes were at ground potential.

Although the scintillation crystals were not placed in the actual beam, the large burst of radiation which scattered from the beam into the counter occurred over such a short period of time that the NaI crystal was unable to resolve the individual events. These combined to form a very large light scintillation. Since this large light output would cause a huge pulse to pass through the phototube, the phototube was switched off during the yield pulse in order to prevent overloading of the electronic equipment. This switching was accomplished by pulsing the photocathode up to or above the potential of the first

dynode during the time that the counter was to be off. The height of the pulse used was 200 volts. When the photomultiplier was turned off there were absolutely no counts observed from the photomultiplier even though the counters might be placed in the beam. A circuit diagram for the photocathode pulser is shown in figure 12.

This circuit would take the counting cycle gate pulse from the master timing circuit, amplify it, and drive the photocathodes of both detectors through a cathode follower output. An additional feature of the circuit was that it contained a univibrator circuit which could be used to generate a shorter "on-pulse" than could be generated by the master timer. This section of the pulser was used in the experimental measurements which utilized merely the dead time between successive beam pulses for the observation time, and will be discussed in the section on gamma-ray and positron energy measurements.

A difficulty which arose in the use of the phototube gating was that of capacitive feed-through between the photocathode and the anode of the photomultiplier. If the gating pulse had a fast rise time and/or a fast decay time, a large pulse would occur at the anode of the photomultiplier. The use of coaxial cable for the cathode and anode lead-in wires inside the counter itself reduced the size of this output pulse, but the ultimate limit was determined by the interelectrode capacitance between the cathode and the anode of the photomultiplier. If the rise time of the photocathode pulse were less than 10 microseconds, the size of this differentiated pulse output on the anode was such as to introduce pulses which were comparable in height to the "real" output pulses of the scintillation detector. Whenever

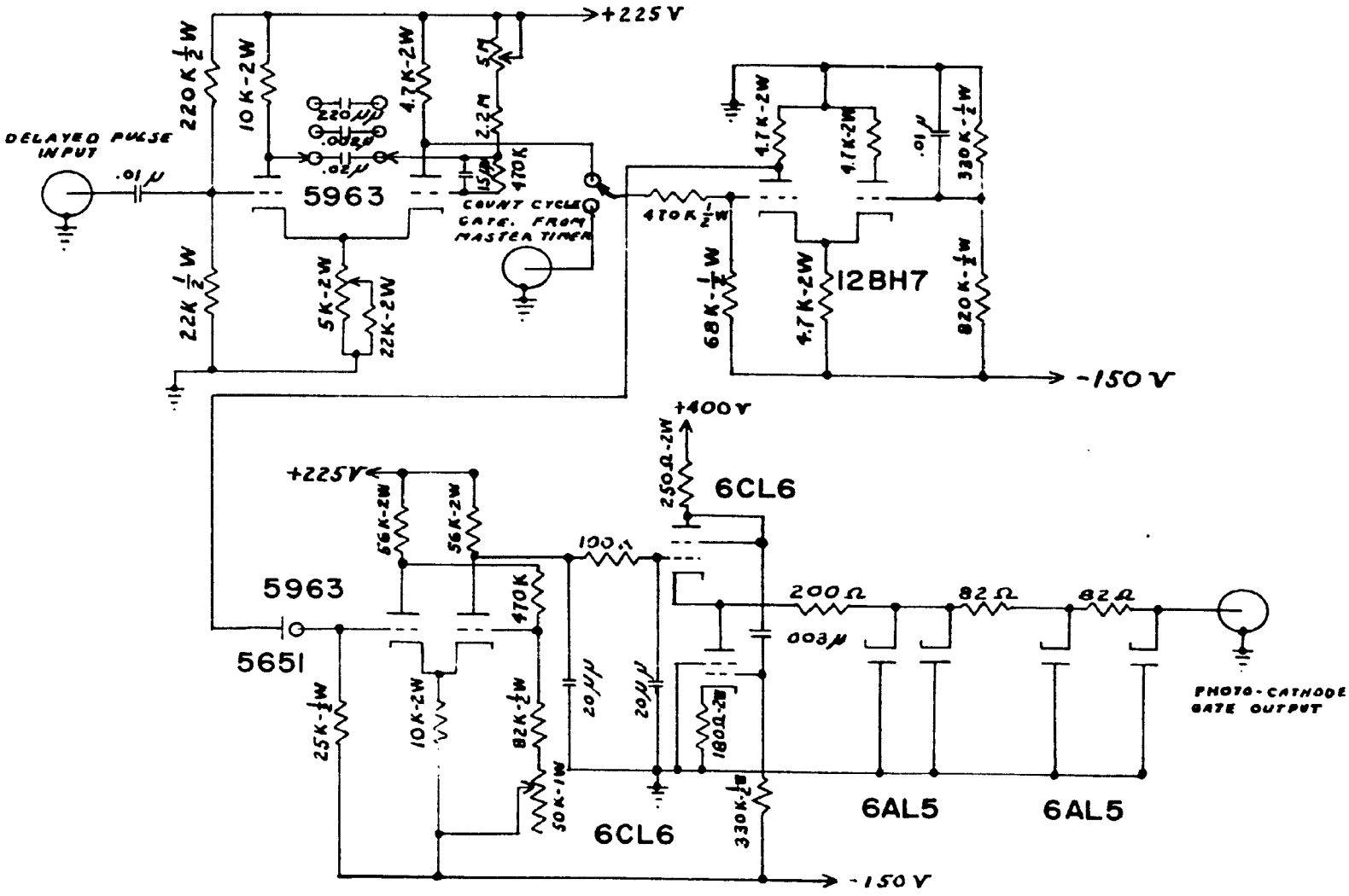


FIGURE 12

PHOTOCATHODE PULSER

possible, therefore, the rise time of this pulse was made longer than the 10 microsecond limit. If the photomultiplier were to be gated on for periods of longer than two seconds, the rise time of the photocathode pulse was set at 100 μ sec. This would introduce an error in the effective length of the first time channel of less than 0.1%, well below statistical counting errors. The rise time was controlled by placing resistances in series with the output, which, in conjunction with the 100 feet of RG/62/U coaxial cable which carried the pulse to the counter, served to integrate the pulse shape slightly.

The remainder of the detection system consisted of parallel systems which contained Atomic Instrument Company model 205b linear preamplifiers, an Atomic Instrument Company model 218 linear amplifier in one system, and a model 204b linear amplifier in the other, Atomic Instrument Company model 510 single channel pulse height analyzers, and Atomic Instrument Company scalers. The high voltage supply for the photomultipliers was an Atomic Instrument Company model 312 supply.

The outputs of the single channel analyzers were fed into a coincidence circuit constructed to operate with the model 510 analyzers. The model 205b preamplifiers were modified slightly to add a pulse shaping network consisting of a delay line. The amplifying systems produced pulses which rose in 0.25 μ sec, were essentially flat for 1 μ sec, and decayed slowly, reaching 1/e of their peak value in about 2 μ sec from the beginning of the pulse.

A block diagram of the electronics is shown in figure 13, indicating that part of the equipment which was in the experimental room,

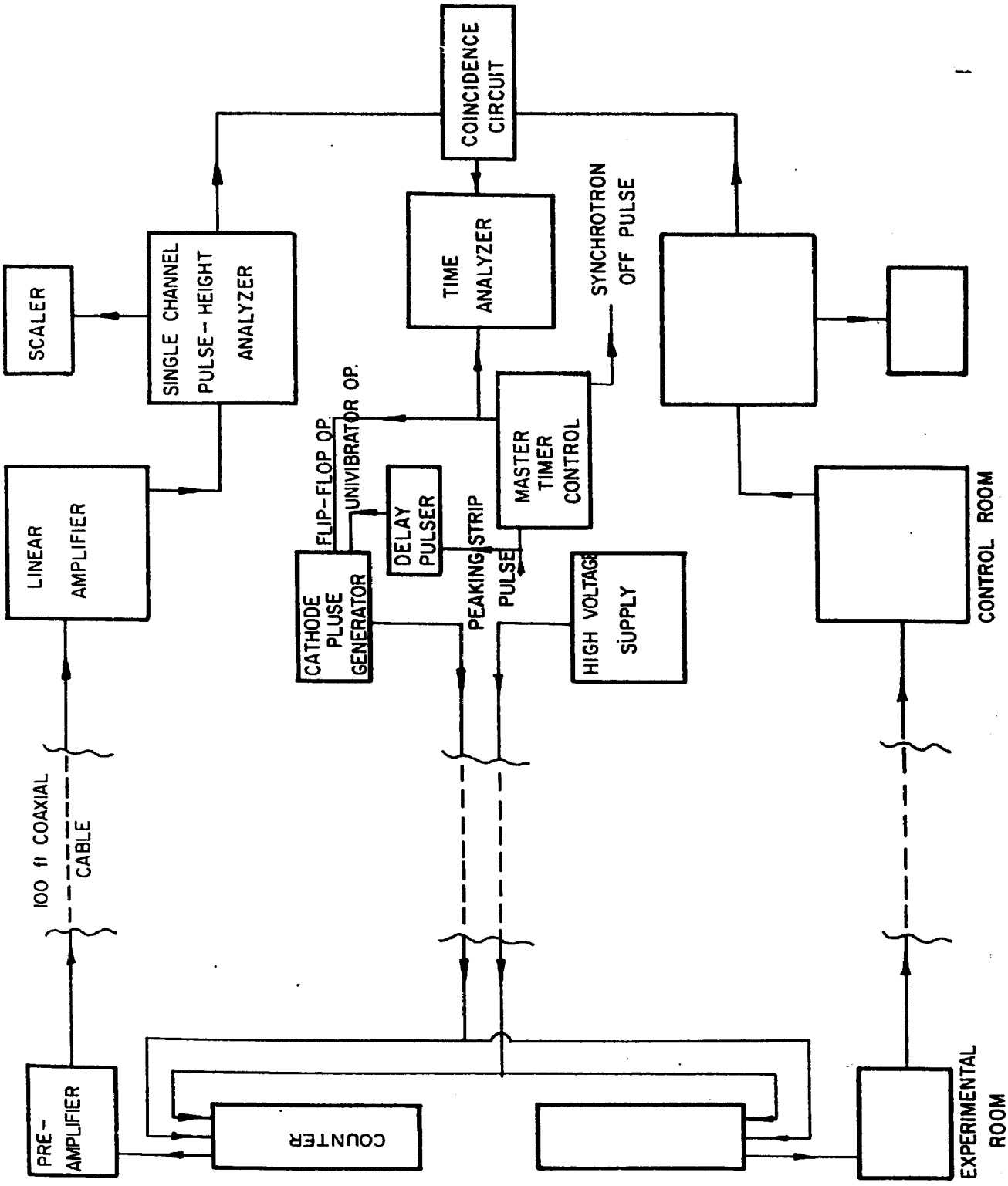


FIGURE 13. DETECTION SYSTEM BLOCK DIAGRAM

and that part which was located in the synchrotron control room.

The parallel systems had resolutions (i.e. ratio of the width (of any energy peak) at half-maximum to the positron of the maximum) for the detection of gamma-rays of energy 0.511 mev of 14.3% and 14.5%.

4. Time Analyzer.

To facilitate a time analysis of the data, a multichannel time analyzer was constructed. This analyzer would automatically sort the counts into twenty separate channels according to when they occurred in the counting period. The length of each channel could be varied in 50 milliseconds steps from 50 milliseconds to 5 seconds.

A block diagram of the time analyzer is shown in figure 14. Each scaler was construced of a 6802 dekatron tube and a Sodeco TCeZ4E - four digit register. The dekatron driver tube was biased so as to require a coincidence between a pulse from the register pulse generator and a pulse from a circuit called the distributor. The register pulse generator provided a pulse whenever it received a count, provided the count cycle gate from the master timer control had provided the proper bias for the triggering tube. The distributor was a ring scale of twenty which was driven by regularly timed pulses from the clock pulse reducer. Each input pulse to the distributor advanced the count one position in the ring, which determined sequentially the scaler that was open to receive register pulses. The clock pulse reducer took the same peaking strip pulses as the master timer and scaled them up to two GS10C dekatron tubes, connected in a decade arrangement. The cathodes of these tubes were fed to a pair of 10

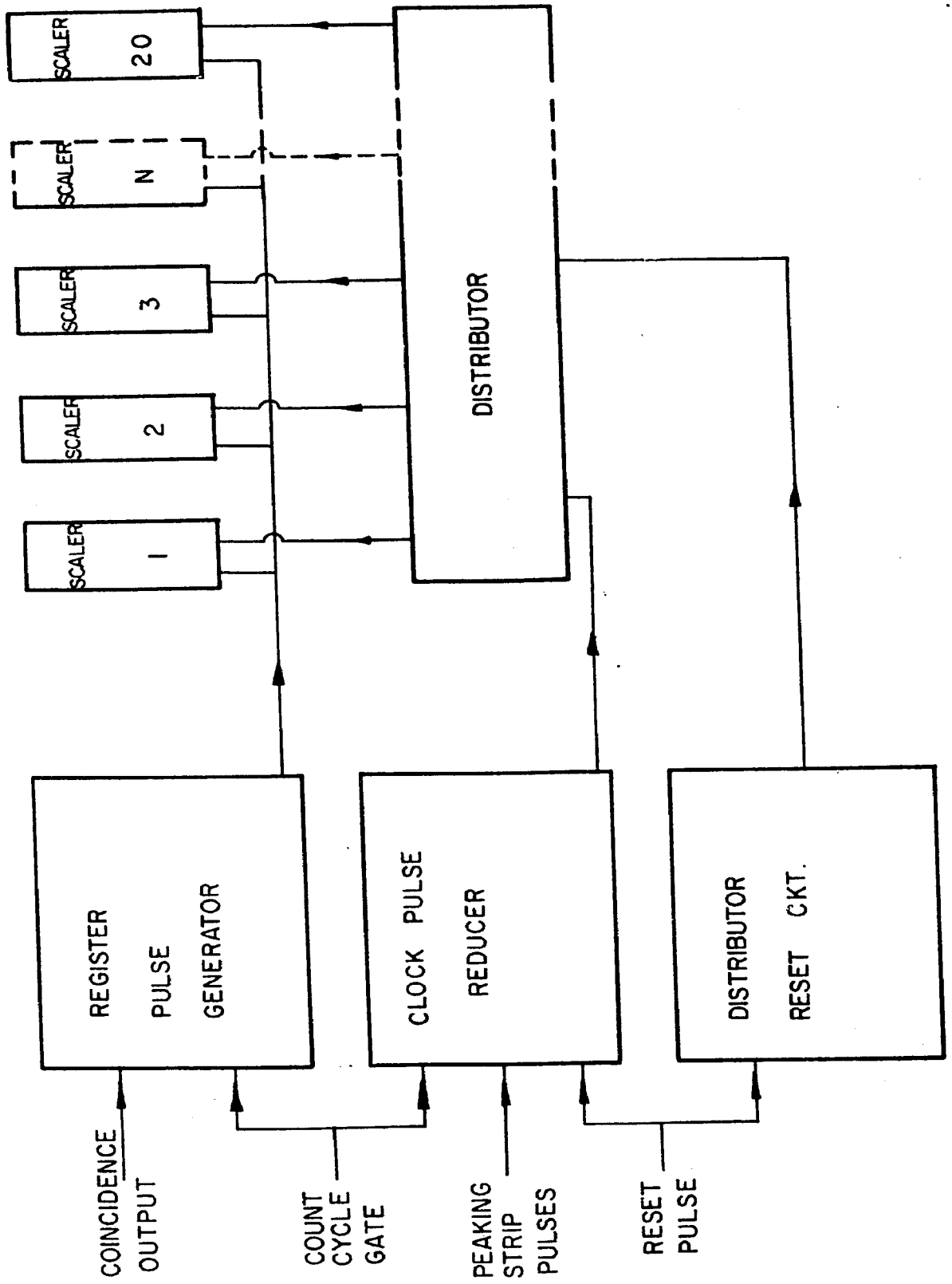


FIGURE 14. DIAGRAM OF TIME ANALYZER

position rotary switches, the outputs of which were fed through a coincidence circuit to trigger the reset mechanism. The reset mechanism reset the dekatron tubes to the zero cathodes and also fed a pulse to the distributor. The clock pulse reducer could scale peaking strip pulses only when the master timer control provided the counting gate signal. The reset pulse from the master control unit also reset the distributor and the clock pulse reducer dekatrons to the zero positions.

The spacing of the peaking strip pulses determined the accuracy of the lengths of the time channels. This accuracy in the timing of the firing of the peaking strip was directly coupled to the twenty cycle operation of the machine, which was in turn, phased to the sixty cps of the A.C. power into the building, thus the accuracy in this timing was roughly the accuracy in the frequency of the sixty cycle A.C. power. This was better than 0.1% over the course of 1 hour, (as quoted by the Detroit Edison Company).

An accurate half-life determination required, in most cases, an experimental decay-curve constructed of more than the twenty points given in a single run of the time analyzer. It was therefore necessary to include 3, and sometimes 4, runs in the compilation of the data for a single decay-curve. With such an experimental procedure it became necessary to normalize the runs accurately to one another. Normalization was accomplished by two methods which provided independent checks on the each other. The first of these was that of using the current integrator; this was driven by an ionization chamber located directly

in the bremsstrahlung beam and placed between the two lead collimators in the synchrotron room itself. Due to the duration of the bombardment process, normally equal to about two half-lives of the decay radiation, the activity produced by the first pulses of beam would be reduced by a factor of four by the beginning of the observation time while the activity produced by the last pulses would be there in its entirety. Accurate normalization by the use of the ionization chamber would require a constant intensity of beam during the bombardment period. Thus, although the ionization chamber provided a direct measurement of the bremsstrahlung flux which passed through the target, it was thought that normalizing by this instrument might introduce errors into the data.

The other normalization procedure that was used was that of overlapping the last five channels of one run with the first five channels of the next run. Since a channel was never shorter than 20% of the shortest half-life, the number of counts in these last five channels of the initial run were significantly fewer than those in the first channel. Consequently, the slope at the overlap section of the decay-curve was usually very small in absolute value. The method that was used was that of normalizing the arithmetic average of the last five channels of one run with the arithmetic average of the counts in the first five channels of the succeeding run, and of adjusting the counts in the remaining channels accordingly. The two normalization procedures were in agreement with each other, in nearly all cases, within the statistical errors of the counts involved. It was always necessary to have nearly equal intensity beams for successive runs in order to keep constant the ratio of signal to background.

5. Data Analysis and Errors.

The data from the lifetime measurements were fitted by the method of least squares to the form

$$y = A + B\, e^{-\alpha t} \qquad \text{IV-18}$$

if a single decay was involved, or

$$y = A + B\, e^{-\alpha t} + C\, e^{(-\beta t)} \qquad \text{IV-19}$$

in the cases where the decay-curve was complex, containing two components. When the half-lives of the two components were very different, the latter expression was approximated by

$$y = A - Dt + Ee^{-\alpha t} \qquad \text{IV-20}$$

where only the shorter lifetime was to be evaluated.

In order to perform a fit of the parameters of equation IV-20 to the data, it was necessary to take the total differential of the equation, as given by

$$\{O\text{-}C\} = (\Delta A) - (\Delta D)t - (\Delta E)e^{-\alpha t} - Et(\Delta \alpha)e^{-\alpha t} \qquad \text{IV-21}$$

and to perform a least squares fit on the differentials. It was necessary, in performing such a fit, to assume definite values for the constants. The results of the calculation would then be corrections to be applied to these assumed constants. $\{O\text{-}C\}$ represents the subtracted difference between the observed value of y at a given value of t, and the computed value, using the assumed values for

A, D, E, and $\alpha$. This method may also be used to compute standard deviations to be attached to the values of the corrected constants. If the values of the calculated corrections, $\Delta$ A, $\Delta$ D, $\Delta$ E, and $\Delta \alpha$ turned out to be greater than twice the computed standard deviations in the constants, it was necessary to perform a second iteration, using the corrected values of the constants for the new values.

Since the calculations involved were extremely time consuming, it was preferable to choose a good set of initial constants. These were chosen by first performing as accurate a fit of the data by graphical means as was possible.

The errors in the measurements of the half-lives should have been small. The experimental decay-curves were taken for at least seven half-lives of the decay and, in many cases, for ten half-lives in order to accurately determine the background. If the background observed in the measurements of the short-lived decays was higher than that expected from measurements of the static background, a decay-curve was taken with 50 second channel lengths to determine whether longer-lived activities were present. In all cases where the background failed to reach the expected value, a longer-lived activity, usually with a half-life greater than 2 minutes, was found, and the decay-curve measured out to seven half-lives or more of the long-lived decay. To obtain a sufficient number of counts in the 50 second channels for good counting statistics, several runs had to be made with 10-15 minute bombardment periods. The background for these measurements was always that of the static background.

It was thus felt that background to which the short-lived activity decayed was very well known and understood, and that any errors in the measured half-lives due to inaccuracies in knowing this background were small.

The errors in the lengths of the time channels have been discussed in the previous section of this chapter. It was thought that these errors were negligible in comparison with those introduced by the counting statistics. It was difficult to estimate the error introduced into the measurement of half-lives by the normalization procedure used when more than one run of the multichannel time analyzer was made to obtain more points on the decay-curve. Since the two normalization methods usually agreed with each other within 3%, it was felt that these errors were also small.

The errors quoted in the results are therefore the standard deviations computed by the least squares fit to the data. They are essentially those involved in the standard number statistics of the counts.

## E. Apparatus and Techniques for Making Energy Measurements.

### 1. Positron Endpoint Determination Equipment and Techniques

#### Targets

Thin targets, 20 mg/cm$^2$, were exposed to the x-ray beam for the purpose of obtaining energy spectra of the various positron decays from the end-products of the photonuclear reactions in the target nuclei. The targets were necessarily made this thin in order to reduce degadation of the emitted positrons in traversing the target, and a consequent altering of the spectrum shape. The targets were made by depositing 20 mg/cm$^2$ of the target substance on a backing of

0.25 mil Mylar. The procedure used in the construction of these targets was to suspend a measured amount of the powdered form of the target material in three cc of amyl acetate to which three drops of collodion had been added. After shaking the mixture well, it was poured out on the surface to be covered. The amyl acetate would then evaporate, leaving the powder deposited in a uniform thin layer over the surface of the Mylar. The collodion acted as a binder to hold the target material together. In this manner were made targets of pure S, Si, $CaF_2$, KI, and P. The aluminum target consisted of a sheet of 2 mil aluminum foil. The collodion, fluorine, and the iodine seemed to have no contaminating influence on the positron spectra at the energies studied.

## Detectors

The detector used to detect positrons was a scintillation counter, employing a Pilot Chemical Company 1 1/2" x 1 1/2" plastic scintillator mounted on a Dumont 6292 photomultiplier. The plastic scintillator was coated on the side, and also in a very thin layer on the top, with MgO. The photomultiplier was magnetically shielded with hypersil foil used in conjunction with aluminum foil, as was described in section D-3 of this chapter.

The experimental arrangement of the targets and the counter is shown in figure 15. Two targets, of the same material were mounted at 45° with respect to each other. The counter was placed directly below the vertex of the two targets, in a vertical position.

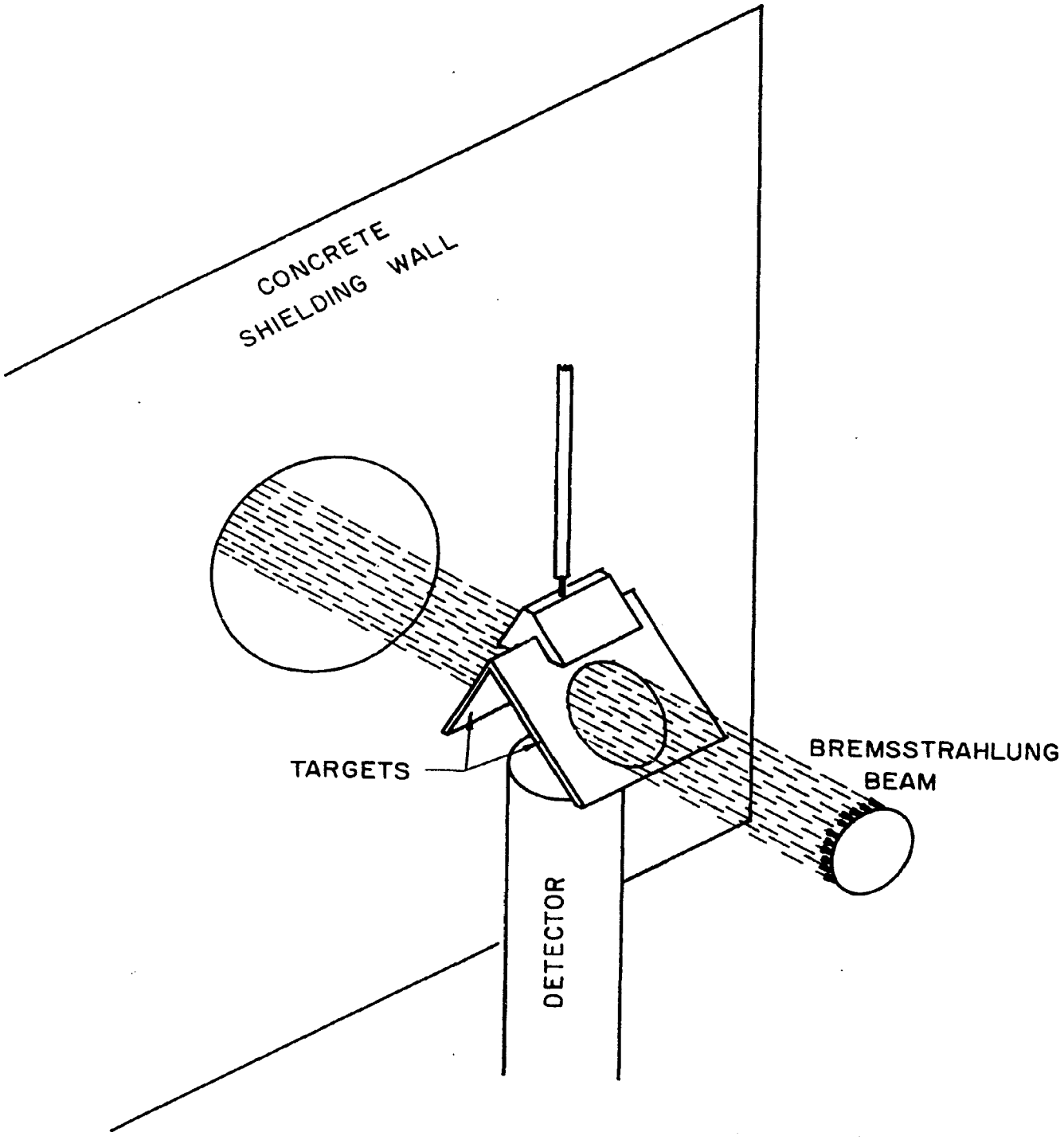


FIGURE 15. DIAGRAM OF TARGET – COUNTER ARRANGEMENT USED IN THE DETECTION OF POSITRONS FROM AN ACTIVATED TARGET

## Analyzing Equipment

To aid in the energy analysis, an auxiliary circuit was constructed which converted the time analyzer into a pulse-height analyzer of the type originated by Wilkinson[31] and further developed by Gatti[32] and others. This involved converting pulse height into time delay while an oscillator fed pulses into the distributor circuit at 50 kcps. In this manner 1000 counts/sec could be resolved into a pulse-height distribution. The widths of the individual channels could be either 2 volts or 4 volts. Thus, the twenty channel analyzer could be used to scan the entire operating range of the linear amplifier in either one run with low attendant resolution, or in two runs with rather good resolution. The remainder of the analyzing system was similar to that described in section IV-D-3.

The counter was gated in a manner described in section IV-D-3 with the photocathode gate generator supplying a pulse 30 milliseconds in length. The pulser was triggered by the output of a delay pulser which, in turn, was triggered by the peaking strip pulse. The delay pulser could render an output pulse at any given delay (from 0 to 100 milliseconds) from the input peaking strip pulse. The delay used was such as to gate on the counter 2 milliseconds after the accelerated beam had passed. This delay of 2 milliseconds was incorporated to allow the neutrons created by the photonuclear reactions in the targets to be eliminated from the background in the room. Experimentally it was noted that about this length of time was required.

The photomultiplier was gated off just before the injection pulse of the succeeding beam acceleration period. If this were not done,

stray electrons would create unwanted background when hitting the internal target of the synchrotron during the acceleration process.

The synchrotron was operated continuously in making the energy measurements, the 30 milliseconds between electron-activity periods in the synchrotron being used as the observation time.

**Calibration Procedure and Corrections to Data**

A difficult problem was that of the energy calibration of the multichannel analyzer. An Atomic Instrument Company model 510 single channel pulse-height analyzer was first calibrated over the entire range of the linear amplifier by using various radioactive sources such as $Na^{22}$, $Cs^{137}$, $Na^{24}$, and $Zn^{65}$, in conjunction with a NaI(Tl) scintillation counter. The pulses were shaped as described in section IV-D-3. The result of this calibration was an establishment of a linear calibration curve for this instrument which intersected the origin. This curve was then used as the basis of a calibration of the multichannel analyzer.

In order to scan the entire voltage output range of the linear amplifier, it was necessary to make at least two runs with the multichannel analyzer, using different base-line voltage settings. It was therefore necessary to know the actual widths of the "2-volt" channels, and to adjust the base-line calibration to correspond to these widths, in order to correlate the runs to one-another. A measurement of the channel widths would also establish (or dis-establish) the linearity of the multichannel analyzer. Such a measurement was made with the aid of a Hamner model N101 mercury switch pulser. This pulser was installed in the electronic system in the place of the scintillation

counter, and its output pulses were shaped to closely resemble those from the scintillation detector. The output pulses of the linear amplifier were fed simultaneously into the single-channel analyzer (whose linearity had been pre-established) and into the multichannel analyzer. In this manner, the widths of the individual channels could be measured in terms of the voltage readings in the single channel analyzer. The width of the twenty individual channels were determined to be equal within 2%. The base-line voltage control was then calibrated to correspond to these widths.

A precision attenuator was constructed which reduced the size of the output pulses from the preamplifier to exactly half of their unattenuated value. This attenuator preserved the 2000 Ω impedance, as seen by pulses from the pre-amplifier. The linearity of the multichannel analyzer having been established, energy calibration would consist of two energy endpoint determinations of the negatron decay from an $Y^{90}$ calibration source; one taken without the attenuator, and one taken with the attenuator in place. The spectrum taken without the attenuator in the circuit would correspond to that with an endpoint energy double the 2.24 mev endpoint reported for the $Y^{90}$ decay.[33] The spectrum taken with the attenuator would correspond to a spectrum having the actual 2.24 mev endpoint. All additional positron endpoint measurements would be made with the precision attenuator in the circuit.

Such a calibration proceedure assumes that the response of the scintillator itself is linear. A measurement of the response of phosphor scintillators was made (for electrons) as a function of the

energy of the electron by Hopkins[34] and others. The results of these measurements indicate that the response is very linear for electron energies above 200 kev.

The positron spectra were corrected for the effects of finite resolution of the scintillation counter by a method reported by Freedman, et al.[35]. In this method, the function which relates the true spectrum to the experimental spectrum is that given by Owen and Primakoff[36] and is given by

$$M(E) = \int_0^{E'_{max}} N^{\alpha}(E') \, L(E,E')dE' \approx \sum_1^{-} N(E'_i) \, L(E,E'_i) \, \Delta_1 E' \qquad \text{IV-19}$$

M(E) is the observed counting rate at the spectrometer energy setting E, N(E') is the true energy spectrum (counting rate per unit energy), and L(E,E') is the fraction of the number of electrons of energy E' which hit the scintillator and are observed in the same range of pulse analyzer setting $\Delta$ E at E as is used in observing M(E).

$$L(E,E') = \frac{S(E,E') \, \Delta E}{\int_0^{\infty} S(E,E')dE} \qquad \text{IV-20}$$

where S(E,E') is the experimental line shape observed with window width $\Delta$ E (on a monochromatic electron source).

An iteration process, used to determine N(E') is based on matching the experimental spectrum M(E) with that calculated from equation IV 19, using a suitable trial function for N(E'). Numerical integration, using a suitably normalized gaussian distribution for L(E,E') which has as the ratio of the width at half maximum to the

position of the maximum, 15%, is performed which obtains a new $M_1(E)$. The first approximation to the true spectrum is given by

$$N_1(E)\ \Delta E = M(E) - \left\{M_1(E) - M(E)\right\} = 2M(E) - M_1(E) \qquad \text{IV-21}$$

Covergence of this iteration process is rapid and for the energy specta measured in this experiment, a first approximation was sufficient to correct the data so that a Kurie plot of the data would yield a straight line.

Many of the spectra studied were complex decay spectra (i.e. more than one positron decay present) and corrections to these data were not made directly but rather inferred from the corrections made to the spectra containing a single component.

The background radiation was measured as a function of energy by placing an aluminum cap over the end of the counter of sufficient thickness to prevent positrons from entering the crystal. So long as the measurements involved energies above 700 kev, the measurements provided a good analysis of the background. Annihilation radiation created in the aluminum cap prevented going to lower energies with this technique. The background was measured for several targets and was found to be independent of the target material. This measured background was subtracted from the raw data for the runs to obtain the true positron spectrum. Successive runs were normalized to one another and to the background runs by the use of the ionization chamber and the current integrator. The objections to the use of this instrument for normalization, discussed in the section on half-life measurements, are invalid for continuous bombardment with a reasonably steady x-ray beam.

Errors

The necessary use of thin targets in beta spectroscopy and the consequent low counting rates from these targets, limited the total number of counts in the individual energy channels to a relatively small number. In addition, in many channels, nearly half of these counts could be attributed to background counts. The primary error in these measurements, therefore, was that of bad counting statistics.

The precision attenuator was felt to be accurate to 1% since the resistors in the circuit were accurate to at least 1%, and the total resistive dividing network was measured to have an attenuation of 2 within 1%. The energy calibration was considered accurate to within 2% due to consistency in the calibration procedure.

As was previously mentioned, several of the decay spectra were complex. Although the endpoint energies of the components were separated by at least 750 kev, the number of points to which a straight line could be fitted in Kurie plots of the data was drastically reduced for these spectra. This further added to errors in the endpoint determinations. In only one case, that of potassium, was it desired to determine the endpoints of both the high and low energy components of the complex decay. In all other cases, only the high energy component of the decay spectra was of interest.

Taking all of the possible errors into account, an error of 5% is attached to the reported endpoint measurements.

## 2. Gamma Ray Energy Measurements

### Targets

The targets used in the search for gamma transitions consisted of the powdered form of the element to be studied, with the exception of potassium which was a solid piece of the metal. The powder was enclosed in iron target holders similar to those discussed in section IV-D-1. The target materials consisted of $CaH_2$, K metal, Si, and S. These targets were used in conjunction with a single scintillation counter located directly above the target.

### Detection Apparatus

The counter used in searching for high energy gamma rays consisted of a 2 inch by 2 inch NaI(Tl) scintillation crystal attached to an R.C.A. 6342 photomultiplier tube magnetically shielded with hypersil foil. Both the crystal and the tube were mounted in a 3 inch diameter brass cylinder. Over the crystal end of the scintillation counter was placed an aluminum cap 1/16 inch thick. The photomultiplier was operated with a positive high voltage and the photocathode was gated by the photomultiplier gate generator. Targets were bombarded by the bremsstrahlung beam in continuous pulsed operation. The remainder of the analyzing system was identical to that used in the measurements of the positron spectra.

### Calibration and Experimental Procedure

The procedure used for gamma-ray searching was to calibrate roughly the multichannel analyzer with a $Na^{24}$ source which has gamma-ray peaks at .51 mev, 1.38 mev, 1.74 mev, 2.25 mev, and 2.76 mev, and to scan the thick targets for gamma-rays in the energy

region from 200 kev to 4.0 mev. The dominant gamma-ray which was always found was the .511 mev annihilation quantum. This peak was of such magnitude as to mask completely any gamma-rays in its vicinity (i.e. 400 kev to 600 kev). The background at 1 mev, if no gamma-rays were present at or above this energy, was down by a factor of 200 from the peak at .511 mev. At 3 mev the background was down by a factor of 2000.

If a gamma-ray were found, the energy region in which it was located was scanned with the single channel analyzer, calibrated with $Na^{24}$. If the quanta were of such an energy that pair production in the scintillation crystal was the dominant interaction process, the two quanta escape peak was normally the peak whose energy was measured by the single channel analyzer since this peak was energetically the closest to the calibration peaks from $Na^{24}$. To ensure that a peak was actually the two quanta escape peak, a 1 1/2 inch by 1 1/2 inch NaI(Tl) crystal was used to scan the target, in which case the relative intensities of the total capture peak, the one quantum escape peak, and the two quanta escape peak would change, the two quanta escape peak becoming larger and the total absorption peak becoming much smaller. The runs were normalized by the use of the current integrator.

Having located the gamma-ray peaks with the single channel analyzer, half-life determinations for these gamma-rays were made by discriminating over the region of the peak with the pulse height analyzer and feeding the output into the time analyzer, used in conjunction with the master timer control. The experimental procedure

was similar to that described in section D of this chapter.

## Errors

The errors in the energy determination of the gamma-rays were small if the gamma peak could be calibrated by known gamma-rays on each side of the unknown peak. The detection system itself, with the 2 inch by 2 inch NaI(Tl) scintillation crystal, had a resolution of 12.3%. The errors assigned to the individual gamma-ray energy determinations are the standard deviations of the finite width peaks.

## CHAPTER V

## DESCRIPTION OF ENERGY LEVEL AND DECAY SCHEMES IN SPECIFIC NUCLEI; RESULTS OF THE MEASUREMENTS

### A. $Ca^{38}$ - $K^{38}$ - $A^{38}$.

1. Energy Level and Decay Schemes.

$K^{38}$ has a ground state nucleon configuration, a (1d3/2) hole in both the proton and neutron levels. $j_n$ and $j_p$ thus being known, Nordheim's rule[17] may be used to predict a value of J for the lowest (T = 0) state. The predicted values of J are 3 and 1, with (J = 3) being the more probable value. Such a level should have even parity since the two nucleons are in equivalent levels. The next (T = 0) state to be expected should have ($J = 1^+$) and should be an excited level.

$Ca^{38}$ and $A^{38}$ are even-even nuclei with a ground state nucleon configuration consisting of two (1d3/2) holes in the neutron orbits in $Ca^{38}$, and in the proton orbits in $A^{38}$. Such nuclei should have ground states with ($T = 1, J = 0^+$) and first excited states with ($T = 1, J = 2^+$). The ground states of $Ca^{38}$ and $A^{38}$ correspond to an isobaric-spin triplet nuclear eigenfunction that is common not only to $Ca^{38}$ and $A^{38}$, but also to $K^{38}$. There should be, therefore, among the low-lying levels of $K^{38}$, a state with ($T = 1, J = 0^+$). The state in $K^{38}$ should be displaced in energy from the similar state in $A^{38}$ by the Coulomb energy. Referring to the calculations of Moszkowski and Peaslee[25] (figure 2), it is found that the ($T = 1, 0^+$) level in $K^{38}$ should lie 5.5 mev above the ground state of $A^{38}$. Similarly, the

ground state of $Ca^{38}$ has been predicted[19] to lie 6.3 mev above the $(T = 1,0^+)$ state in $K^{38}$. There should be, in $K^{38}$, competition between the $(T = 0,3^+)$ level and the $(T = 1,0^+)$ level for the position of ground state.

An energy level diagram for the $Ca^{38}$ - $K^{38}$ - $A^{38}$ triad is shown in figure 16. The $Ca^{38}$ nuclide had not been observed prior to this research. The location of the $(T = 0,1^+)$ state in $K^{38}$ was also completely unknown. For a long time it has been known that a low-lying state in $K^{38}$ undergoes positron decay with a half-life of about 7.5 minutes[37] to the $(T = 1,2^+)$ state in $A^{38}$. That the transition goes to the first excited state of $A^{38}$ was verified by a half-life measurement of the 2.18 mev gamma transition which follows the positron decay [38]. Since the gamma transition would be an E-2 transition with a very small lifetime, a half-life measurement would yield the half life of the preceding beta-decay. The positron endpoint energy of this transition has been given as 2.6 mev[39] which, in conjunction with the half-life, gives $\log_{10}$ ft = 5.0 for the transition. The transition is therefore classed as allowed (i.e. $|\Delta J| = |\Delta T| = 1$). From this knowledge, the state in $K^{38}$ was deduced as having $(T = 0)$ and either $(J = 1^+)$ or $(J = 3^+)$. In addition, a .95 second positron activity was observed from the bombardment of potassium with $\gamma$-rays[40] which had an endpoint energy of 5.0 mev[41] and a subsequent $\log_{10}$ ft value of about 3.4. This transition was classed as a $(0^+ \rightarrow 0^+)$ superallowed positron transition between the isobaric-spin triplet states in $K^{38}$ and $A^{38}$.

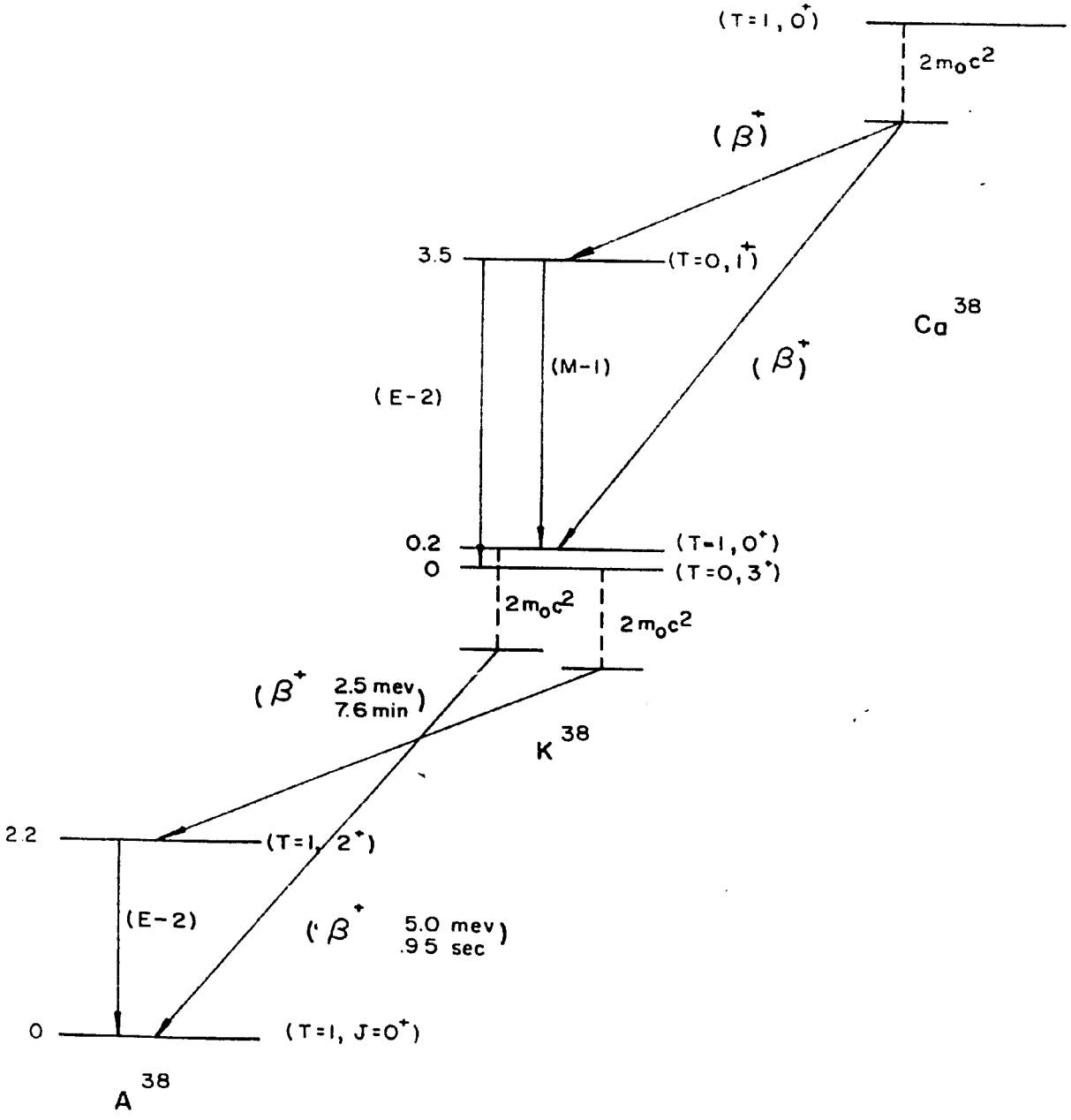


FIGURE 16. ENERGY LEVEL DIAGRAM FOR THE NUCLEI, $A^{38}$, $K^{38}$, $Ca^{38}$

The existence of independent positron decay from these two states in $K^{38}$ would be impossible if the lowest (T = 0) state had ($J = 1^+$). This state and the ($T = 1, 0^+$) level would be, in such a case, connected by M1 radiation with a much shorter half-life than that for either positron decay. The conclusion was therefore drawn that the spin of the (T = 0) state was ($J = 3^+$).[40]

It is not altogether clear which of these two low-lying states in $K^{38}$ is the ground state, although present indications seem to indicate that the ($J = 3^+$) level is probably the lower level. Green and Richardson[42] attempted to find an internal conversion line caused by an (M3) transition between the ($J = 3^+$) level and the ($J = 0^+$) level with negative results. The line should have been observed if the ($J = 0^+$) level were the ground state. It was therefore concluded from intensity considerations that the ($J = 0^+$) level must either lie above the ($J = 3^+$) level or not more than 80 kev below it.

$Ca^{38}$ may be produced in the ($T = 1, 0^+$) ground state by a ($\gamma$,2n) reaction on $Ca^{40}$ and should undergo positron decay to the corresponding state in $K^{38}$. Since the transition would be a ($0^+ \rightarrow 0^+$) transition, the $\log_{10}$ ft value is given by equations III-5 and III-9 as 3.4. The half-life for such a decay has been predicted from the ft value to be .7 seconds[19]. If a ($T = 0, 1^+$) excited state in $K^{38}$ lies energetically below the ground state of $Ca^{38}$, then a branching in the positron decay should occur to this state with subsequent (E2) and (M1) gamma transitions to the lower lying ($T = 0, 3^+$) and ($T = 1, 0^+$) states respectively in $K^{38}$. The fractional intensity x for such a branching has been calculated by Moszkowski and Peaslee for the

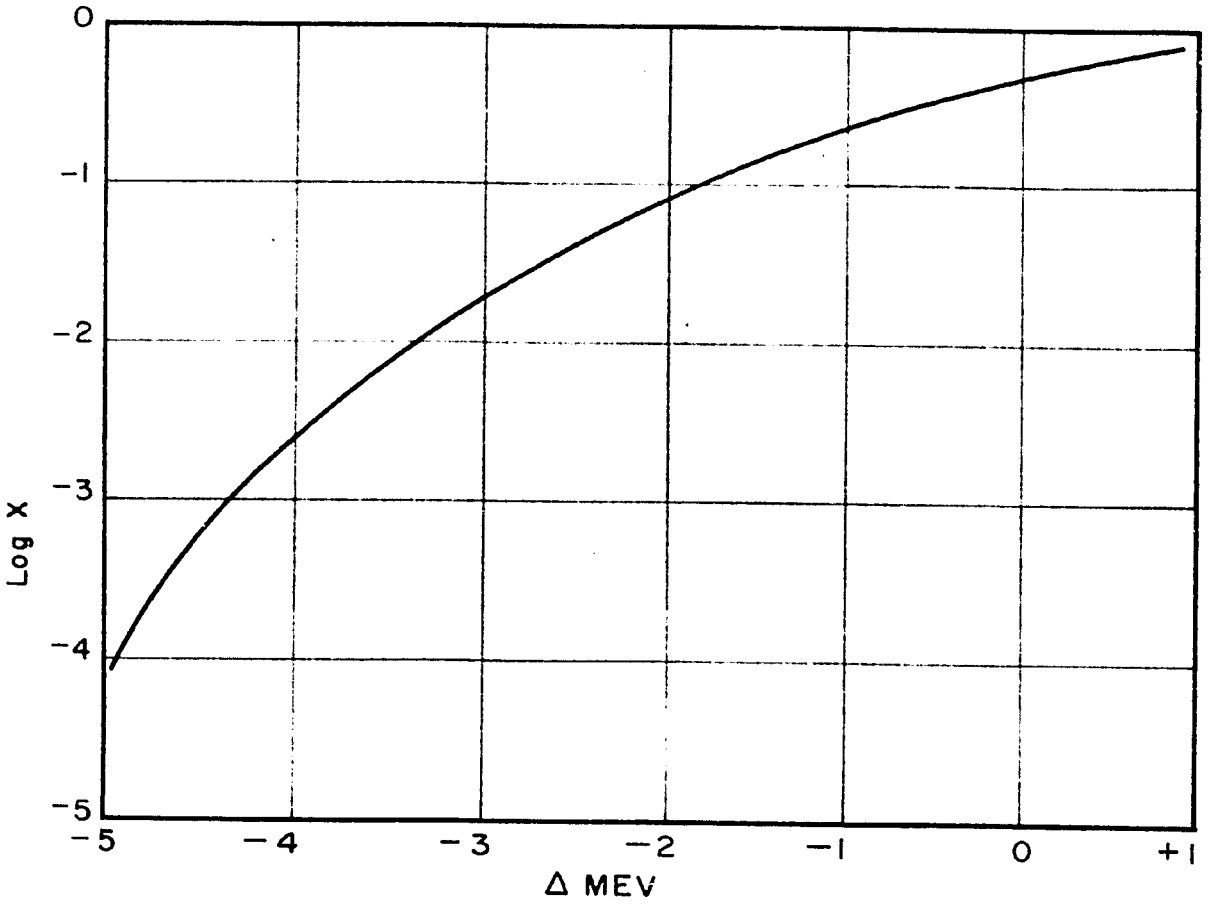


FIGURE 17. FRACTIONAL INTENSITY X OF $0^+ \rightarrow 1^+$ TRANSITION IN $\beta^+$ DECAY OF $Z = N+2$, $A = 4n+2$ NUCLEI. Δ EQUALS HEIGHT OF $\theta^+$ STATE ABOVE $1^+$ STATE IN $N = Z$ NUCLEI.

A = 38 nuclei[25] as a function of the energy separation of the $(1^+)$ state and the $(0^+)$ state. The results of their calculation are shown in figure 17.

2. Experimental Results and Analysis.

The experimental results for the measurements of the decay radiations from nuclei in the A = 38 triad are summarized in Table I.

Potassium

Typical decay curves for the 7.67 minute and the 0.95 second positron decays from $K^{38}$ are shown respectively in figures 18 and 19. Both of these decay curves were experimentally determined three separate times, and an analysis was performed on each distinct curve to obtain the half-life of the decay. The result of each analysis is listed in Table I as well as the average of each group of three measurements. The individual runs took about two hours to complete and were made at widely separated intervals over the course of a month.

Potassium has two stable isotopes, $K^{39}$ and $K^{41}$. Since the potassium used as the target material was not an isotopically enriched material, the relative abundance may be taken as those occuring in nature, namely 93.4% and 6.6% respectively. $K^{38}$ would be, in the main, produced by the reaction $K^{39}(\gamma,n)\ K^{38}$. The primary competing photonuclear reactions in $K^{39}$ would be the $(\gamma,n^dp)$, the $(\gamma,2n)$, the $(\gamma,2p)$, and the $(\gamma,p)$ reactions. The neutron and proton yields from the $(\gamma,n^dp)$ reaction are estimated from the data of Smith[43] and others to be about 5% of the neutron yield from the $(\gamma,n)$ reactions, while the yield from either the $(\gamma,2n)$ or the $(\gamma,2p)$ reactions is estimated

TABLE I

Results of the Measurements of the Decays From the Nuclei in the Nuclear Triad with ( A = 38)

| TARGET ISOTOPE | GAMMA-RAY ENERGY | POSITRON ENDPOINT ENERGY | MEASURED HALF-LIFE OF GAMMA-RAY | $LOG_{10}ft$ | ASSIGNMENT OF TRANSITION |
|---|---|---|---|---|---|
| $K^{39}$ | $m_oc^2$ | 2.60 ± 0.15 mev<br>2.58 ± 0.15 mev<br>2.60 ± 0.15 mev<br>avg.<br>2.59 ± 0.09 mev | 7.68 ± 0.06 min.<br>7.62 ± 0.04 min.<br>7.72 ± 0.06 min.<br>avg.<br>7.67 ± 0.03 min. | 4.89 ± 0.07 | allowed positron transition from $K^{38}(T=0,3^+)$ to $A^{38}$ $(T=1,2^+)$ |
| $K^{39}$ | 2.20 ± 0.11 mev<br>2.15 ± 0.11 mev<br>2.22 ± 0.11 mev<br>avg.<br>2.19 ± 0.06 mev | ------- | 7.67 min. | ----- | E-2 transition from $(T=1,2^+)$ level in $A^{38}$ to the ground state following the 7.67 minute decay to this state. |
| $K^{39}$ | $m_oc^2$ | 4.92 ± 0.28 mev<br>4.91 ± 0.28 mev<br>5.13 ± 0.29 mev<br>avg.<br>4.99 ± 0.16 mev | 0.956 ± 0.010 sec.<br>0.950 ± 0.011 sec.<br>0.946 ± 0.014 sec<br>avg.<br>0.951 ± 0.007 sec. | 3.48 ± 0.05 | $(0^+ \rightarrow 0^+)$ super-allowed transition from $K^{38m}$ to ground state of $A^{38}$ |
| $Ca^{40}$ | $m_oc^2$ | ------- | 7.67 min. | ----- | decay from $K^{38}$ |
| $Ca^{40}$ | 2.2 mev | ------- | 7.67 min. | ----- | transition in $A^{38}$ |
| $Ca^{40}$ | 3.54 ± 0.25 mev<br>3.50 ± 0.25 mev<br>3.45 ± 0.25 mev<br>avg.<br>3.50 ± 0.14 mev | ------- | 0.73 ± 0.09 sec.<br>0.63 ± 0.09 sec.<br>0.61 ± 0.09 sec.<br>avg.<br>0.66 ± 0.05 sec. | ----- | decay from excited state in $K^{38}$ follow a braching in the decay of $Ca^{38}$ to this state. |

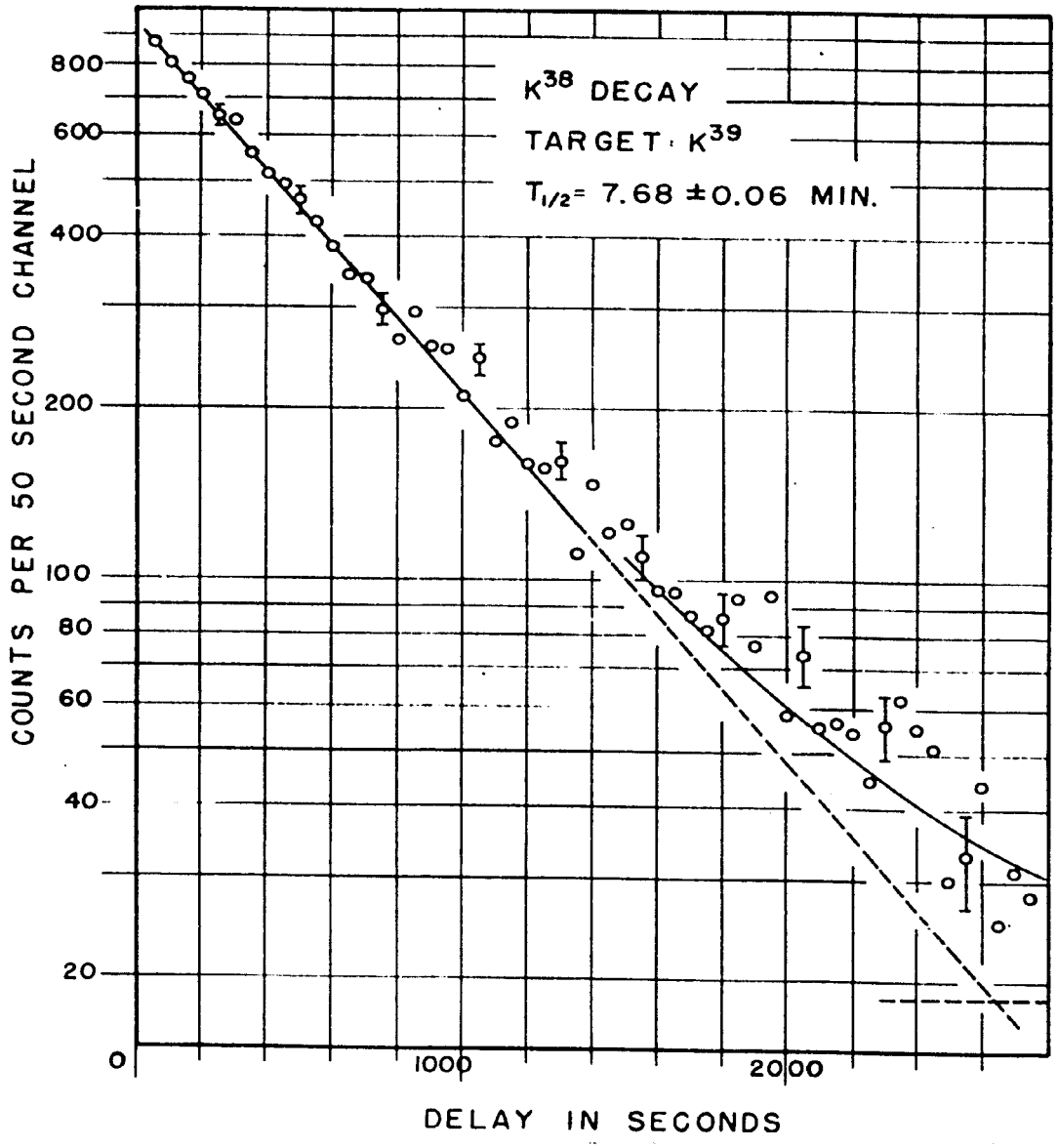


Figure 18. Decay Curve for $K^{38}$.

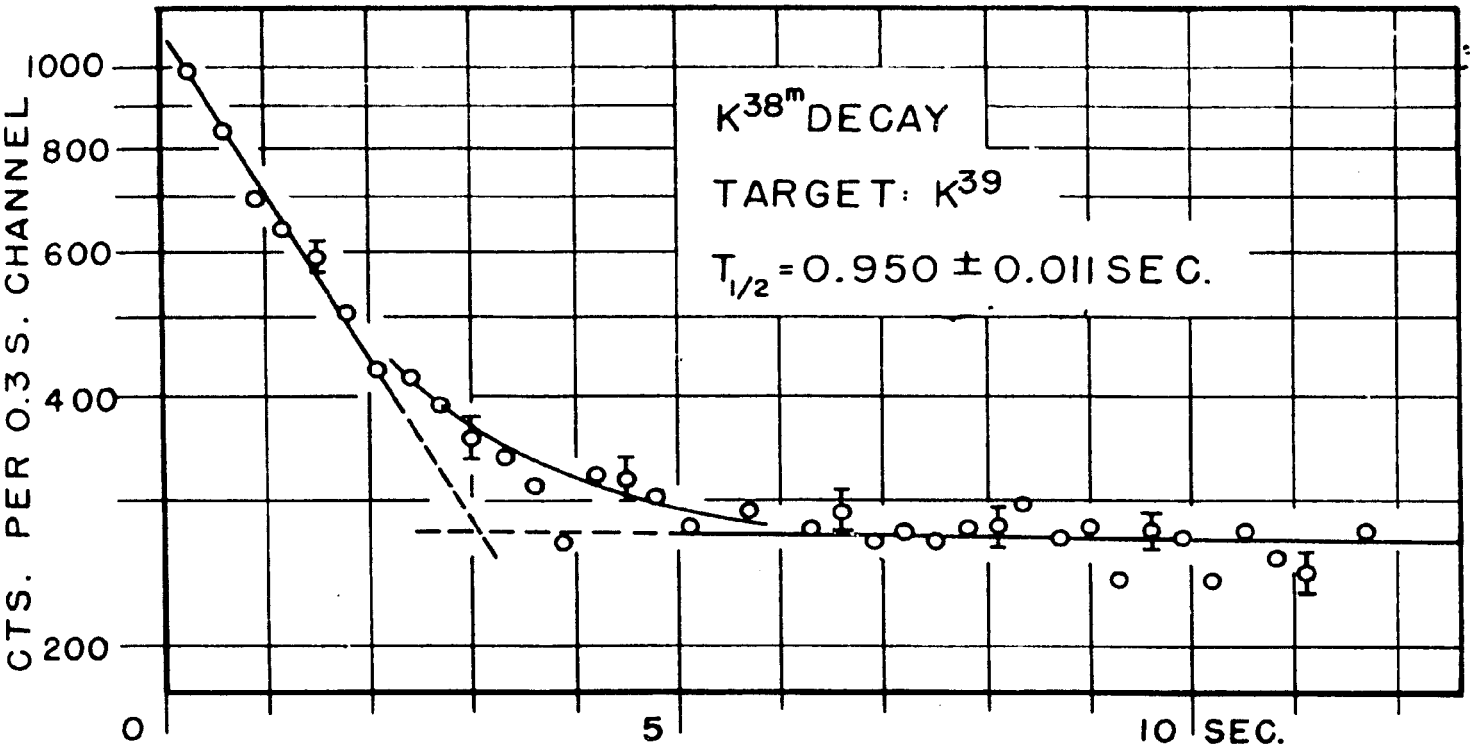


Figure 19. Decay Curve for $K^{38m}$.

to be about 6%[44] of the neutron yield from the $(\gamma,n)$ reaction. The yield from the $(\gamma,p)$ reaction should be about the same as that from the $(\gamma,n)$ reaction[10]. A $(\gamma,n^dp)$ reaction in $K^{39}$ creates $A^{37}$, a nucleus which undergoes K and L capture with a half-life of 35 days. There are no positron or gamma transitions associated with $A^{37}$ which could contaminate the data from the decay of $K^{38}$. The $(\gamma,p)$ and the $(\gamma,2p)$ reactions on $K^{39}$ produce $A^{38}$ and $Cl^{37}$ respectively, both of which are stable isotopes. The $(\gamma,2n)$ reaction on $K^{39}$ produces $K^{37}$, about which very little is known. $K^{37}$ should be a positron emitter, and should have a half-life of about 1 second. Any other photonuclear reaction on $K^{39}$ is estimated to have a yield, relative to that from the $(\gamma,n)$ reaction, of less than 1.%, and should contribute no observable distortion in the decay curve of the radiation from $K^{38}$ and $K^{38m}$.

None of the above mentioned photonuclear reactions will produce any positron unstable nuclei from the 6.6% abundant $K^{41}$ isotope in the target. The only gamma activity produced by such reactions on $K^{41}$ would be the 1.5 mev gamma-ray from the $10^8$ year $K^{40}$ isotope.

Activity in the potassium target, other than that from $K^{38}$ and $K^{38m}$, should, therefore, be present in insignificant amounts, with the exception of the activity from $K^{37}$. Since the half-life of $K^{37}$ is unknown, it is difficult to estimate how much of an error a 3% contamination of $K^{37}$ would make in the measured half-life of the decay from $K^{38m}$. Nevertheless, such an error is believed to be less than 0.8%.

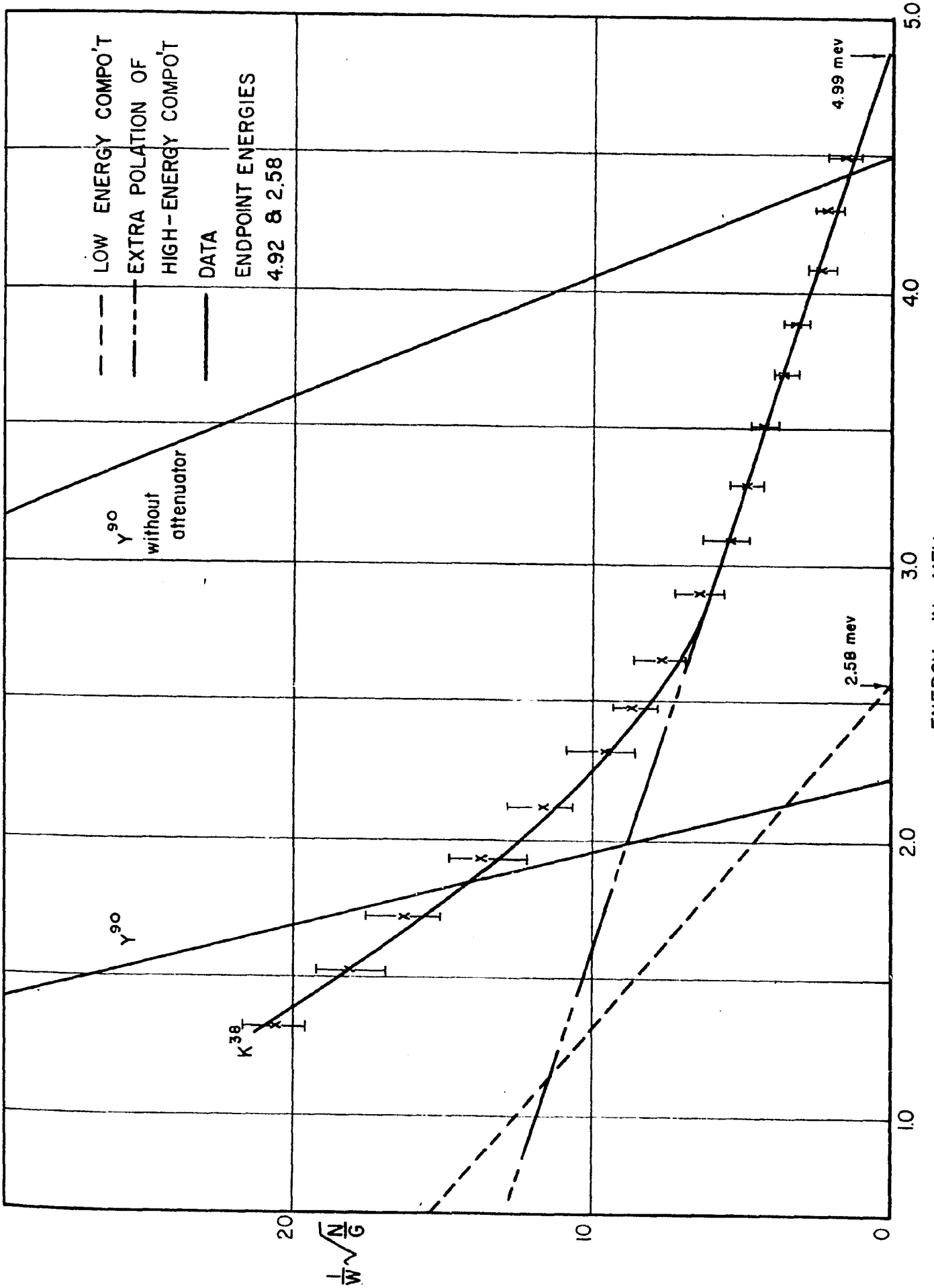


FIGURE 20. KURIE PLOT OF POSITRON SPECTRUM FROM $K^{38}$ and $K^{38m}$

A Kurie plot of the positron spectrum from the decay of $K^{38}$ is shown in figure 20. It is noticed from the shape of the spectrum that it represents a complex decay containing at least two components. The components of this curve have been taken to be the decays which occur from $K^{38}$ and $K^{38m}$. The Kurie plot was resolved into its two components by making a Kurie plot of the data beyond 3 mev, and extrapolating the straight line back to the origin. The difference between the extrapolated curve and the true curve at any point, as well as the value on the extrapolated curve, was then used to calculate the portion of the total counts in any energy channel that belong to each decay curve. A new Kurie plot was then made for the component with the lower endpoint energy. This was done for the three independent measurements of the positron decay spectra from $K^{38}$.

In the positron spectra from the decay of $K^{38}$, there should be little effect from the 6% contamination of $K^{40}$ produced by the reaction $K^{41}(\gamma,n)\ K^{40}$, since the half-life of $K^{40}$ is about $10^8$ years. In addition, the energy endpoint of the $\beta^-$ decay from $K^{40}$ is 1.35 mev which is below the energy region of interest (> 1.5 mev for $K^{38}$). The only other contamination would be that from the decay of $K^{37}$, and should consist of at most 3% of the counts in any one energy channel, which is within the statistical counting errors. The positron spectrum from $K^{38}$ should, therefore, not be affected in any measureable quantity (in the energy region of interest) by the decay of the end products of the competing photonuclear reactions.

The gamma-ray spectrum obtained from the bombardment of potassium by high-energy gamma-rays is shown in figure 21. This spectrum is

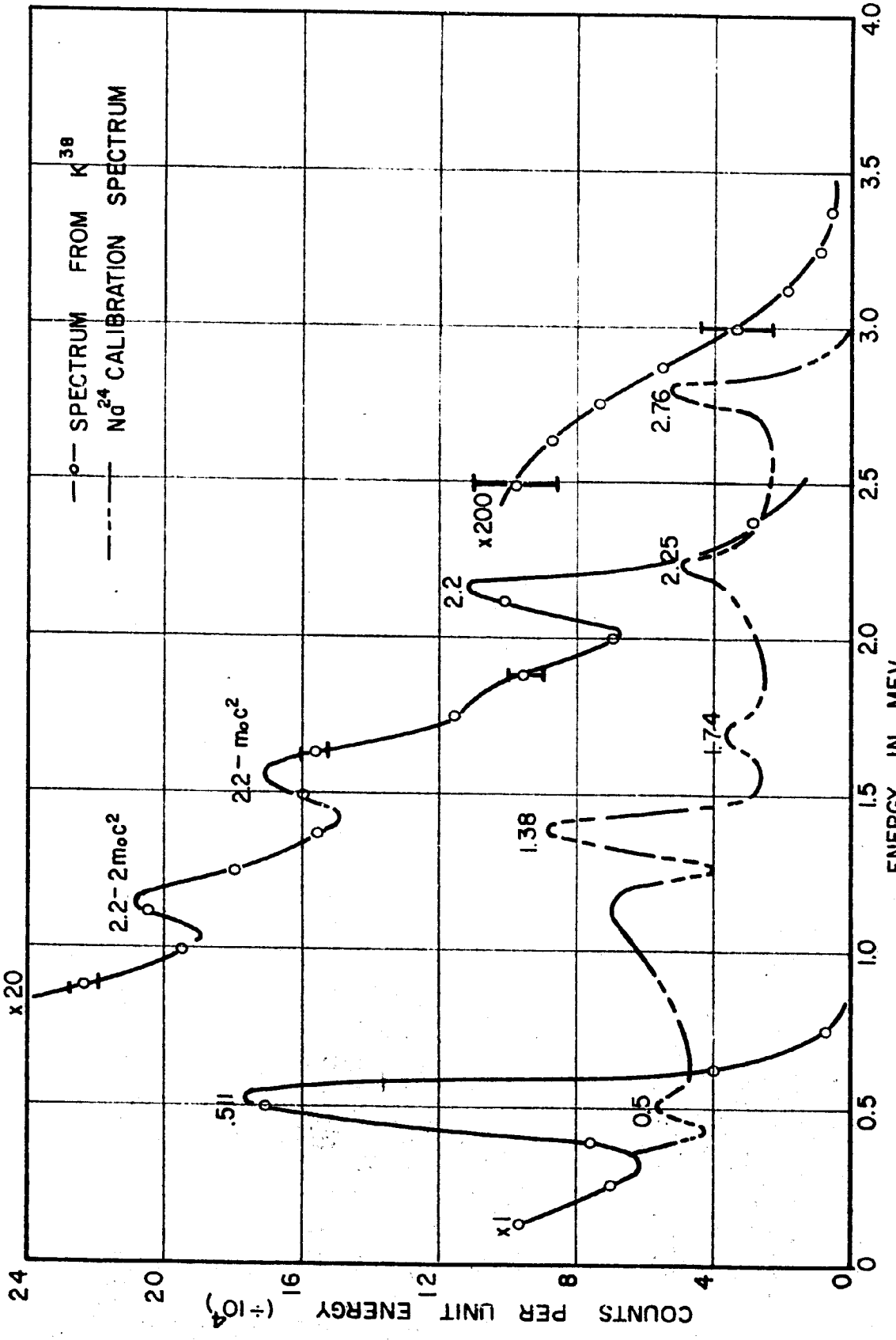


FIGURE 21. GAMMA RAY SPECTRUM FROM THE DECAY OF $K^{38}$ AND $K^{38m}$ SHOWING CALIBRATION SPECTRUM FROM $Na^{24}$

continuous from 300 kev up to 3.5 mev. Super-imposed upon the spectrum is the calibration spectrum from a $Na^{24}$ calibration source. The spectra show the 2.2 mev transition in $A^{38}$ which follows the 7.67 minute positron from $K^{38}$ to the ($T = 1, 2^+$) state in $A^{38}$. A half-life measurement of this gamma transition, obtained by discriminating over the total absorption peak with the single channel analyzer, is shown in figure 22. There should be no gamma-ray present from the contaminating influence of competing photonuclear processes beyond the 1.35 mev gamma-ray from the decay of $K^{40}$. Since the decay of $K^{40}$ has such a long half life, it is felt that this transition should not be seen in the data. This is accentuated by the fact that such a peak in the spectrum could easily be masked by the one quantum escape peak from the 2.2 mev transition in argon.

## Calcium

The gamma-ray spectrum from the bombardment of a calcium target is shown in figure 23. This spectrum shows the 2.2 mev gamma-ray present from the bombardment of a potassium target and, in addition, shows a 3.5 mev transition which is present only with a calcium target. Discrimination over the peaks was made with a single channel analyzer, and a half-life measurement was made. The decay-curve is shown in figure 24.

Calcium occurs naturally in six stable isotopes; $Ca^{40}$, $Ca^{42}$, $Ca^{43}$, $Ca^{44}$, $Ca^{46}$, and $Ca^{48}$, with respective relative abundances of 96.9%, .6%, .1%, 2.1%, .003%, and .2%. The ($\gamma$,n) or ($\gamma$,p) reaction on any of these isotopes produces no nuclei to which a 3.5 mev gamma

DECAY CURVE FOR
GAMMA-RAY IN $A^{38}$

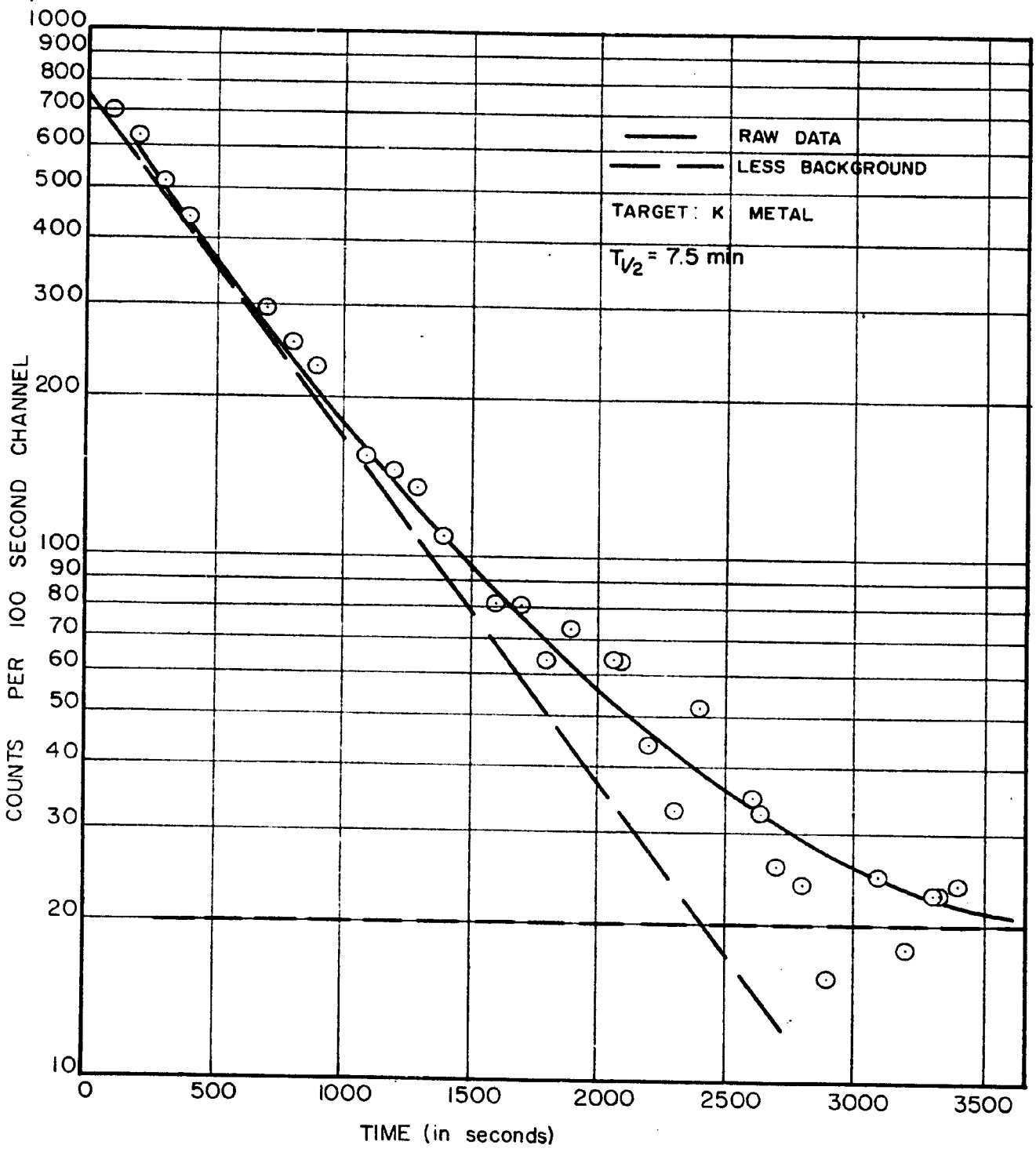


FIGURE 22 DECAY CURVE FOR ARGON GAMMA-RAY

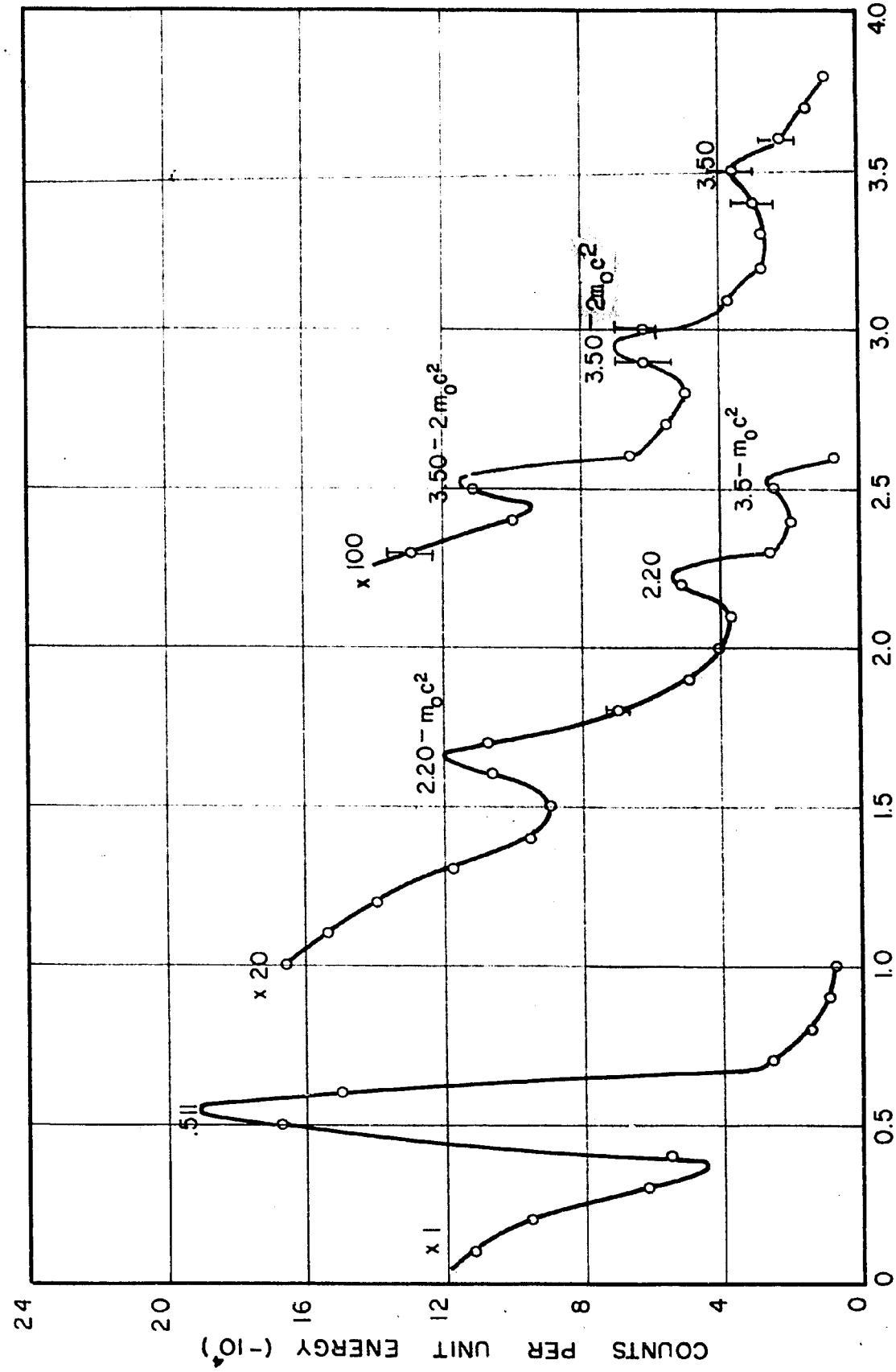


FIGURE 23. GAMMA-RAY SPECTRUM FROM CALCIUM TARGET SHOWING 2.2 MEV. GAMMA-RAY FROM ARGON AND 3.5 MEV GAMMA-RAY, SPECIFICALLY OBTAINED ONLY FROM A CALCIUM TARGET

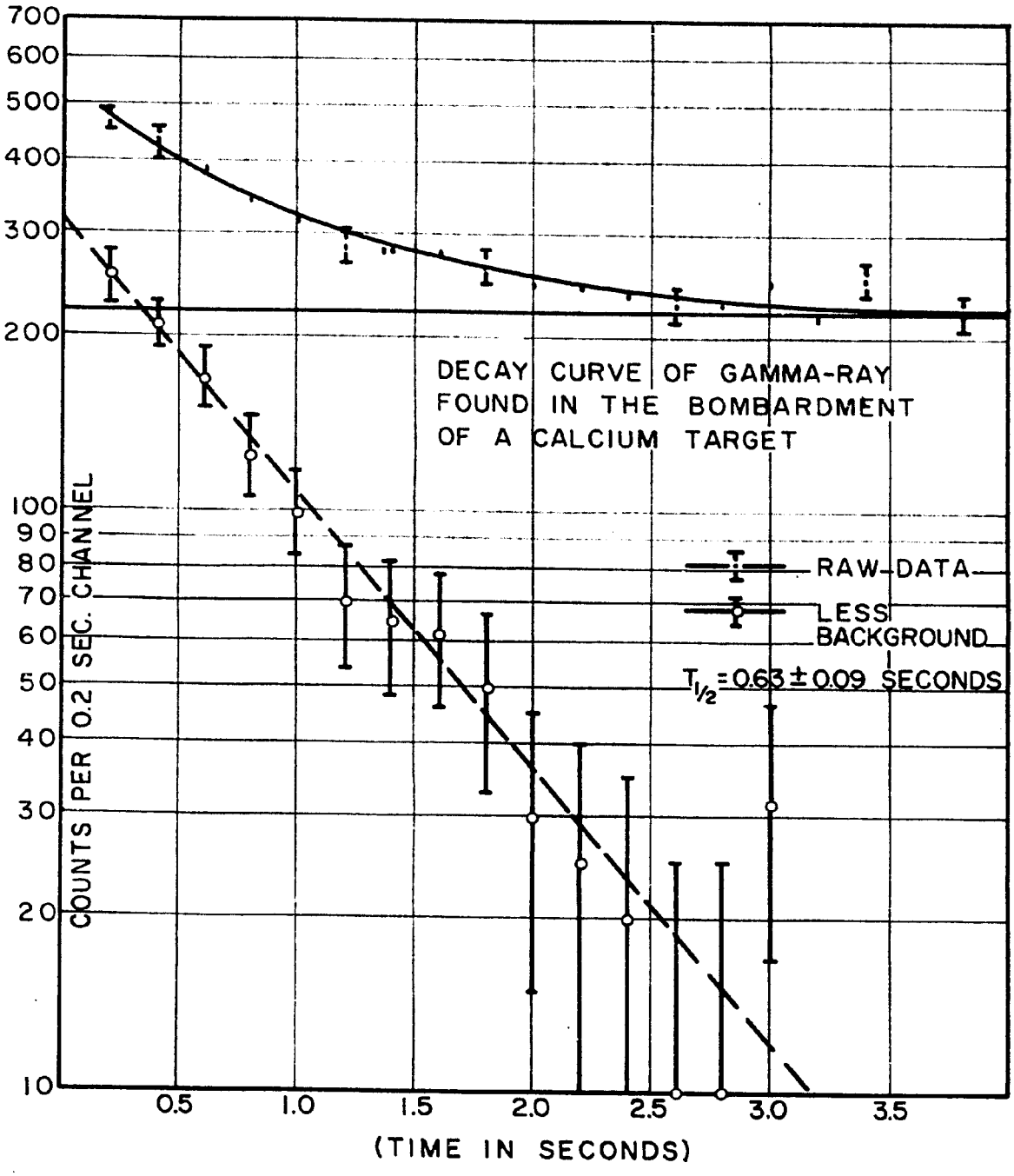


FIGURE 24 DECAY CURVE OF GAMMA-RAY FOUND FROM THE BOMBARDMENT OF A CALCIUM TARGET

transition could be assigned. Any of the multiple nucleon emission processes would produce too few nuclei for any measurable activity to occur, in all the isotopes except $Ca^{40}$ and $Ca^{44}$. A $(\gamma,n^dp)$ reaction on $Ca^{44}$ produces $K^{42}$, which has a half-life of 12.5 hours and a gamma-ray of 1.5 mev. That this gamma-ray was not seen in the spectrum is attributed to the fact that the half-life is so long, and also to the fact that such a peak would most likely be masked by the one-quantum escape peak from the 2.2 mev gamma transition in $A^{38}$. The $(\gamma,n)$ and $(\gamma,2n)$ reactions on $Ca^{44}$ produce stable isotopes of calcium. The $(\gamma,2p)$ reaction on $Ca^{44}$ produces $A^{42}$ which has a half-life of 3.5 years and would not be observed in the two hour bombardment periods used in performing the experiment. Any other reaction in $Ca^{44}$ would have a cross-section so small that any subsequent activity could not be observed in these measurements. Thus, it is argued that the activity is an activity specifically obtained from the bombardment of $Ca^{40}$.

An attempt was made to establish the fact that the gamma-ray was in coincidence with a positron decay. This attempt failed due to the low intensity of the gamma-ray. The three peaks in the spectra were determined to be the two quantum escape peak, the one quantum escape peak, and the total absorption peak by two separate experiments. The first of these was that of scanning the spectrum with a smaller crystal of NaI(Tl), which should make the total absorption peak nearly disappear, and should increase the height of the two quantum escape peak relative to the others. Such an effect was observed when a 1 1/2 inch by 1 1/2 inch crystal was substituted for the 2 inch by

2 inch crystal. The second experiment consisted in discriminating over the total absorption peak with the single channel analyzer, determining if this peak had a half-life less than 1 second. Such a measurement was made, and the results indicated that this peak had a half-life of about 0.5 seconds. Both of the experiments indicated that the three new peaks in Ca were from a 3.5 mev gamma-ray with a half-life of 0.66 seconds.

When calcium was bombarded with the bremsstrahlung beam, time analysis of the long-lived positron activity present yielded the 7.67 minute half-life of $K^{38}$. The quantity of this radiation that was present indicated an amount of $K^{38}$ produced which was inconsistent with the amount produced by the decay of $Ca^{38}$. Hence, the majority of the $K^{38}$ that was present was felt to be produced by the reaction $Ca^{40}$ $(\gamma,n^dp)$ $K^{38}$. The amount of $K^{38}$ present was consistent with the measured $(\gamma,n^dp)$ cross-section in other elements[45]. No other activity in calcium with a half-life greater than 1 second was found. A distortion in the 7.67 minute decay curve in the first few channels was investigated and found to be a small amount of contaminating 2.1 minute positron activity from $O^{15}$. The 4.5 minute activity from calcium reported in 1937[46] and 1940[47], was not found.

3. Summary and Conclusions

The results of the preceding set of measurements may be summarized by stating that the transitions in the isobaric triad $Ca^{38}$-$K^{38}$-$A^{38}$ are consistent with those indicated in figure 15. $Log_{10}ft = 4.87$ for the lower energy transition from $K^{38}$, which shows that the transition is allowed, but unfavored. The 2.2 mev gamma transition exhibits the

half-life of the low energy positron transition from $K^{38}$, which indicates that the positron transition proceeds to the $(T = 1, 2^+)$ level in $A^{38}$ and that the gamma-ray is the subsequent transition to the ground state. That no other gamma-rays were observed from potassium also indicates that the parent level of this decay is a $(3^+)$ level. The high energy positron decay from $K^{38}$ with $\log_{10} ft = 3.48$ is in agreement with the predicted value of 3.4 for the $(0^+ \rightarrow 0^+)$ transitions, which indicates that this is the transition from the $(T = 1, 0^+)$ level in $K^{38}$ to the ground state $(T = 1, 0^+)$ level in $A^{38}$.

The value of 2.59 mev for the positron endpoint of the lower energy decay, and the value of 4.99 mev for the high energy component of the decay from $K^{38}$, coupled with the measurement of 2.2 mev for the gamma transition in $A^{38}$ indicates that the $(T = 0, 3^+)$ state is the ground state in $K^{38}$, while the $(T = 1, 0^+)$ level lies above this state by $(210 \pm 190)$ kev.

The 3.5 mev gamma-ray , observed only in the bombardment of calcium, has been interpreted as the transition from an excited level in $K^{38}$ following a branching in the positron decay from $Ca^{38}$ to this excited state. An alternative assignment might be the decay from an isomeric state in $K^{39}$ following the creation of this state by the reaction $Ca^{40}$ $(\gamma, p)$ $K^{39}$. States with approximately the correct energy have been found in $K^{39}$ [48]. However, for such an assignment to be consistent with the observed half-life of the gamma-ray, 0.66 seconds, the transition would need to be a transition with $|\Delta J| \geq 5$. Since the $(\gamma, p)$ reaction is essentially a dipole absorption phenomenon[49], it is

thought to be highly improbable that such a state could be created in large quantity.

The assignment of the gamma-ray to a transition from an excited state following a branching in the positron decay from $Ca^{38}$ is consistent with predicted half-life of $Ca^{38}$ of 0.7 seconds[19]. The fractional intensity for this branching is then given from the graph in figure 16 to be 1%. This value is also consistent with the assignment since the intensity of the radiation observed compares favorably with the expected ratio of yields for the $(\gamma,n)$ and $(\gamma,2n)$ reactions of 3% and with the fractional intensity of 1%.

The 3.5 mev excited level in $K^{38}$, to which this branching may be supposed to occur, could either be a $(T = 0,1^+)$ level or a $(T = 1,0^+)$ level. A level with either assignment could be found with the proper excitation energy from an $(S\ \frac{1}{2})^{-2}$ configuration[50], although lower lying $(J = 1^+)$ states are possible with other configurations. If the level is a $(T = 0,1^+)$ level, then the positron decay to the state, from the ground state of $Ca^{38}$, would be an allowed, but unfavored, decay. The gamma-decay from such a state would present a competition between an E2 transition to the ground $(J = 3^+)$ state of $K^{38}$, and an M1 transition to the $(J = 0^+)$ isomeric state. A rough calculation of the transition probabilities for the two decays indicates that the M1 transition would be slightly favored over the E2 transition. In such a case, the observed gamma peak would actually be a doublet, with a separation of the two components equal to the separation of the ground and the first excited states in $K^{38}$. It was not experimentally possible to determine whether the observed gamma peak was, or was not a doublet.

If on the other hand, the newly observed state had ($T = 1, 0^+$), the positron decay to this state would be an allowed and favored decay. The subsequent gamma-decay could then be an M3 transition to the ($J = 3^+$) ground state. In this case, it would also be expected that there would exist an alternate mode of decay, consisting of a cascade through an intermediate ($T = 0, 1^+$) state, theoretically predicted to lie below 3.5 mev[50]. Since this alternate decay mode would consist either of a pair of M1 transitions to the lowest ($J = 0^+$) state or an M1 followed by an E2 transition to the ($J = 3^+$) ground state, the transition probability would be so high, compared to the transition probability for the direct 3.5 mev M3 transition to the ground state, that no 3.5 mev gamma-ray should have been seen.

In view of the above argument, it is deemed more probable that the state at 3.5 mev has ($T = 0, J = 1^+$). Such a statement is based wholly on the assumption, however, that a ($T = 0, J = 1^+$) state also lies energetically lower than 3.5 mev. A branching in the decay from $Ca^{38}$ should also occur to this state. Due to the presence of the 2.2 mev gamma-ray (from the transition in $A^{38}$), with the associated single and double quantum escape peaks, and the .511 mev annihilation quantum in the experimental spectrum, it was not possible to determine whether a gamma-ray, indicating a transition from such a state to the lower states of $K^{38}$, existed.

## B. $S^{30}$ - $P^{30}$ - $Si^{30}$

### 1. Energy Level and Decay Schemes.

The ground state nucleon configuration in $P^{30}$ consists of a ($S\ \frac{1}{2}$) neutron and proton beyond the closed nucleon orbits. Nordheim's rule[17]

thus predicts ($J = 1^+$) for the lowest ($T = 0$) state. In addition, among the low lying states in $P^{30}$, $S^{30}$, and $Si^{30}$. The other two nuclei in the ($A = 30$) triad, $S^{30}$ and $Si^{30}$ have ground states with ($T = 1, J = 0^+$) and probably have first excited states with ($T = 1, J = 2^+$). Figure 2 predicts an energy separation of the ($T = 1, 0^+$) state in $P^{30}$ and the ground state of $Si^{30}$ of 4.62 mev. Similarly, the ground state of $S^{30}$ has been predicted to lie 5.2 mev above the ($T = 1, 0^+$) state in $P^{30}$ [19].

The positron decay from $P^{30}$ has an energy endpoint of about 3.3 mev[51] and a half-life of 2.5 minutes [52] ($\log_{10} ft = 4.8$). This decay is, therefore, allowed but unfavored, and the ground state assignment is given to the ($T = 0, J = 1^+$) level. The ground state of $S^{30}$ should decay by an allowed transition to the ground state of $P^{30}$. In addition, a branching in the decay should occur to the ($T = 1, 0^+$) excited level in $P^{30}$ with a subsequent M1 transition to the ground state. The predicted half-life for the decay from $S^{30}$ is 1.8 seconds[19]. This value would be reduced by the branching in the decay.

An energy level diagram for the ($A = 30$) nuclei is shown in figure 25. States in $P^{30}$ have been reported at .7 mev, 1.4 mev, and 2.0 mev.[54,51,53,55]. The state at 700 kev was identified as having ($J = 0$) on the basis of excitation energy and gamma-ray angular distribution following the $Si^{29}$ (p,$\gamma$) $P^{30}$ reaction [51,53]. Moreover, this same level was identified as having ($T = 0$), due to its production by the $S^{32}$(d,$\alpha$) $P^{30}$ reaction[55]. If the isobaric-spin selection rules for nuclear reactions of Adair[9] and others are valid, then the (d,$\alpha$) reaction on $S^{32}$ should produce no ($T = 1$) states. Thus, the

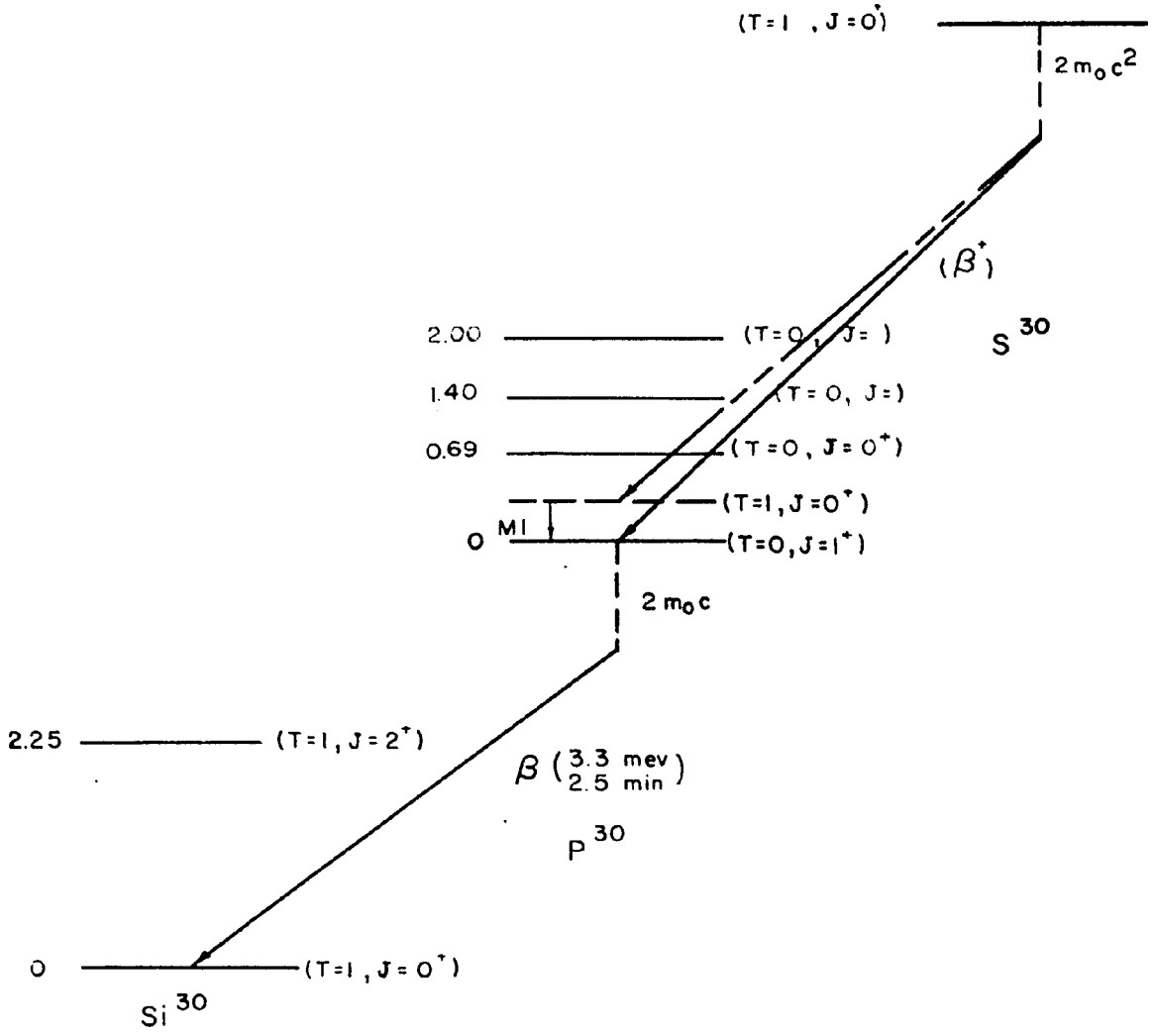


FIGURE 25 ENERGY LEVEL DIAGRAM FOR NUCLEI $S^{30}$, $P^{30}$, $Si^{30}$.

available information on the 700 kev state in $S^{30}$ would seem to indicate that the state is a (T = 0,J = 0) level. Such a state could theoretically occur from a mixed nucleon configuration.[5] Positron branching to this state would then not be allowed since it would violate the isobaric-spin selection rules in beta-decay. If the other levels at 1.4 mev and at 2.3 mev have (T = 0), as was also reported by Lee and Mooring[55], then no appreciable branching should occur to these states either, since they presumably have J > 1, and the transitions would be forbidden.

The positron decay from $P^{30}$ should not consist of two independent decays (as in the case of $K^{38}$ and $K^{38m}$). The ($T = 1,0^+$) state may decay to the ($T = 0,1^+$) ground state by M1 radiation with a transition probability much higher than that for the positron decay from the excited level.

2. Experimental Results and Analysis

The results of the experimental measurements of the decay processes in this chain of nuclei are given in Table II.

Phosphorus

A typical decay-curve for the positron decay from $P^{30}$ as a function of time is shown in figure 26. $P^{30}$ was produced by the reaction $S^{32}(\gamma,n^dp)\ P^{30}$. The four stable isotopes of sulfur are $S^{32}$, $S^{33}$, $S^{34}$, and $S^{36}$ with relative abundances of 95.1%, 0.7%, 4.2%, and 0.016% respectively. Only reactions on $S^{32}$, $S^{33}$, and $S^{34}$ could produce any measurable quantity of activity in this experiment. In addition, any measurable positron activity could have been produced only by photonuclear reaction on $S^{32}$. The ($\gamma$,n)

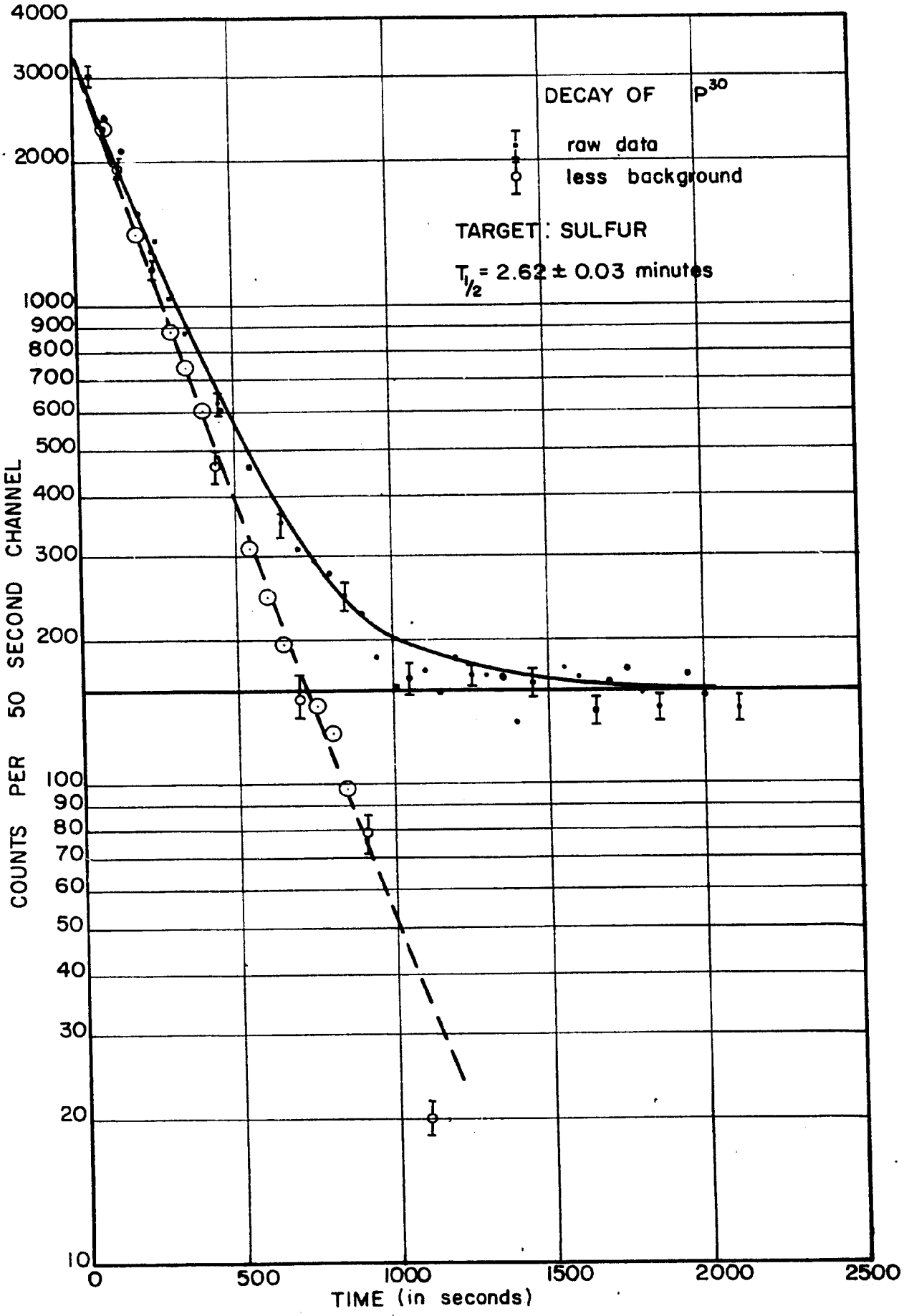


FIGURE 26. DECAY OF $P^{30}$

TABLE II

Results of the Measurements of the Decays From the Nuclei in the Nuclear Triad with ( A = 30)

| TARGET IS TOPE | GAMMA-RAY ENERGY | MEASURED HALF-LIFE OF GAMMA-RAY | POSITRON ENDPOINT ENERGY | $Log_{10}ft$ | ASSIGNMENT OF TRANSITION |
|---|---|---|---|---|---|
| $S^{32}$ $P^{31}$ | $m_0c^2$ | 2.62 ± 0.03 min.<br>2.59 ± 0.03 min.<br>2.70 ± 0.04 min.<br>avg.<br>2.62 ± 0.02 min. | 3.24 ± 0.19mev<br>3.22 ± 0.19mev<br>3.21 ± 0.19mev<br>avg.<br>3.22 ± 0.11mev | 4.81±0.07 | allowed positron transition from $P^{30}$ ($T = 0,1^+$) to ground state of $Si^{30}$ ($T = 1,0^+$). |

reaction on $S^{32}$ produces $S^{31}$, a positron emitter with a half-life of about 3 seconds. The $(\gamma,2n)$ reaction would produce $S^{30}$, a positron emitter whose half-life has been estimated[19] to be 1.8 seconds. The $(\gamma,p)$ and $(\gamma,2p)$ reactions would produce $P^{31}$ and $Si^{30}$ respectively; both are stable nuclei. Thus, the only photonuclear reaction which would produce any positron activity with a half-life of the order of minutes would be the reaction $S^{32}(\gamma,n^dp)\ P^{30}$. There should, therefore, be no contamination present in the decay-curve, and a half-life analysis, using such a decay curve, should yield an accurate measurement of the positron decay from $P^{30}$.

A measurement of the positron energy spectrum from the decay of $P^{30}$ was made using a target of amorphous phosphorus, which is 100% $P^{31}$. The spectrum, unlike the complex decay spectrum from the decay of $K^{38}$, is that of a single decay. A Kurie plot of the data (figure 27) yielded a straight line. The $(\gamma,2n)$ reaction on $P^{31}$ produces $P^{29}$, a positron emitter with a half-life of 4.6 seconds and an energy end-point of 3.5 mev. The $(\gamma,2p)$ reaction creats $Al^{29}$, a negatron emitter

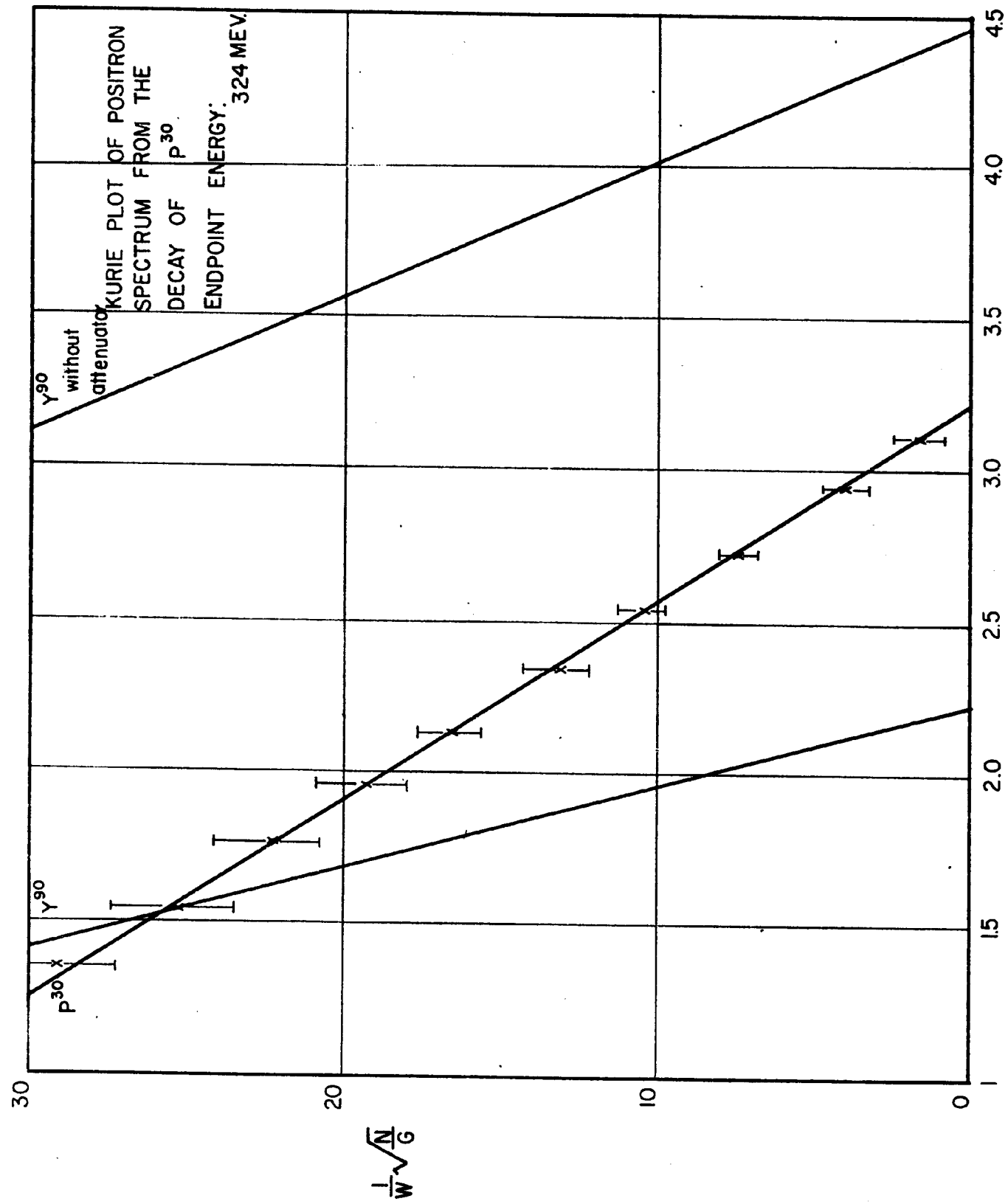


FIGURE 27. KURIE PLOT OF POSITRON SPECTRUM FROM THE DECAY OF $P^{30}$

with a half-life of 6.6 minutes and endpoint energies of 3.5 mev and 1.4 mev. Both the 3.6 mev activity in $P^{29}$ and the 2.5 mev activity in $Al^{29}$ should have contributed a contaminating influence on the spectrum shape. However, since neither activity should have been present in amounts greater than 5% of the primary $P^{30}$ activity, such influence is felt to be negligable in comparison to the influence of the statistical errors in the individual points of the positron spectrum.

Sulfur

An energy spectrum of the gamma-rays produced when a sulfur target is exposed to the x-ray beam is shown in figure 28. The target material was natural sulfur, which, as was previously mentioned, contains the four stable isotopes of sulfur. The only gamma-ray expected to be present in the spectrum, with the exception of the ever present annihilation quantum, would be that representing the transition, in $P^{30}$, from the excited ($T = 1, 0^+$) state to the ground state. Such a transition should follow a branching in the positron decay from $S^{30}$, created by the $S^{32}$ $(\gamma, 2n)$ reaction. The experimental spectrum, however, shows no such gamma-rays present in sufficient quantity to be resolved from the background. Of particular interest was the region around 700 kev. If the state previously reported at this energy did not have ($T = 0, J = 0$), but instead, had either ($T = 0, 1^+$) or ($T = 1, 0^+$), then a gamma-ray of 700 kev should have been observed.

3. Summary and Conclusions

The results of the measurements made of the decay radiation from the nuclei in the isobaric triad $S^{30}$-$P^{30}$-$Si^{30}$ are in accordance with the level scheme presented in figure 25. The value of $\log_{10} ft = 4.8$

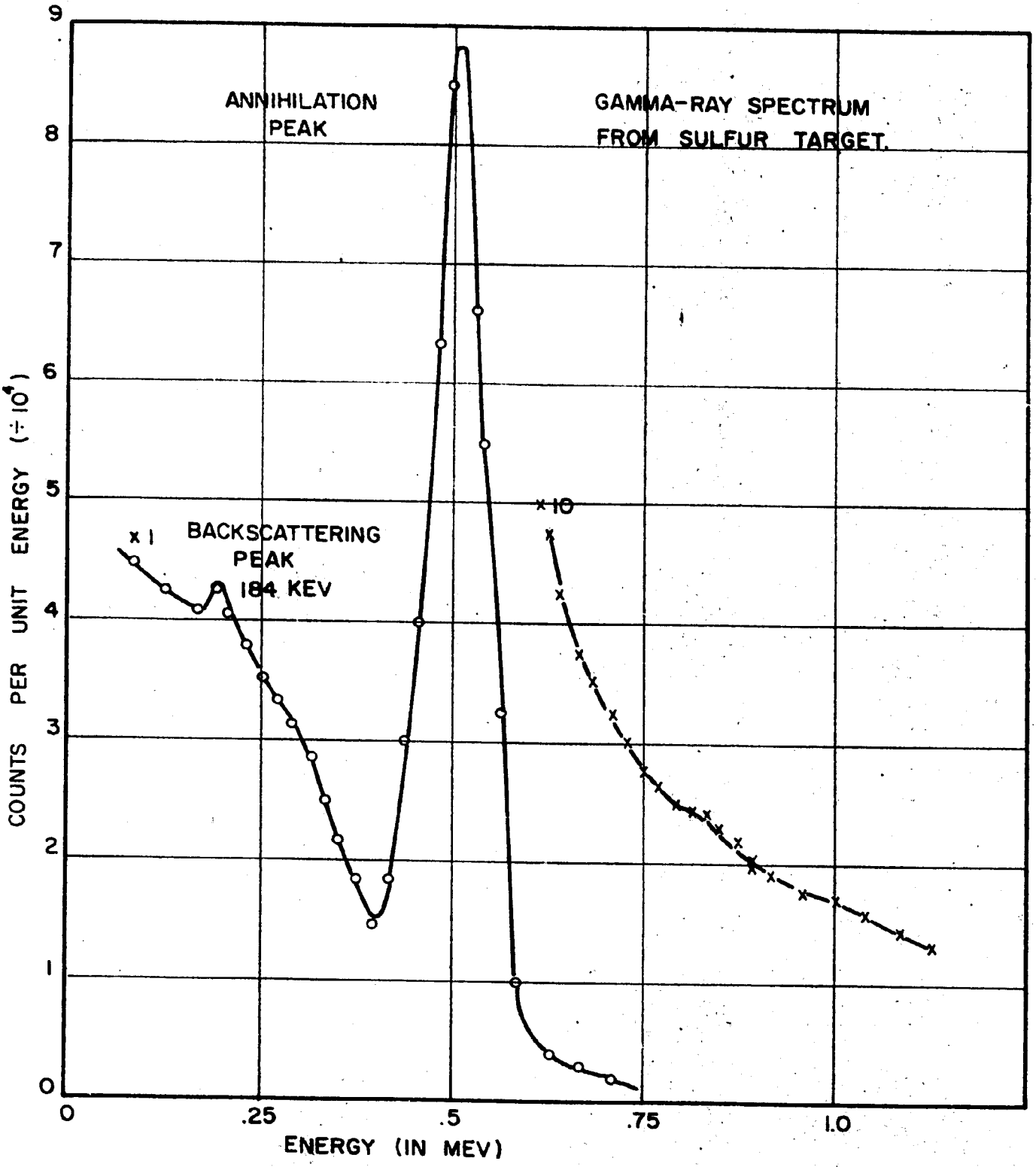


FIGURE 28. GAMMA-RAY SPECTRUM FROM SULFUR TARGET.
ENERGY REGION 0 → 1.0 MEV

for the positron decay from $P^{30}$ ensures that the decay is allowed, but unfavored. That there is no gamma transition accompaning the decay shows that it goes to the ($T = 1,0^+$) ground state of $Si^{30}$. Both the $\log_{10}ft$ value and the absence of a subsequent gamma transition indicate that the parent state in $P^{30}$ is a ($T = 0,1^+$) state.

The fact that no gamma-ray at 700 kev was found, even though a photopeak of three times less than the expected intensity could have been resolved from the background, would indicate an assignment of ($T = 0, J = 0$) for the level at .7 mev. Such an assignment is the only assignment consistent with all the previous information known about the state and with the additional information that the state was not fed by a branching in the decay from $S^{30}$. The missing ($T = 1,0^+$) state still has not been located. From Coulomb energy considerations (figure 2), the state should lie about 300 kev above the ground state. Moszkowski and Peaslee state that the level probably occurs about 0.5 mev above the ground state. Branching in the positron decay from $S^{30}$ should go to this state with the subsequent gamma-decay to the ground state. If the state were lower than 600 kev, the gamma-ray peak in the spectrum could not have been resolved from the background in this experiment, since the annihilation peak at .511 mev would completely mask it out.

C. $Si^{26}$ - $Al^{26}$ - $Mg^{26}$

1. Energy Level and Decay Schemes.

The lowest ($T = 0$) state of the self-conjugate nucleus in the nuclear triad with $A = 26$, $Al^{26}$, has a nucleon configuration which consists of a ($d\ 5/2$) particle in both the neutron and proton orbits.

The coupling rules of King and Peaslee[56] and Nordheim[17] predict a J value for this state of $5^+$. A ($T = 1, J = 0^+$) level should also occur among the low-lying states of $Al^{26}$, as in all the self-conjugate nuclei of the ($4n + 2$) triads. This level should be displaced in energy from the ground state of $Mg^{26}$ by about 4.4 mev (figure 2). Similarly, the ground state of $Si^{26}$ has been predicted[19] to lie 4.7 mev above the ($T = 1, 0^+$) state in $Al^{26}$. The first excited state of $Mg^{26}$ has been found at 1.83 mev and has been identified as a ($T = 1, J = 2^+$) level[57].

The two lowest-lying states in $Al^{26}$ (i.e. the $J = 5$ and the $J = 0$ levels) should be expected to present close competition for the position of the ground state. Positron decay from the ($J = 5^+$) state would most probably go to the ($J = 2^+$) level in $Mg^{26}$. Such a decay would be a second-forbidden transition, with $\log_{10} ft \approx 13$. Consequently, the half-life of the decay would be about $10^4$ years. Positron decay from the ($T = 1, 0^+$) state in $Al^{26}$ would be a superallowed decay to the ground state of $Mg^{26}$ with a half-life of about 7 seconds. If the ($J = 5^+$) state were the first excited state, then such a state would decay by M5 radiation to the ground state, with an estimated half-life of about 10 years, rather than directly to $Mg^{26}$ (through the $10^4$ year positron emission). If, however, the ($J = 5^+$) level were the ground state, then the two states in $Al^{26}$ would undergo independent positron decay to $Mg^{26}$. An energy level diagram for the nuclei $Si^{26}$, $Al^{26}$ and $Mg^{26}$ is shown in figure 29.

From the findings of Haslam, et al.[58], that the neutron yield from the reaction $Al^{27}(\gamma,n)\ Al^{26}$ was three times the positron yield,

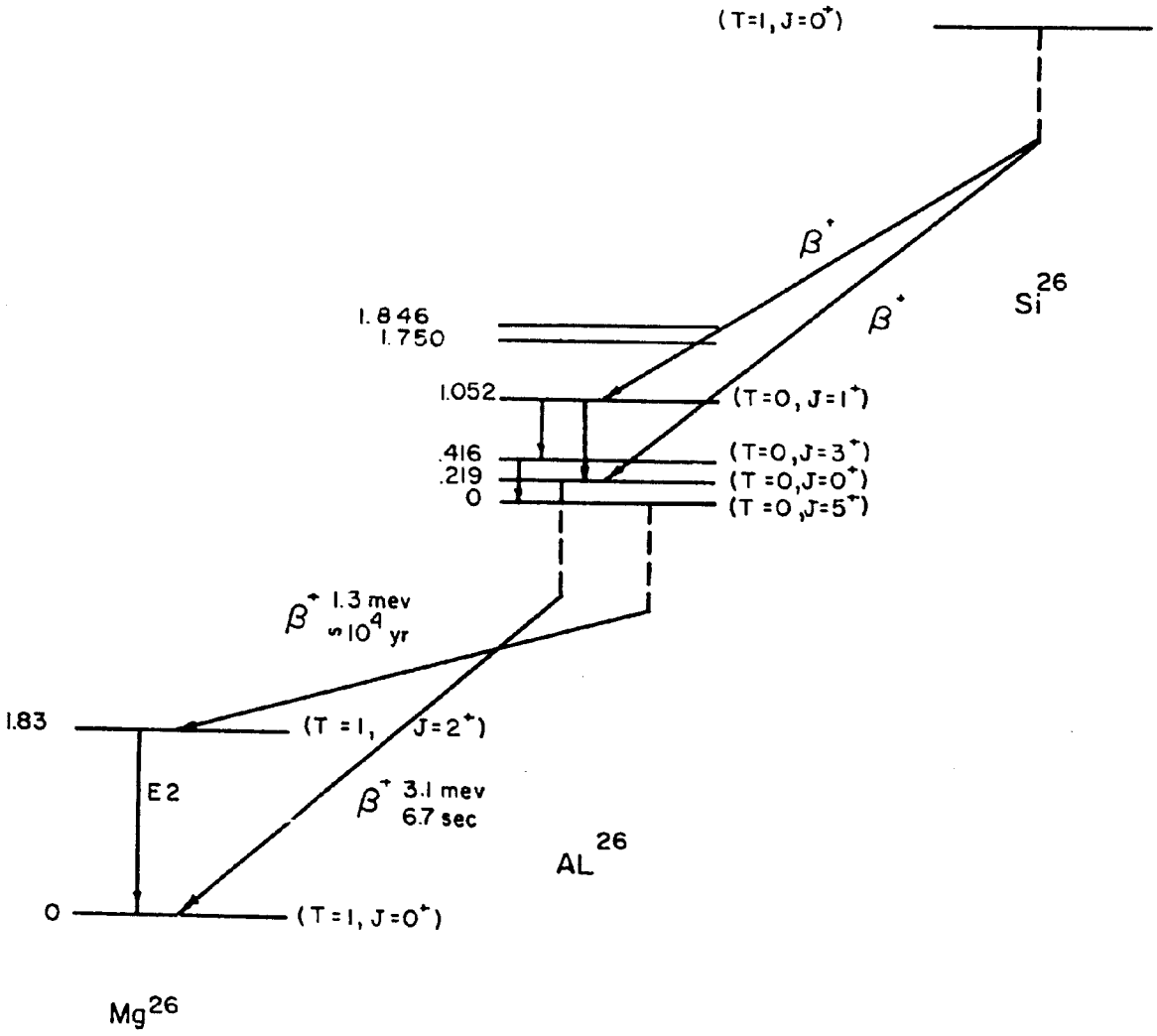


FIGURE 29. ENERGY LEVEL DIAGRAM FOR NUCLEI : $Mg^{26}$, $AL^{26}$, $Si^{26}$.

and also from the noted discrepancy between the Q value for reactions involving $Al^{26}$, and the positron decay energy, $E_{\beta^+} + 2m_oc^2$ [59], it has been shown that not only does the lowest-lying (T = 0) state in $Al^{26}$ have ($J = 5^+$), but that it is the ground state. Excited states in $Al^{26}$ have been found at .219 mev[60], .416 mev[60,61,62], 1.052 mev [60,62], 1.750 mev[60,62] and 1.846 mev[60,62]. The state at .416 mev was first stated to be the ($T = 1, J = 0^+$) state[61]. This assignment was later refuted by Browne[62] when it was produced by the reaction $Si^{28}$ (d,α) $Al^{26}$, which feeds only (T = 0) states. A later assignment of the level at .219 mev as the ($T = 1, 0^+$) level was consistent with the Q values for the creation of $Al^{26}$ and with the positron decay energy from the state[60]. The remainder of the excited states in $Al^{26}$ were tentatively identified[60] as shown in figure 29. The assignments were consistent with the data on the gamma-rays from the decay of these states, and with the coupling rules for the creation of low-lying states in the self-conjugate, odd-odd nuclei[27,25,56].

A long-lived positron activity in $Al^{26}$ has been recently observed [63,64] with a positron energy endpoint of 1.30 mev. These positrons were in coincidence with a 1.83 mev gamma transition. The positron transition was identified as the transition from the ($T = 0, 5^+$) ground state of $Al^{26}$ to the ($T = 1, 2^+$) excited state of $Mg^{26}$. The gamma-ray was the decay of the excited state.

The ground state of $Si^{26}$ is predicted to decay to the corresponding state in $Al^{26}$ with a half-life of 3.4 seconds and a positron endpoint energy of 3.6 mev[29]. If the assignment of the excited states of $Al^{26}$ [60] is correct, then a branching in the decay should also

occur to the ($T = 0,1^+$) state in $Al^{26}$. This excited state should decay by an M1 transition to the ($T = 1,0^+$) state. An alternative mode of decay would be a decay to the ($T = 0,3^+$) ground state by a cascade of E2 transitions via the ($T = 0,3^+$) state. The actual decay would be a competition between the two modes. Three gamma-rays should then be observed following the decay of $Si^{26}$; .416 mev, .638 mev, and .833 mev. The direct M1 transition to the ($1,0^+$) state should dominate over the E2 cascade by a factor of $10^4$, hence, for the intensity of the bombarding beam used in this experiment, only the 0.833 mev transition should be observed.

2. Experimental Results and Analysis

The results of the measurements of the decay radiation from the nuclei in the triad $Si^{26}$- $Al^{26}$- $Mg^{26}$ are listed in Table III.

Aluminum

A decay curve for the positron decay from a target of silicon powder, bombarded by the x-ray beam, is shown in figure 30. The decay curve is seen to be that of a complex decay, containing two components with half-lives of 6.7 and 4.3 seconds. The 6.7 second component is that from the decay of $Al^{26}$, while the other represents the decay of $Si^{27}$. These two active nuclei were created by $(\gamma,n^dp)$ and $(\gamma,n)$ reactions respectively on the target of silicon powder.

Silicon, in its natural form, has three stable isotopes, $Si^{28}$ $Si^{29}$, and $Si^{30}$, with relative abundances of 92.3%, 4.7%, and 3.0% respectively. Only photonuclear reactions on $Si^{28}$ could produce positron activity in any measurable quantity. The $(\gamma,n)$ reaction produces $Si^{27}$, a positron-unstable mirror nucleus with a decay half-life of about 4.5 seconds. A $(\gamma,2n)$ reaction would produce $Si^{26}$, a

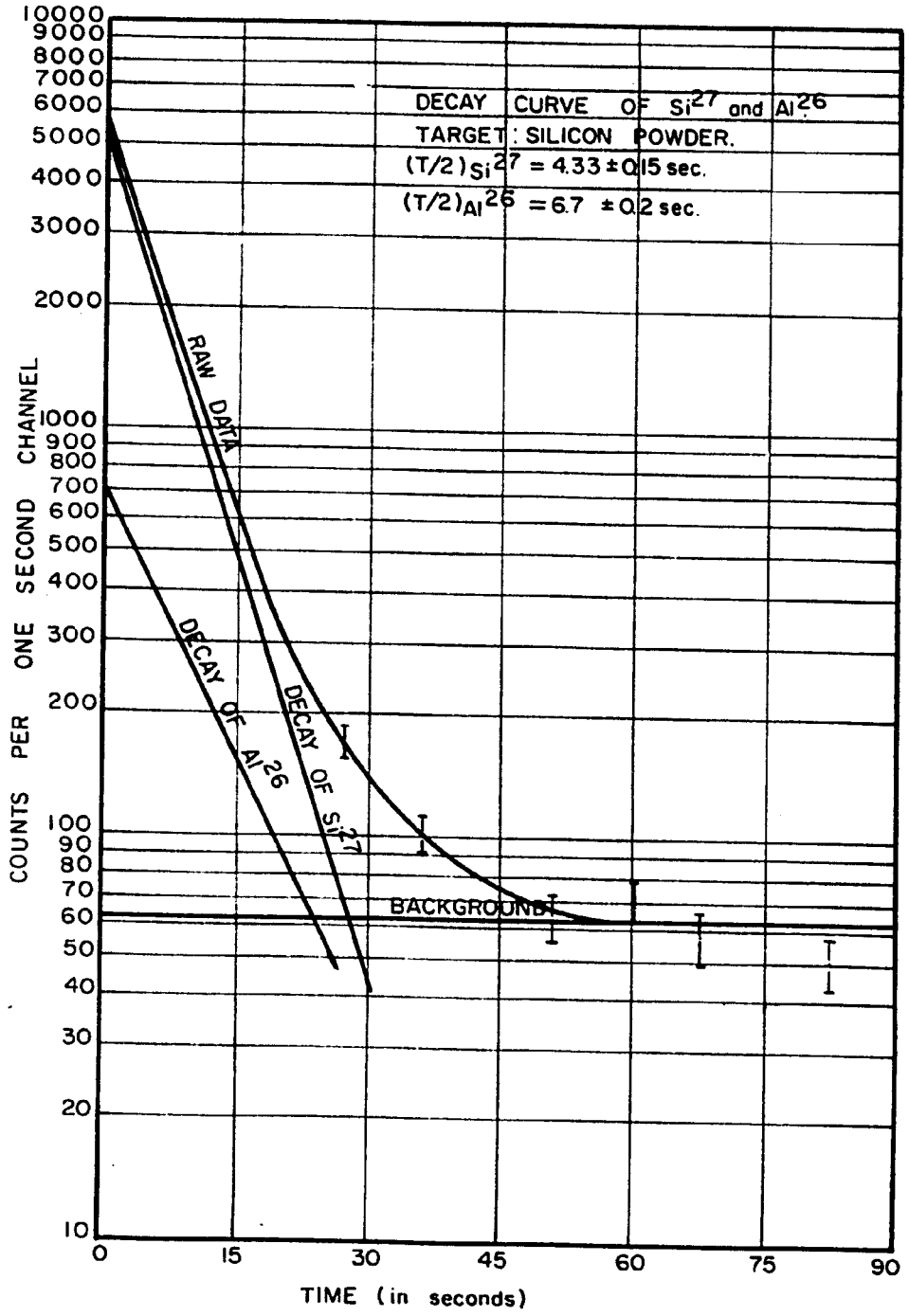


FIGURE 30. DECAY CURVE FOR $Si^{27}$ and $Al^{26}$ FOR 85 mev BOMBARDING ENERGY.

TABLE III

Results of the Measurements of the Decays From the Nuclei in the Nuclear Triad with ( A = 26)

| TARGET ISOTOPE | GAMMA-RAY ENERGY | MEASURED HALF-LIFE OF GAMMA-RAY | POSITRON ENDPOINT ENERGY | $\log_{10} ft$ | ASSIGNMENT OF TRANSITION |
|---|---|---|---|---|---|
| $Si^{28.29.30}$ | $m_o c^2$ | 6.70 ± 0.20 sec.<br>6.60 ± 0.19 sec.<br>6.75 ± 0.22 sec.<br>avg.<br>6.68 ± 0.12 sec. | 3.08 ± .19 mev<br>3.13 ± .19 mev<br>3.10 ± .19 mev<br>avg.<br>3.11 ± .11 mev | 3.38±.07 | $(0^+ \rightarrow 0^+)$ super-allowed transition from $Al^{26m}$ to ground state of $Mg^{26}$. |
| $Si^{28.29.30}$ | 1.28mev | 6.6 minutes | ----- | ----- | decay of $Al^{29}$ |
| $Si^{28.29.30}$ | 1.78mev | 2.3 minutes | ----- | ----- | decay of $Al^{28}$ |

proton-rich (A = 4n + 2) nuclei whose decay half-life has been predicted to be 3.4 seconds. The $(\gamma,p)$ and $(\gamma,2p)$ reactions produce $Al^{27}$ and $Mg^{26}$ respectively, both stable nuclei, and the $(\gamma,n^dp)$ reaction produces $Al^{26}$. Thus, it is seen that the measured decay curve of the radiations from the silicon target should represent only the decays from $Si^{26}$, $Si^{27}$, and $Al^{26}$. $Si^{26}$ should be present in approximately 3% abundance relative to the amount of $Si^{27}$ present, and hence, the decay from $Si^{26}$ should not have been able to be resolved from the decay from $Si^{27}$. Such was the case, and the measured half-life of $Si^{27}$ is felt to be slightly in error (about 1%) due to this presence of $Si^{26}$.

A measurement of the positron energy spectrum was made using a target of three mil aluminum foil. A Kurie plot of the spectrum, figure 31, shows a straight line intersecting the energy axis at 3.11 mev. The spectrum was expected to contain little contamination

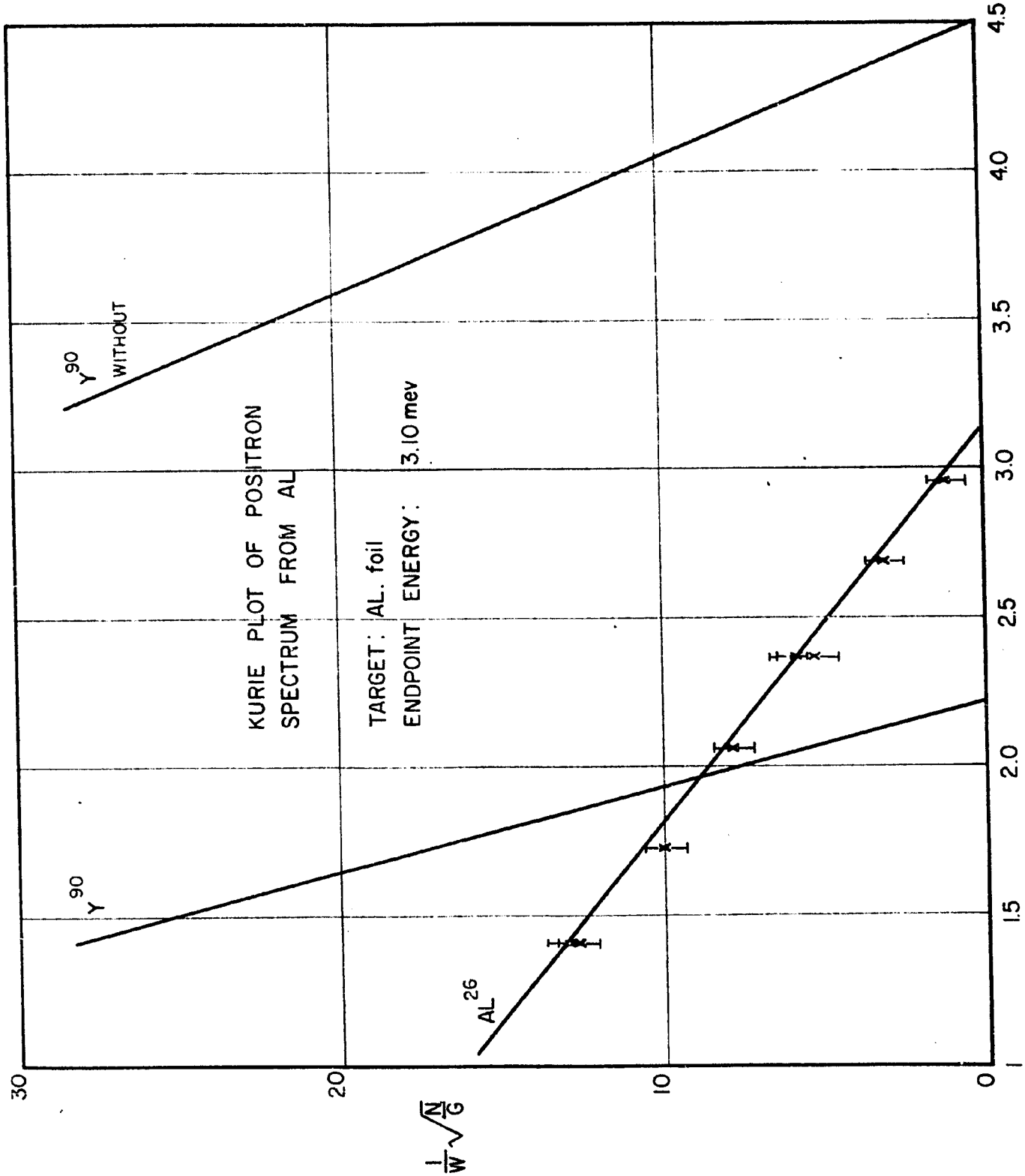


FIGURE 31. KURIE PLOT OF POSITRON SPECTRUM FROM $AL^{26}$

from other decays. The target was 100% $Al^{27}$ and the only other beta emitters, beyond $Al^{26}$, produced by photonuclear reactions on such a target (in any measurable quantity) would be $Al^{25}$ and $Na^{25}$, both expected to be present in 3% abundance relative to $Al^{26}$.

Silicon

The gamma-ray spectrum, taken after the bombardment of a target of silicon powder, showed gamma-rays of three energies, .511, 1.28, and 1.78 mev. Half-life measurements were made on the photo peaks at 1.28 and 1.78 mev and yielded the results of 6.6 minutes and 2.3 minutes respectively. The gamma rays were thus identified as being from $Al^{29}$ and $Al^{28}$. The relative heights of the three peaks was consistent with the relative abundance of the three stable isotopes of silicon. The active aluminum isotopes were thus created by a $(\gamma,p)$ reaction on $Si^{29}$, and $Si^{30}$, and by the $(\gamma,n^dp)$ reaction on $Si^{30}$ and $Si^{28}$. The contaminating gamma-rays were present in quantities about 7 times greater than the expected intensity of the 0.833 mev transition in $Al^{26}$. In addition, the peak for an 833 kev gamma-ray would occur just short of the Compton edge of the 1.28 mev peak. Hence, it was felt that the presence of any radiation with an energy of 833 kev and with an intensity expected in this experiment would not have been resolved from the background. No attempt was made to observe the 1.83 mev transition in $Mg^{26}$ following the decay from the $(J = 5^+)$ ground state in $Al^{26}$.

3. Summary and Conclusions.

The results of the measurements made on the nuclei in the isobaric chain $Si^{26}$ - $Al^{26}$ - $Mg^{26}$ are consistent with the level scheme shown in

figure 29. The value for $\log_{10}$ft of 3.4 for the 6.7 second transition shows that the positron decay is, indeed, a $(0^+ \rightarrow 0^+)$ superallowed transition. The attempt to completely identify the level at 1.052 as a $(T = 0, 1^+)$ level, by observing the decay from this level following a branching in the decay from $Si^{26}$ to the level, failed due to the contaminating presence of $Al^{28}$ and $Al^{29}$.

D. Decay From the Mirror Nuclei, $Ca^{39}$, $S^{31}$, $Si^{27}$.

When $Ca^{40}$, $S^{32}$, and $Si^{28}$ are bombarded with the 85 mev bremsstrahlung beam in an attempt to produce the positron unstable isotopes $Ca^{38}$, $S^{30}$, and $Si^{26}$ by the $(\gamma,2n)$ reaction, the mirror nuclei, $Ca^{39}$, $S^{31}$, and $Si^{27}$ are produced in great quantity by the dominant $(\gamma,n)$ reaction. This reaction has a total integrated cross-section roughly 20 times the cross-section for the $(\gamma,2n)$ reaction and about twice that for the $(\gamma,n^dp)$ reaction. Although the primary aim of this research was to study the $(4n + 2)$ nuclei, the mirror nuclei were studied as well. This was done due to the fact that the mirrors were produced as an abundant by-product, and the fact that the positron transition from these nuclei, although not $(0^+ \rightarrow 0^+)$ transitions as in the $(4n + 2)$ nuclei, are, nevertheless, superallowed transitions and, as such, are of considerable interest.

1. Energy Level and Decay Schematics

The low-lying energy levels in the mirror nuclei are formed from one particle configurations, this particle being either a hole or an extra particle in the outer nucleon orbit. For the beta-unstable member of the pairs, there is an excess of protons. This excess occurs either as a single proton in a nucleon orbit in conjunction with a

closed neutron orbit, or as a single hole in the outer neutron orbit in conjunction with a closed proton orbit. In either case, the excess proton is transformed into a neutron with the emission of a positron. The nuclear configuration for the transformed nucleus is then identical to that for the original nucleus except that the extra proton is now a neutron. There should be complete overlap of the nuclear wave functions even considering the effect of spin-dependent nuclear forces. The level schemes in the mirror pairs should be identical except for the Coulomb differences which would raise the levels in the proton-rich member several mev above the corresponding levels in the neutron-rich member.

The ground states of the mirror pair $Ca^{39}$ and $K^{39}$ arise from a nucleon configuration of a single hole in the (1d 3/2) shell and would, consequently, be ($T = 1/2, J = 3/2^+$) states. The ground state of both $S^{31}$ and $P^{31}$ is formed from a single particle in the (2s1/2) shell and would have ($T = 1/2$, $J = 1/2^+$). Similarly, $Si^{27}$ and $Al^{27}$ ground states are formed from a (1d 5/2) hole and are ($T = 1/2$, $J = 5/2^+$) states.

Since the ground states in the mirror pairs are the states corresponding to an isobaric-spin doublet nuclear eigenfunction, the Fermi nuclear matrix element for the beta transition between the states does not vanish, but assumes the value of 1 for all cases (from equation III-5). The evaluation of the Gamow-Teller nuclear matrix element depends upon the ground state configuration and, hence, is different in all cases. These matrix elements have been evaluated using Wigner coupling which assumes spin-independent nuclear forces,

and Mayer Jensen coupling (equation III-6). The results are listed in Table IV, for the three transitions studies. In these cases, the results for Wigner coupling and Mayer-Jensen coupling are the same. The $\log_{10} ft$ values were then computed from equation III-8.

TABLE IV

Theoretical Values of the Nuclear Matrix Elements for the Positron Decay of the Mirror Nuclei, $Ca^{39}$, $S^{31}$, and $Si^{27}$

| PARENT NUCLEUS | DAUGHTER NUCLEUS | NUCLEON CONFIGURATION GIVING RISE TO GROUND STATE | $\lvert\int 1\rvert^2$ | $\lvert\int \sigma\rvert^2$ j-j | $\lvert\int \sigma\rvert^2$ L-S | $\log_{10} FT$ |
|---|---|---|---|---|---|---|
| $_{14}Si^{27}_{13}$ | $_{13}Al^{27}_{14}$ | (1d 5/2) hole | 1.0 | 1.4 | 1.4 | 3.55 |
| $_{16}S^{31}_{15}$ | $_{15}P^{31}_{16}$ | (2 s 1/2) hole | 1.0 | 3.0 | 3.0 | 3.22 |
| $_{20}Ca^{39}_{19}$ | $_{19}K^{39}_{20}$ | (1d 3/2) hole | 1.0 | 0.6 | 0.6 | 3.95 |

2. Experimental Results and Analysis

The results of the measurements of the decay from the mirror nuclei are shown in Table V.

Half-Life Measurements

Calcium$^{39}$ was formed by a $(\gamma,n)$ reaction on calcium$^{40}$. A typical decay-curve from which a determination of the half-life of the decay is made is shown in figure 32. Included in this decay curve, however, was the decay from $K^{38m}$ which had a half-life of 0.95 seconds. $K^{38m}$ was created along with $K^{38}$, by the reaction $Ca^{40}(\gamma,n^d p)\ K^{38m}$. The

TABLE V

| TARGET ISOTOPE | GAMMA-RAY ENERGY | POSITRON ENDPOINT ENERGY | MEASURED HALF - LIFE OF GAMMA-RAY | ADJUSTED VALUE OF HALF-LIFE | $LOG_{10}ft$ | ASSIGNMENT OF TRANSITION |
|---|---|---|---|---|---|---|
| $Ca^{40}$ | $m_oc^2$ | 5.70 ± 0.30 mev<br>5.55 ± 0.30 mev<br>5.49 ± 0.30 mev<br>avg.<br>5.58 ± 0.17 mev | 0.894 ± 0.016 sec.<br>0.904 ± 0.012 sec.<br>0.865 ± 0.015 sec.<br>avg.<br>0.888 ± 0.008 sec. | 0.876 ± 0.008 seconds | 3.65 ± 0.06 | mirror transition from $Ca^{39}$ to $K^{39}$. |
| $S^{32}$ | $m_oc^2$ | 4.51 ± 0.27 mev<br>4.75 ± 0.28 mev<br>4.58 ± 0.27 mev<br>avg.<br>4.61 ± 0.16 mev | 2.78 ± 0.03 sec.<br>2.60 ± 0.03 sec.<br>2.68 ± 0.03 sec.<br>avg.<br>2.72 ± 0.02 sec. | 2.80 ± 0.03 seconds | 3.79 ± 0.07 | mirror transition from $S^{31}$ to $P^{31}$. |
| $Si^{28}$ | $m_oc^2$ | 3.80 ± 0.22 mev<br>3.77 ± 0.22 mev<br>3.70 ± 0.22 mev<br>avg.<br>3.76 ± 0.13 mev | 4.33 ± 0.15 sec.<br>4.27 ± 0.16 sec.<br>4.39 ± 0.16 sec.<br>avg.<br>4.33 ± 0.12 sec. | ------- | 3.41 ± 0.07 | mirror transition from $Si^{27}$ to $Al^{27}$. |

TABLE V

Results of the Measurements of
the Decays from the Mirror Nuclei

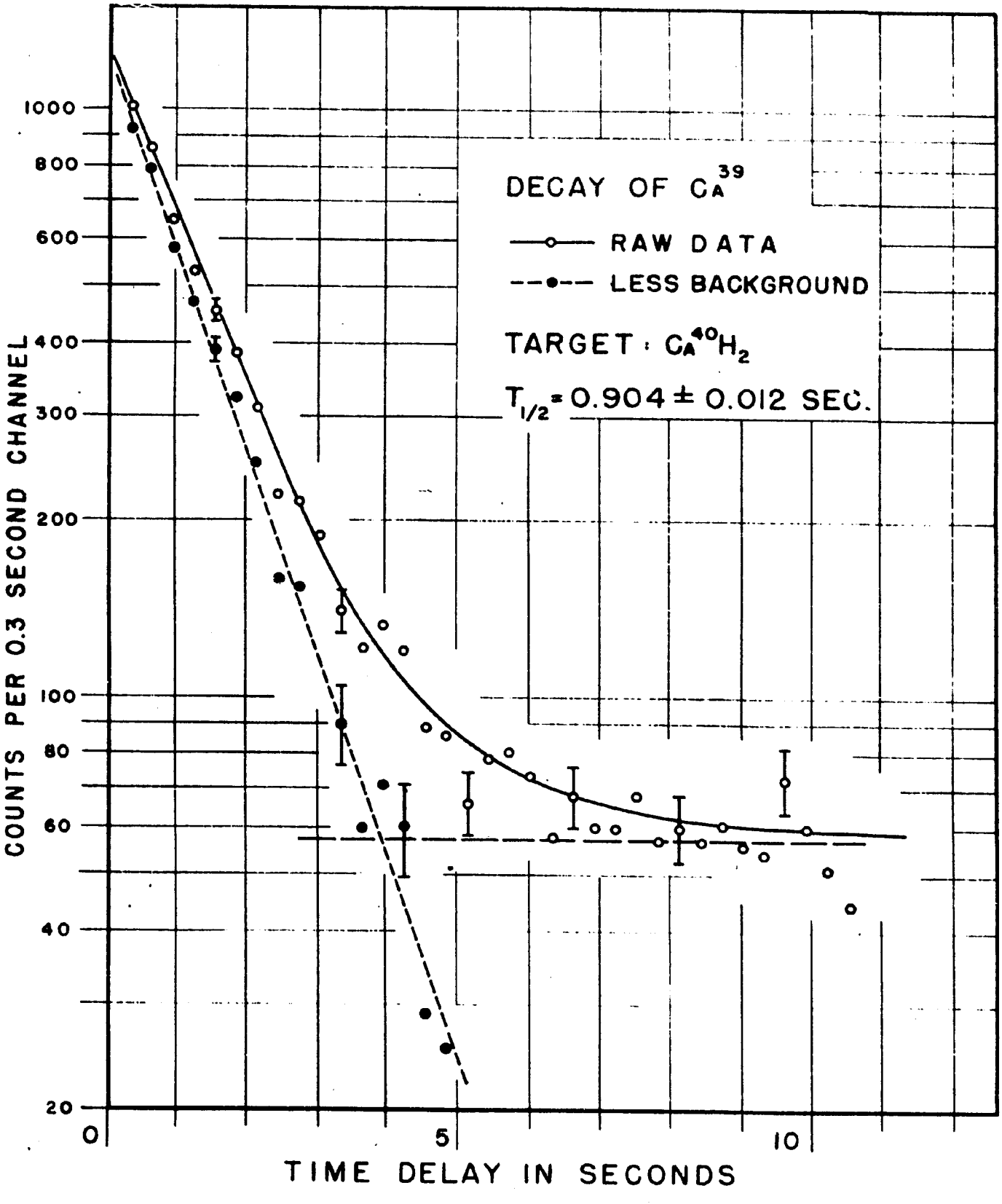


FIGURE 32. DECAY CURVE FOR $Ca^{39}$

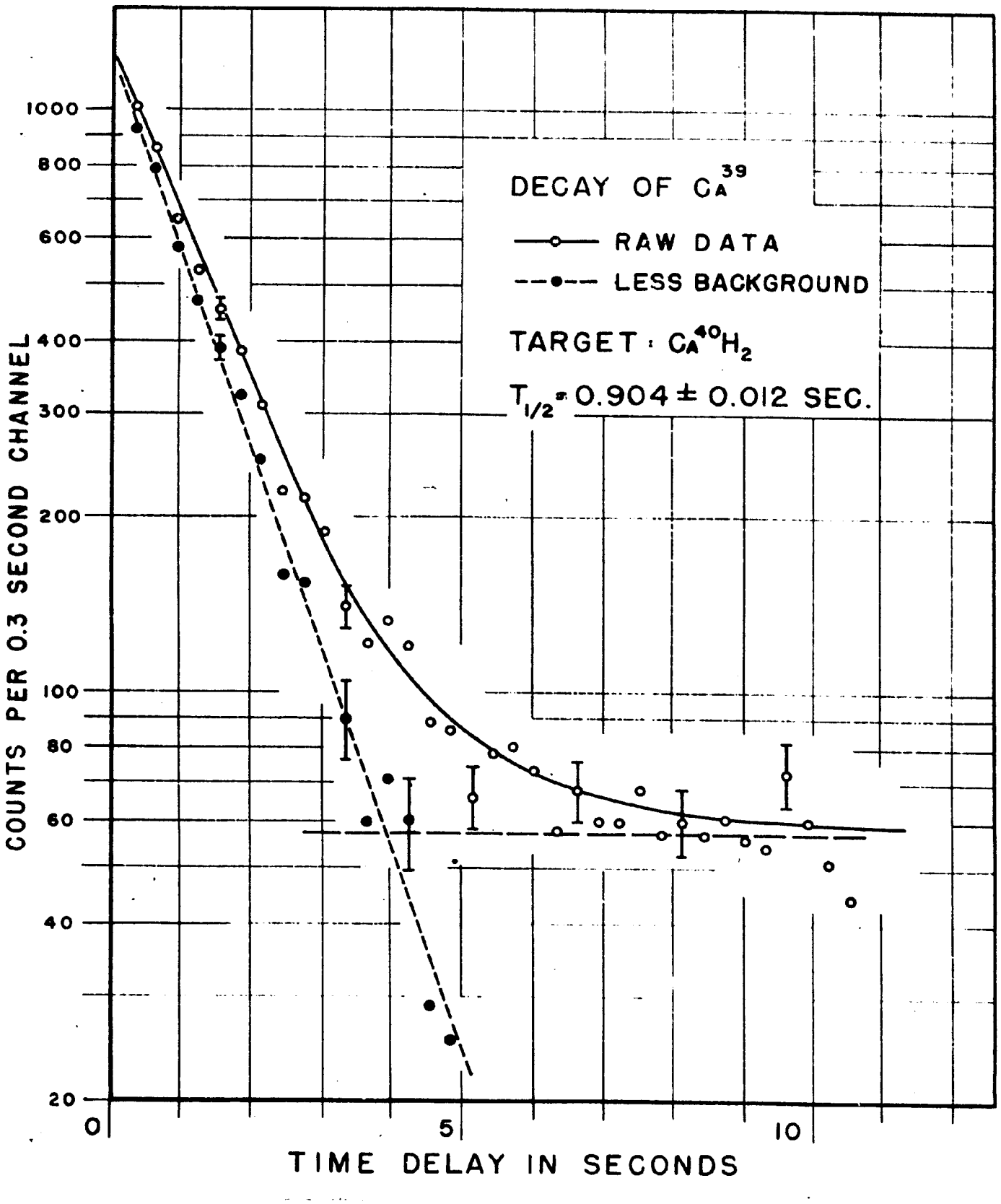


FIGURE 32. DECAY CURVE FOR $Ca^{39}$

amount of $K^{38}$ that was present, in relation to the amount of $Ca^{39}$, could be calculated from a measurement of the amount of the 7.67 minute background in the decay-curve of the radiation from $Ca^{39}$. It was impossible to know exactly the relative amounts of $K^{38m}$ and $K^{38}$ background that was created by the $(\gamma,n^dp)$ process. Such a ratio could be calculated, however, for the relative creation of these states by the $(\gamma,n)$ reaction on $K^{39}$. This has been done, and the value for the ratio of ($K^{38}$ : $K^{38m}$ 2.1: 1.0) has been used to estimate the relative creation of the two states by the $(\gamma,n^dp)$ reaction on $Ca^{40}$. The value of the measured half life for $Ca^{39}$ has been adjusted, using the above ratio to compute the amount of $K^{38m}$ contamination in the curve. The adjusted value is also shown in table V. There is no a priori reason why the rel tive abundances of $K^{38m}$ and $K^{38}$ should be the same when produced by the two reactions. It was, nevertheless, felt that the ratio for the production of the two states of $K^{38}$ should be of the same order for both reactions.

The .66 second positron activity from $Ca^{38}$ would also contribute some short lived contamination in the decay-curve. However, since $Ca^{38}$ is thought to be produced in a quantity about 3% of the amount of $Ca^{39}$ produced, and is accompanied in the main by the .95 second decay of $K^{38m}$, the effect the presence of $Ca^{38}$ on the half-life determination is thought to be negligible. Since $Ca^{39}$, $Ca^{38}$, and $K^{38m}$ are the only positron emitters produced in any measurable quantity from the bombardment of calcium, the adjusted half-life is thought to be the true half-life of $Ca^{39}$.

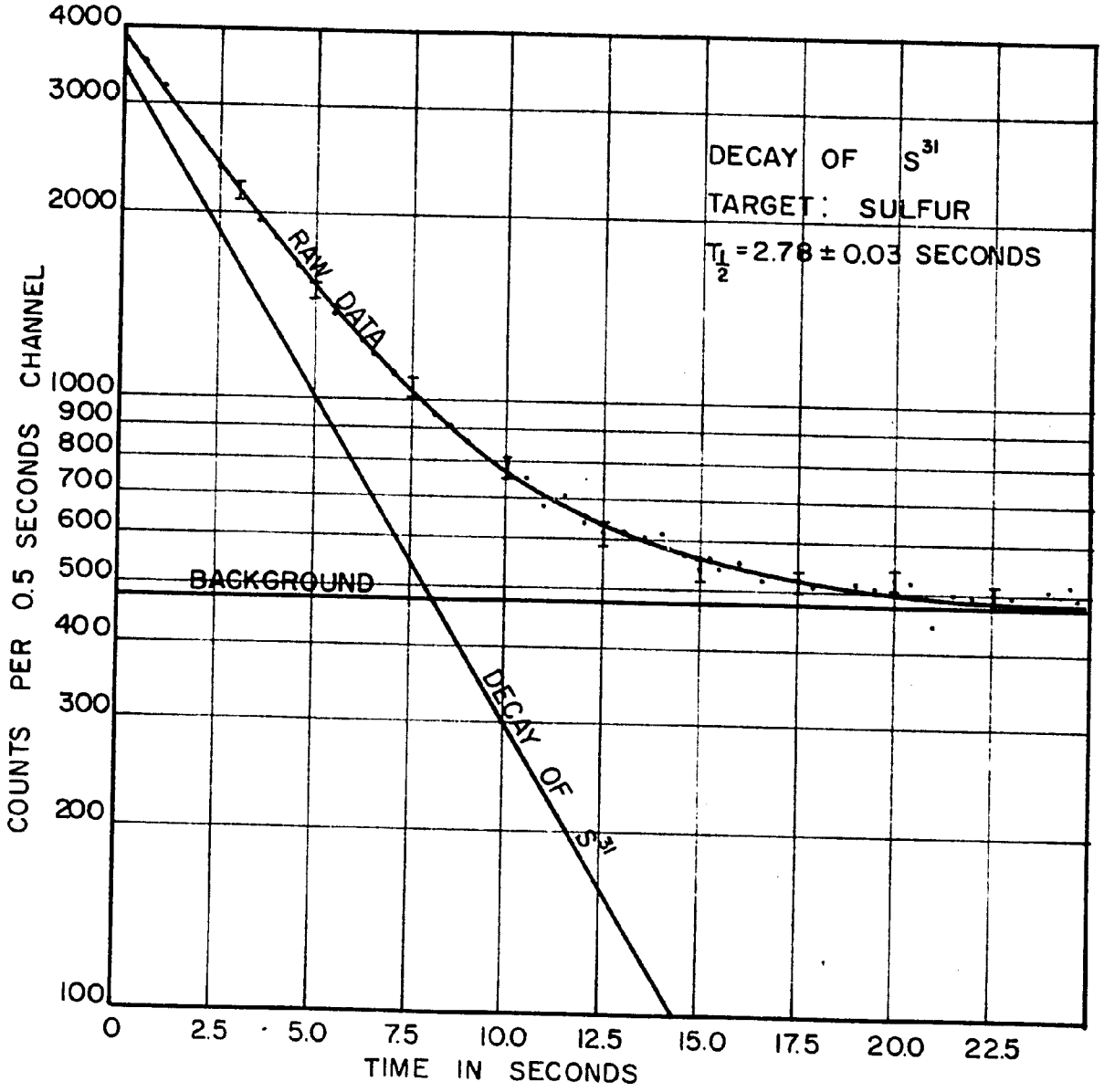


FIGURE 33. DECAY OF $S^{31}$

The mirror nucleus $S^{31}$ was formed by the reaction $S^{32}$ $(\gamma,n)$ $S^{31}$. A half-life curve for the decay from $S^{31}$ is shown in figure 33. The half-life of 2.72 seconds, as determined from an analysis of the data, would be contaminated only by the estimated half-life of 1.8 seconds from the decay of $S^{30}$. The amount of $S^{30}$ created in the target should represent a contamination of about 3%, which would make an upward adjustment in the half-life of $S^{31}$ of 2.9%. This would make the adjusted value, 2.80 seconds.

The mirror isotope of silicon, $Si^{27}$, was produced by the reaction $Si^{28}$ $(\gamma,n)$ $Si^{27}$. The competing $(\gamma,n^dp)$ photonuclear reaction produced $Al^{26}$ which has a half-life of 6.7 seconds. This value of 6.7 seconds was sufficiently different from the 4.3 second half-life of $Si^{27}$ to be resolved, but the two values were too close to be resolved well enough to attain the accuracy reached in the other half-life measurements in this research. The errors attached to the results are therefore significantly higher than in the other measurements. The decay curve was shown in figure 32. The value of 4.3 seconds should also be adjusted for contamination due to the predicted presence of $Si^{26}$ which should be present in 3% abundance, and is assumed to have the predicted half-life of 3.5 seconds. However, since this would amount to only a 0.6% correction to data which has a quoted error of 3%, an adjustment was not made on the measured half-life.

## Endpoint Measurements

Kurie plots for the positron spectra from $Ca^{39}$, $S^{31}$, and $Si^{27}$ are shown in figure 34 along with the Kurie plot of the $Y^{90}$ spectrum, taken with and without an attenuator. It is noticed that all of these spectra

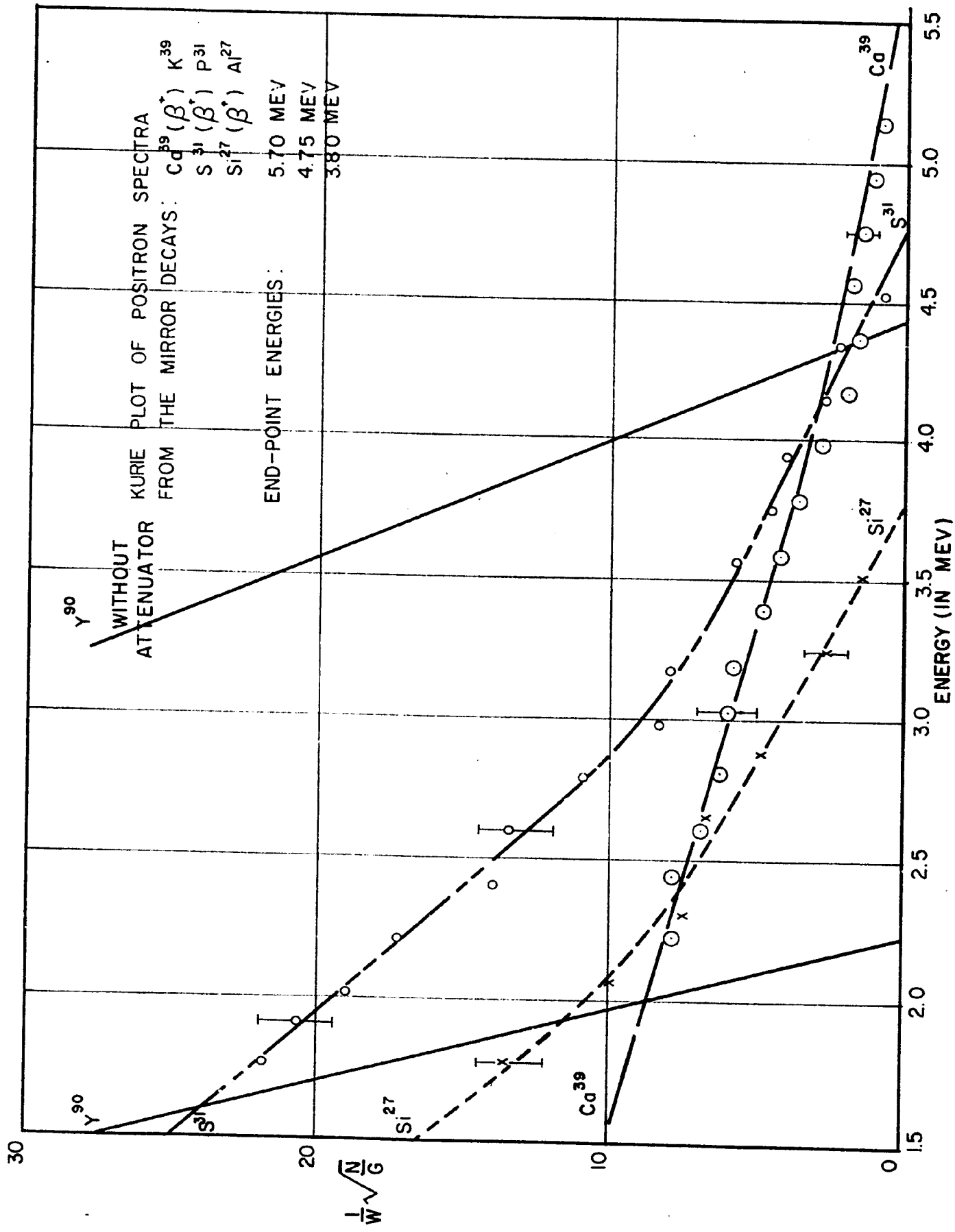


FIGURE 34. KURIE PLOTS OF THE POSITRON SPECTRA FROM THE MIRRORNUCLEI

exhibit the shape of a complex spectrum. The two components of these spectra are the decays from the product nuclei of the $(\gamma,n)$ and $(\gamma,n^{d}p)$ reactions. In all cases, the decay from the mirror nuclei had the higher endpoint energy. Since only the mirror decays were to be analyzed from these spectra, only the high energy component was of interest and the spectra were not accurately resolved into their components any more than was necessary to establish the origin of the curvature in the Kurie plot.

3. Summary and Conclusions.

The results as shown in table V show values of $\log_{10}ft$ which indicate that the transitions are allowed and favored. That the results do not agree exactly with the theoretical predictions is not considered to be a difficulty, as the agreement is not bad. The values are consistent with the work done at Iowa State College by Zaffarano et al.[65,66,41].

## CHAPTER VI

## RELATIVE YIELDS FROM THE $(\gamma,n)$ AND THE $(\gamma,n^dp)$ REACTIONS ON $Ca^{40}$, $S^{32}$ and $Si^{28}$

The first experimental evidence that high-energy photons could produce nuclear disintegrations was presented by Chadwick and Goldhaber[67] in 1934. It was shown that the deuteron could be split into its neutron and proton components with gamma-rays. Since this initial experiment, there have been numerous additional measurements of the cross-sections for photonuclear reactions. The experimental results have indicated that the photon absorption cross-section for all elements, as a function of energy, except hydrogen, consists of a pronounced peak in the neighborhood of 20 mev, and a flat tail at higher energies[68,69,70]. To describe these processes of photonuclear disintegrations, several theories were proposed. Of these theories, the compound nucleus theory of Bohr[71] has been the most successful. In this theory the disintegration process and the absorption process are assumed to be completely independent processes. The absorption process has been found to be basically a dipole absorption process[49]. Probably the most satisfactory model for the decay of the compound nucleus is the statistical model of Weisskopf and Ewing[72]. In this theory, the excited nucleus is presented as a high temperature nucleon gas, with all the nucleons sharing the energy. In such a nucleus, there would be a constant interchange of energy, and eventually a particular nucleon would be "boiled-off" and escape from the nucleus. For high excitation energies additional particles may be emitted until the final nucleus has disposed of all the excess energy.

Although much information has been obtained concerning single nucleon emission processes, relatively little experimental information is available concerning the processes of multiple nucleon emission. This lack of information is due chiefly to the difficulty of separating the reaction products from those of the single neutron or proton reactions. Cross-sections for the $(\gamma,2n)$ reactions have been studied in copper[44], nitrogen[73], and tantalum[74,75]. It was found that the $(\gamma,2n)$ cross-section as a function of energy exhibits a resonance peak which occurs in the high energy tail of the $(\gamma,n)$ cross-section resonance. The height of the $(\gamma,2n)$ resonance peak was about 20% of that for the $(\gamma,n)$ reaction. Several other multiple nucleon photonuclear disintegrations have been studied; among them being the $(\gamma,\alpha)$ reaction and the $(\gamma,3n)$ reaction in various nuclei.

A. Deuteron Emission Photonuclear Reactions.

The multiple nucleon emission process with the highest reaction cross-section is that for the ejection of a deuteron (or a neutron and a proton) from a nucleus. Three experiments have been carried out which indicate that more deuterons are emitted in photonuclear reactions than would be expected from considerations of the statistical theory of nuclear reactions[72]. The reactions $S^{32}$ $(\gamma,n^dp)$ $P^{30}$ may readily be detected at energies down to the photodeuteron threshold;[45,76] only one mev above this threshold the $(\gamma,d)$ to $(\gamma,p)$ cross-section ratio reaches the value 0.001[77]. Byerly and Stephens[78] found that the ratio of deuterons to protons produced in copper irradiated with 24 mev bremsstrahlung is 0.31. For 65 mev x-rays, this ratio rises to 0.5[48]. These ratios are several orders of magnitude larger than the statistical theory would predict[78].

The observed cross-sections, when plotted as a function of energy, have a shape characteristic of a double peak. For this reason the curve is assumed to be a superpositron of the curves for the $(\gamma,d)$ and $(\gamma,np)$ reactions[79]. The threshold for the $(\gamma,np)$ reaction in Cu is higher than that for the $(\gamma,d)$ reaction by 2.18 mev[79]. This is simply the binding energy of the deuteron.

B. Results and Analysis.

In this experiment, the decay-curves obtained after the bombardment of $Ca^{40}$, $S^{32}$, and $Si^{28}$ could be used to calculate the relative yields for the $(\gamma,n^dp)$ and $(\gamma,n)$ reactions on these isotopes. The calculations are based, not upon a direct measurement of the neutrons and deuterons created by the reactions, but upon a measurement of the relative amounts of the reaction product nuclei present in the target sample. The measurements, therefore, represent the ratio of the yield from the $(\gamma,np)$ and $(\gamma,d)$ reactions to that from the $(\gamma,n)$ reaction rather than the ratios from the $(\gamma,d)$ reaction alone. The results of the calculations are given in Table VI.

For two of the isotopes bombarded, the reaction products of the $(\gamma,n)$ and $(\gamma,n^dp)$ reactions have half-lives which are significantly different, and had to be measured on different time scales. The background after the decay of the shorter half-life had to be broken up into its components, namely those of the true background (infinite half-life) and of the longer-lived decay. By a careful analysis of this background after the long-lived nuclei were gone, such a division could be made. The relative abundance of the short-lived nuclei and the long lived nuclei could then be calculated by correcting the observed ratio for the effects of half-life differences

TABLE VI

| TARGET ISOTOPE | PEAK BREMSSTRAHLUNG ENERGY | YIELD-RATIO $\frac{Y_d}{Y_N}$ | ADJUSTED YIELD-RATIO |
|---|---|---|---|
| $Ca^{40}$ | 85 mev | 0.16 ± 0.03<br>0.17 ± 0.03<br>0.17 ± 0.03<br>avg.<br>0.17 ± 0.02 | 0.40 ± 0.05 |
| $S^{32}$ | 85 mev | 0.41 ± 0.09<br>0.43 ± 0.09<br>0.45 ± 0.09<br>avg.<br>0.43 ± 0.05 | ----- |
| $Si^{28}$ | 85 mev | 0.16 ± 0.06<br>0.17 ± 0.06<br>0.15 ± 0.06<br>avg.<br>0.16 ± 0.04 | ----- |
| | 60 mev | 0.16 ± 0.05<br>0.10 ± 0.05<br>0.13 ± 0.05<br>avg.<br>0.13 ± 0.03 | ----- |
| | 40 mev | 0.11 ± 0.05<br>0.09 ± 0.04<br>0.12 ± 0.05<br>avg.<br>0.11 ± 0.03 | ----- |

for the effect of using the interrupted beam cycle procedure (Section IV-D-2) to obtain the decay curve.

Such a correction factor may be calculated from equation IV-12. This gives as the total number of active nuclei (with a particular half-life) in the target after an infinite number of operation cycles (consisting of $\underline{k}$ peaking strip pulses bombarding time and $\underline{p}$ peaking strip pulses observation time),

$$N = \alpha_\gamma \left(\frac{e^{-\lambda\gamma t_o} - e^{-k\lambda\gamma t_o}}{1 - e^{-\lambda\gamma t_o}}\right) e^{-p\lambda\gamma t_o}\left(\frac{1}{1-e^{-\lambda\gamma(k+p)t_o}}\right) + \alpha_\gamma\left(\frac{e^{-\lambda\gamma t} - e^{-k\lambda\gamma t_o}}{1 - e^{-\lambda\gamma t_o}}\right) \qquad \text{VI-1}$$

$\alpha_\gamma$ is the number of nuclei created per 30 μ-sec beam pulse, $\lambda_\gamma$ is the decay-constant of nuclei in question, and $t_o$ is the time between pulses.

Therefore, the number of counts from type $\gamma$ nuclei in the first channel is given by

$$N_\gamma = \frac{(20t)}{(k+p)} \lambda_\gamma N t' \epsilon \qquad \text{VI-2}$$

where t = length of run in seconds, $t'$ is the length of the time channel in seconds and $\epsilon$ is the proportionality factor. $\alpha_\gamma$, is the number of nuclei of type $\gamma$ created in each beam pulse, is now given by

$$\alpha_\gamma = \frac{N_\gamma(k+p)}{t'(20t)\lambda_\gamma\epsilon}\left(\frac{1}{\left[\frac{e^{-p\lambda\gamma t_o}(e^{-\lambda\gamma t_o} - e^{-k\lambda\gamma t_o})}{(1-e^{-\lambda\gamma t_o})(1-e^{-\lambda\gamma(k+p)t_o})} + \frac{(e^{-\lambda\gamma t_o} - e^{-k\lambda\gamma t_o})}{(1 - e^{-\lambda\gamma t_o})}\right]}\right) \qquad \text{VI-3}$$

$\frac{\alpha_{\gamma_1}}{\alpha_{\gamma_2}}$ is then the ratio of the number of nuclei created with decay-constant $\lambda_\gamma$, per beam pulse, to the number of nuclei created with decay-constant $\lambda_{\gamma_2}$

If the nuclei with decay-constant $\lambda_{\gamma_1}$ were created by the $(\gamma,n^dp)$ reaction, and the nuclei with decay-constant $\lambda_{\gamma_2}$ were created by the $(\gamma,n)$, the ratio of $\frac{\alpha_{\gamma_1}}{\alpha_{\gamma_2}}$ represents the actual yield ratio for the two photonuclear reactions.

The reaction products of the $(\gamma,n^dp)$ and $(\gamma,n)$ reaction in $Si^{28}$ had half-lives of 6.7 and 4.3 seconds respectively. Therefore, the decay-curve for each product isotope could be obtained from the same measurement. The background from this complex decay-curve served as a check on the calculated static background for the decay-curves from calcium and sulfur. The yield ratio from the bombardment of silicon was obtained for bombarding energies of 85 mev, 60 mev, and 40 mev. The accuracy in the quoted bombarding energy is felt to be about 5%.

The observed ratio from the bombardment of calcium was further corrected to take into account the fact that the long-lived activity represented only that portion of the $(\gamma,n^dp)$ reaction products created in the $K^{38}$ ground state. The portion created as $K^{38m}$ would be observed in the decay-curve of $Ca^{39}$, the reaction product of the $(\gamma,n)$ process. Assuming the computed ratio of 2.0/2.1 for the creation of $K^{38m}$ and $K^{38}$ from the $(\gamma,n)$ reaction on $K^{39}$, to hold also in the creation of these states by the reaction $Ca^{40}$ $(\gamma,n^dp)$ $K^{38m}$, the observed yield ratio from $Ca^{40}$ was corrected. The adjusted value is also shown in Table VI.

C. Summary and Conclusion.

The observed ratios of the yields from the $(\gamma,n^dp)$ reaction and the $(\gamma,n)$ reaction on $Ca^{40}$ and $S^{32}$ are consistent with the previous measurements in sulfur[43,73] and in copper[76,77]. The yield ratio from the bombardment of $Si^{28}$ was better than a factor of 2 smaller than the corresponding

ratios from $Ca^{40}$ and $S^{32}$ at 85 mev bombarding energy. This is consistent with the findings that the neutron yield of the reaction $Al^{27}$ $(\gamma,n)$ $Al^{26}$ is three times the positron yield[58,59].

## CHAPTER VII

## SUMMARY AND CONCLUSIONS

A state has been found in $K^{38}$ which lies at 3.5 mev above the ground state. This state has been identified as having either $(T = 1, 0^+)$, or $(T = 0, 1^+)$. The latter assignment of the 3.5 mev state is the preferred assignment. Both assignments are possible from an $(s\ \frac{1}{2})^{-2}$ configuration[50]. From measurements of the positron endpoints of the decays from $K^{38}$ and $K^{38m}$, and from an energy measurement of the gamma-ray which follows the decay from $K^{38}$, the energy separation of $K^{38}$ and $K^{38m}$ has been measured to be $(210 \pm 190)$ kev. The $(T = 0, 3^+)$ state is probably the ground state.

The half-life of the positron decay from $Ca^{38}$ has been measured to be $0.66 \pm 0.05$ seconds. Since the decay is assumed to be, in the main, a $(0^+ \rightarrow 0)$ transition between the corresponding states $Ca^{38}$ and $K^{38m}$, the decay should be a superallowed transition with $\log_{10} ft = 3.5$. This value, together with the measured half-life, predicts an endpoint energy of 6.3 mev for the positron decay. Such an endpoint may account for the wide discrepancies in the measured values of the decay from $Ca^{39}$. The $Ca^{39}$ was produced in many such measurements by a $Ca^{40}$ $(\gamma,n)$ reaction. Since the bombarding energies were usually above 30 mev, $Ca^{38}$ was also produced in about 3% relative abundance. This presence of $Ca^{38}$, with the predicted endpoint of 6.3 mev could cuase a distortion in the positron spectrum of $Ca^{39}$, particularly at the higher energies.

The ratio of the activities produced by the $(\gamma,n^dp)$ reaction and the $(\gamma,n)$ reaction on $Ca^{40}$ agrees with previous measurements, showing that the $(\gamma,n^dp)$ cross-section is much higher than that predicted by Weisskopf

and Ewing[72]. This is in accordance with similar yield measurements on $S^{32}$ [43,45,76] and on $Cu^{63}$ [78,79].

When sulfur was bombarded by the bremsstrahlung beam, no gamma-rays were found with an energy of 700 kev. The absence of such a gamma-ray is interpreted as indicating that the reported state at 700 kev in $P^{30}$ [51,53,55] is a (T = 0,0) state. The existence of such a state violates the rule that in the odd-odd, self-conjugate nuclei the (T = 0) states may have only odd values of J[25]. Such a state could, however, be formed from a mixed nucleon configuration. The $(T = 1,0^+)$ state probably lies between this state at 700 kev and the ground state. Transitions from this state would not have been seen due to the proximity of the energy of the gamma-ray to the very intense annihilation radiation. In the bombardment of sulfur, as in the bombardment of calcium, the ratio of $(\gamma,n^dp)$ reaction induced activity to $(\gamma,n)$ reaction induced activity is too high to be consistent with the Weisskopf-Ewing theory.

The data from the bombardment of silicon indicated that the deuteron emission induced activity is much lower than that from the bombardment of either calcium or sulfur. This has been interpreted as a substantiation of previous experiments which indicate the production of two states in $Al^{26}$ [58,64]. One of these states has a very long half-life and decay from this state was not observed as deuteron emission induced activity.

It is to be hoped that further experiments could be designed and carried out which would further verify the findings of this research, would indicate the location of the $(T = 1,0^+)$ level in $P^{30}$, and would verify the existence of the same state in $Al^{26}$ at 1083 kev.

BIBLIOGRAPHY


1. Fermi, E., Zeit. fur Physik. 88, 161, 1934.
2. Gamow, G., & Teller, E., Phys. Rev. 49, 895, 1936.
3. Blatt & Weisskopf, Theoretical Nuclear Physics, Wiley & Sons, 1952.
4. Cassen B., and Condon, E. U., Phys. Rev. 50, 846, 1936.
5. Wigner, E. P., Phys. Rev. 51, 106, 1937.
6. Rustad B.M. & Ruby, S.L., Phys. Rev. 89, 880, 1953.
7. Radicatti, L. A., Phys. Rev. 87, 521, 1952.
8. Gell-Mann, M., and Telegdi, V. L., Phys. Rev. 91, 169, 1953.
9. Adair, R. K., Phys. Rev. 87, 1041, 1952.
10. Morinaga, H., Phys. Rev. 97, 444, 1955.
11. Harkins, W. D., Jour. Am. Chem. Soc. 39, 856, 1917.
12. Elsasser, W. M., Jour. Phys. et Ra. 4, 549, 1933.
13. Elsasser, W. M., Jour. Phys. et Ra. 5, 389 (1934) 635 (1934).
14. Haxel, O., Jensen, J. D., Suess, H. E., Phys. Rev. 75, 1766, 1949.
15. Mayer, M. G., Phys. Rev. 75, 1969, 1949.
16. Inglis, D. R., Rev. Mod. Phys. 25, 390, 1953.
17. Nordheim, L. A., Rev. Mod. Phys. 23, 322, 1951.
18. Mayer, M. G. and Jensen, J. H. Elementary Theory of Nuclear Shell Structure. Wiley & Sons, 1955.
19. Kofoed-Hansen, Phys. Rev. 92, 1075, 1953.
20. Wigner, E. P. Phys. Rev. 51, 95, 1937.
21. Trigg, G., Phys. Rev. 86, 506, 1952.
22. Winther, A., Physica, 18, 1079, 1952.
23. Arber, W., and Stahelin, P., Helv. Phys. Acta. 26, 433, 1953.

24. Morinaga, H., Phys. Rev. 100, 431L,,1955

25. Moszkowski, S. A., Peaslee, D. C., Phys. Rev. 93, 455, 1954.

26. Bethe, H. A., Bacher, R. F. Rev. Mod. Phys. 8, 162, 1936.

27. von Weitzsacher, C. F., Zeit. Physik. 96, 431, 1935.

28. Cooper, L. N. and Henley, E. M. Phys. Rev. 92, 801, 1953.

29. Rossi, B., and Greisen, K. Rev. Mod. Phys. 13, 253, 1941.

30. Paul, W., and Steinwedel, H. Interactions of Electrons with Materials, Beta and Gamma Spectroscopy, K. Seigbahn Interscience Publishers Inc. 1955.

31. Wilkinson, D. H., Proc. Cambr. Phil. Soc. 46, 508, 1950.

32. Gatti, E. Nuovo Cimento 7, 655, 1950.

33. Laslett, L. J., Jensen, E., and Paskin, A. Phys. Rev.. 79, 412, 1950.

34. Hopkins, J. I. Rev. Sci. Inst. 22, 29, 1951.

35. Freedman, M. S., Novey, T. B., Porter, F. T. and Wagner, F.,Jr. Rev. Scient. Inst. 27, 716, 1956.

36. Owen, G. E., and Primakoff, H., Phys. Rev. 74, 1406, 1948.

37. Henderson, Ridenour, White, and Henderson, Phys. Rev. 51, 1107L, 1937.

38. Tricho, H. K., Phys. Rev. 84, 847, 1951.

39. Bleuler, E. and Zunti, W., Helv. Phys. Acta. 19, 375, 1946.

40. Stahelin, P. Helv. Phys. Acta. 26, 691, 1953.

41. Hunt, W. A., Doctoral Thesis, Iowa State College, 1954.

42. Green, D. and Richardson, J. R., Phys. Rev. 101, 776, 1956.

43. Smith W. H. Bull. Am. Phys. Soc. 27, #1,18, 1952.

44. Sagane, R., Phys. Rev. 83, 174L, 1951.

45. Katz and Penford, Phys. Rev. 81, 815, 1951..

46. Pool, Cork, and Thornton, Phys. Rev. 52, 239, 1937.

47. Walke, Thompson, and Holt, Phys. Rev. 57, 177, 1940.

48. Sperduto, A,. and Buechner, W. W. Phys. Rev. 100, 961A, 1955

49. Wilkinson, D. H., Notes of remarks made at the Glasgow Nuclear Physics Conference (July 1954).

50. Satchler, G. R., Private Communication.

51. Endt, P. M., Kluyver, J. C. and VanderLeun, C. Phys. Rev. 95, 580L, 1954.

52. Ridenour, L. N., and Henderson, W. J. Phys. Rev. 82, 889, 1951.

53. Broude, Green, Singh, and Wilmott, Phys. Rev. 101, 1052, 1956.

54. Mandeville, Swann, Chatterjee, and van Patter, Phys. Rev. 85, 193, 1952.

55. Lee, L. L.,Jr.. & Mooring, F. P. Phys. Rev. 104, 1342, 1956.

56. King, R. W. and Peaslee, D. C. Phys. Rev. 93, 455, 1954.

57. Hausman, Allen, Arthur and McPole, Phys. Rev. 88, 1296, 1952.

58. Haslam, Roberts, and Robb., Can. Jour. Phys. 32, 361, 1954.

59. Montalbatti, Katz, and Goldemberg. Phys. Rev. 91, 659, 1953.

60. Kavanaugh, Mills, and Sherr. Phys. Rev. 97, 248L, 1955.

61. Kluyver, J. C., VanderLeun, and Endt, P. M. Phys. Rev. 94, 1794L, 1954.

62. Browne, C. P. Phys. Rev. 95, 860, 1954.

63. Simanton, J. R., Richtmare, R. A., Long, A. L., and Kohman, T. Phys. Rev. 96, 1711, 1954.

64. Handley, T. R. and Lyon, W. S. Phys. Rev. 99, 755, 1955.

65. Kline, R. M. and Zaffarano, D. J. Phys. Rev. 96, 1620, 1954.

66. Phipps, P. L. Masters Thesis, Iowa State College.

67. Chadwick, J. and Goldhaber, M. Nature 134, 237, 1934.

68. Sagane, R. Phys. Rev. 85, 926, 1952.

69. Terwilliger, K. M. Doctoral Thesis, University of California, 1952.

70. Jones, L. W. Doctoral Thesis, University of California, 1952.

71. Bohr, N. Nature, 137, 344, 1936.

72. Weisskopf, V. F. and Ewing, D. H., Phys. Rev. 57, 472, 1940.

73. Panofski, W. K. H., and Reagon, D., Phys. Rev. 87, 324L, 1953.

74. Whalin, E. A., Hanson, A. D. Phys. Rev. 89, 324L, 1953.

75. Carver, T. H., Edge, E. D. and Wilkinson, D. H. Phys. Rev. 89, 658L, 1953.

76. Katz, L., and Cameron, A. G. W., Can. Journ. Physics, 29, 518, 1951.

77. Cameron, A. G. W., Phys. Rev. 86, 437L, 1952.

78. Byerly, P. R. Jr., and Stephens, W. E. Phys. Rev. 83, 54, 1951.

79. Harrington, Katz, Haslam, and Johns, Phys. Rev. 81, 660A, 1951.